REGULATION OF THE ERROR-PRONE DNA POLYMERASE POLK BY ONCOGENIC SIGNALING

by

Kelsey Rene Temprine

A Dissertation

Presented to the Faculty of the Louis V. Gerstner, Jr.

Graduate School of Biomedical Sciences,

Memorial Sloan Kettering Cancer Center

in Partial Fulfillment of the Requirements for the Degree of

Doctor of Philosophy

New York, NY

September, 2018

_____ _____

Richard M White, MD, PhD Date
Dissertation Mentor

DEDICATION

I would like to dedicate this thesis to my parents, Raeneen and Luke Temprine. From the very beginning, they were always there for me, providing a helping hand and the inspiration to chase after my dreams. Without them, none of this would be possible.

ABSTRACT

The acquisition of mutations over time plays an important role in tumor progression for many different types of cancer by promoting processes such as proliferation, survival, and metastasis. The rate at which cells acquire mutations over time is dependent upon the interplay between the fidelity, or error rate, of the DNA polymerases utilized and the ability of repair pathways, such as mismatch repair, to fix any mistakes that are made. While high fidelity DNA polymerases perform the majority of DNA replication, cells also contain a large number of more "error-prone" DNA polymerases that function in DNA repair but have high mutation rates when replicating on undamaged DNA. Affecting any of these processes can result in an increased mutation rate and therefore contribute to cancer. While there are many examples of mutations that turn cells into constitutive mutators, it could be beneficial for cells to instead use more of an induced system where they can turn the high mutation rate on and off depending on how well-adapted they are to their environment. An example of such an induced system is stress-induced mutagenesis (SIM) in bacteria, where in response to stress (such as starvation or treatment with antibiotics), cells can temporarily increase their mutation rate by activating the error-prone DNA polymerase DinB. We hypothesized that a similar process could occur in human cancer via DNA polymerase kappa (polκ), DinB's closest vertebrate ortholog.

To test this, we treated the $BRAF^{V600E}$-mutant human melanoma cell line A375 with the $BRAF^{V600E}$ inhibitor PLX4032 (vemurafenib) and observed a significant increase in polκ mRNA levels and a dramatic shift of polκ protein from the cytoplasm into the

nucleus. Similar results were also observed with other MAPK inhibitors and in other melanoma cell lines as well as with breast and lung cancer cell lines treated with relevant targeted inhibitors. We next worked to determine the mechanism behind the observed shift. In bacterial SIM, the two major requirements are activation of the DNA damage response pathway (SOS) and induction of a stress response (RpoS). Whereas we found no evidence of a role for DNA damage in our system, we found that additional stressors such as glucose deprivation and ER stress could induce similar effects on polκ. All these pathways appear to converge on mTOR, a central stress sensor in vertebrate cells. Direct inhibition of mTOR or its upstream activator PI3K rapidly induced polκ nuclear localization at a timepoint much earlier than that observed for MAPK inhibition. These data suggest that similar to bacteria, induction of a stress response, via mTOR, is the most proximate regulator of polκ localization.

Finally, we examined the functional consequences of high levels of nuclear polκ, focusing on mutagenesis, drug resistance, and tumorigenesis. To study these, we generated dox-inducible and constitutive polκ overexpression constructs for use in our human melanoma cell lines and zebrafish model of melanoma, respectively. Cells exposed to a period of polκ overexpression showed increased mutagenesis and resistance to PLX4032. In addition, we monitored tumor incidence in sibling melanoma-prone zebrafish with or without polκ overexpression and saw a decrease in melanoma-free survival. Overall, these studies provide important insights into how stress may act to induce new genetic heterogeneity in cancer via error-prone DNA polymerases such as polκ. In the future, one open question is whether these observations could lead to therapies designed to reduce the chances of acquiring resistance by interfering with tumor cell evolvability.

BIOGRAPHICAL SKETCH

Kelsey was born to Raeneen and Luke Temprine on November 21, 1989 in Dallas, Texas. Kelsey attended the local elementary, middle, and high schools in her hometown of Coppell, Texas before transferring to the Texas Academy of Mathematics and Science (TAMS) at the University of North Texas for her junior and senior years of high school. She graduated from TAMS in May 2008 with a 4.0 GPA and then began college at the University of Texas at Austin (UT) as part of the Dean's Scholars Honors Program. After three years at UT, she graduated with a Bachelor of Science (BS) in Biology, a 4.0 GPA, and highest honors. During her undergraduate career, Kelsey performed research in a variety of labs both at UT and abroad before completing an undergraduate senior thesis project in the College of Pharmacy under the mentorship of Dr. Shawn Bratton. In June 2011, Kelsey moved to Bethesda, Maryland to work as a NIH Postbaccalaureate Intramural Research Training Award (IRTA) Trainee in the lab of Dr. Hari Shroff. In July 2012, Kelsey moved to New York City, New York where she began the first year of her PhD at the Louis V. Gerstner Jr. Graduate School of Biomedical Sciences. During her graduate studies, Kelsey investigated the role of the error-prone DNA polymerase polκ in stress-induced mutagenesis and cancer with her mentor Dr. Richard White at Memorial Sloan Kettering Cancer Center.

ACKNOWLEDGMENTS

First, I would like to thank my mentor, Dr. Richard White, for being with me throughout my entire Ph.D. He provided me with guidance, encouragement, and feedback while helping me build a project from the ground up that straddled the diverse fields of mutagenesis/evolution, cancer, and zebrafish. He also supported me in my more creative outlets, such as crocheting zebrafish and decorating the lab. Without him, this work would not have been possible.

Second, I am extremely grateful for the exceptional guidance provided by the members of my thesis committee, Dr. John Petrini and Dr. Sarat Chandarlapaty. From the start, they have provided useful feedback, reagents, protocols, and suggested experiments. Also, I would like to thank Dr. Xiaolan Zhao for agreeing to chair my Dissertation Defense Committee and Dr. Itai Yanai for acting as my external examiner.

Third, I would like to thank all of my labmates (past and present): Yan Zhang, Scott Callahan, Milena Zimmer, Bili Yin, Nate Campbell, Josh Weiss, Mohita Tagore, Maomao Zhang, Richard Huang, Thijs Van Boxtel, Liz Perry, Kajan Ratnakumar, Izzy Kim, Terri Simon-Vermot, Emily Kansler, Erin Langdon, Grant Robinson, Thomas Beckham, Sara Fisher, and Emily Johnson. It has been amazing working with such a talented and fun group of people, and they all helped me both scientifically and creatively. I would also like to thank the wonderful summer students who have worked with me over the years: Averill Clapp, Mollie Chipman, Krisha Mehta, and Langley Grace Wallace. They performed great work, and it was a pleasure mentoring them.

Fourth, I would like to thank the graduate school, particularly Dr. Ken Marians, Dr. Linda Burnley, Maria Torres, Iwona Abramek, David McDonagh, Ivan Ruban, and Alex Woodside. Thank you so much for your support throughout my graduate career. Additionally, I would like to thank the staff at the Rockefeller University Science Outreach Program, specifically Dr. Beth Waters and Dr. Jeanne Garbarino. Volunteering for the LAB Initiative and Science Saturday were extremely enjoyable experiences that helped remind me of the joy in science when all my experiments were failing.

Finally, I would like to present my sincerest thanks to my family and the friends who are basically family. They kept me sane, helped satisfy my ice cream cravings (a special shout out to Vicki Crosson for the many different ice cream places we have tried together), and provided unwavering support and encouragement. There is no way I would be where I am today without them.

TABLE OF CONTENTS

LIST OF TABLES

LIST OF FIGURES

LIST OF ABBREVIATIONS

3’-OH: 3’-hydroxyl

4E-BP1: eukaryotic translation initiation factor 4E (eIF4E) binding protein 1

5’-dRP: 5’-deoxyribose-5-phosphate

53BP1: p53-binding protein 1

6-TG: 6-thioguanine

9-1-1 complex: RAD9-RAD1-HUS1 complex

AGC subfamily: protein kinase A, G, and C subfamily

AGT: O6-alkylguanine DNA alkyltransferase

AID: activation-induced deaminase

Akt/PKB: protein kinase B

ALKBH: AlkB homolog

ANOVA: analysis of variance

APE1: apurinic/apyrimidinic (AP) endonuclease-1

APOBEC: apolipoprotein B mRNA editing enzyme, catalytic polypeptide-like

ATCC: American Type Culture Collection

ATF4/6: activating transcription factor 4/6

ATM: ataxia-telangiectasia-mutated

ATR: ataxia telangiectasia and RAD3-related protein

ATRIP: ATR interacting protein

BER: base excision repair

BRCA1/2: breast cancer 1/2

BRCT: BRCA1 C-terminus

C-terminus: carboxyl-terminus

cAMP: cyclic adenosine monophosphate

CAS: cellular apoptosis susceptibility

Cas9: CRISPR associated protein 9

CDK4/6: cyclin-dependent kinase 4/6

cDNA: complementary DNA

Chk1/2: checkpoint kinase 1/2

CHOP: CCAAT-enhancer-binding protein (C/EBP) homologous protein

CML: chronic myeloid leukemia

CPD: cyclobutane pyrimidine dimers

CREB: cAMP-response-element-binding protein

CRISPR: clustered regularly interspaced short palindromic repeats

crRNA: CRISPR RNA

CSD: chronically sun damaged

D-loop: displacement loop

dCMP: deoxycytidine monophosphate

DDR: DNA damage response

DEPTOR: DEP domain containing mTOR-interacting protein

dHJ: double Holliday junction

DMSO: dimethyl sulfoxide

DNA-PK: DNA-dependent protein kinase

DNA-PK_{cs}: DNA-PK catalytic subunit

DNA: deoxyribonucleic acid

dNTP: deoxyribonucleoside triphosphate

dox: doxycycline

DSBR: double-strand break (DSB) repair

dsDNA: double-stranded DNA

dsNLS: dimer-specific NLS

E. coli: *Escherichia coli*

eGFP: enhanced GFP

EGFR: epidermal growth factor receptor

ELISA: enzyme-linked immunosorbent assay

ER: endoplasmic reticulum

ERK: extracellular signal-related kinase

Exo1: exonuclease 1

FAK: focal adhesion kinase

FBS: fetal bovine serum

FEN1: flap endonuclease 1

FG-NUP: phenylalanine and glycine-rich repeat NUP

FOXO: forkhead box O

GAB: GRB2-associated-binding protein

GAP: GTPase-activating protein

GDP: guanosine diphosphate

GEF: guanine nucleotide exchange factor

GFP: green fluorescent protein

GPCR: G-protein coupled receptor

Grb2: growth factor receptor-bound protein 2

GRP78: glucose-regulated protein 78

GSK3β: glycogen synthase kinase 3β

GTP: guanosine triphosphate

H&E: hematoxylin and eosin

HER2: human epidermal growth factor receptor 2

HGF: hepatocyte growth factor

HhH: helix-hairpin-helix

HIV: human immunodeficiency virus

HJ: Holliday junction

hpf: hours post fertilization

HPRT: hypoxanthine phosphorybosyl transferase

HR: homologous recombination

hrGFP: humanized *Renilla* GFP

HSF1: heat shock factor 1

HSP90: heat shock protein 90

hTERT: human telomerase reverse transcriptase

ICL: interstrand crosslink

IDL: insertion/deletion loop

Ig: immunoglobulin

IGF1: insulin-like growth factor 1

IGF1R: IGF1 receptor

IKK: IκB kinase

IPZ: importazole

IR: ionizing radiation

IRE1: inositol-requiring enzyme 1

IκB: inhibitor of NF-κB

JNK: c-Jun N-terminal kinase

kDa: kilodalton

Lig1/3α: DNA ligase 1/IIIα

LMB: leptomycin B

MAP2K: MAPK kinase

MAP3K: MAPK kinase kinase (MAP2K kinase)

MAP4K: MAPK kinase kinase kinase (MAP3K kinase)

MAPK: mitogen-activated protein kinase

MEK: MAPK ERK kinase

MITF: microphthalmia-associated transcription factor

MLH1/3: MutL homolog 1/3

mLST8: mammalian lethal with sec-13

MMEJ: microhomology-mediated end joining

MMR: mismatch repair

MRN complex: Mre11-RAD50-Nbs1 complex

mRNA: messenger RNA

MSH2/3/4/5/6: MutS homolog 2/3/4/5/6

MSI: microsatellite instability

mSIN1: mammalian stress-activated map kinase interaction protein 1

mtDNA: mitochondrial DNA

mTOR: mammalian/mechanistic target of rapamycin

mTORC1/2: mTOR complex 1/2

N-terminal: amino-terminal

NER: nucleotide excision repair

NES: nuclear export signal

NF-κB: nuclear factor kappa-light-chain-enhancer of activated B cells

NF1: neurofibromin 1

NFAT: nuclear factor of activated T-cells

NHEJ: non-homologous end joining

NLS: nuclear localization signal

NPC: nuclear pore complex

NTD: nuclear transport domain

NTF2: nuclear transport factor 2

NTR: nuclear transport receptor

NUP: nucleoporin

PAK: p21-protein activated kinase

PARP: poly (adenosine diphosphate-ribose) polymerase

PCNA: proliferating cell nuclear antigen

PCR: polymerase chain reaction

PDGFRβ: beta-type platelet-derived growth factor receptor

PDK1/2: phosphatidylinositol-dependent kinase 1/2

PERK: protein kinase R (PKR)-like ER kinase

PI3K: phosphatidylinositol-4,5-bisphosphate 3-kinase

PIP_2: phosphatidylinositol 4,5-bisphosphate

PIP_3: Phosphatidylinositol (3,4,5)-trisphosphate

PNPK: polynucleotide phosphatase/kinase

polα: DNA polymerase alpha

polβ: DNA polymerase beta

polγ: DNA polymerase gamma

polδ: DNA polymerase delta

polε: DNA polymerase epsilon

polζ: DNA polymerase zeta

polη: DNA polymerase eta (POLH)

polθ: DNA polymerase theta

polι: DNA polymerase iota (POLI)

polκ: DNA polymerase kappa (POLK)

polλ: DNA polymerase lambda

polμ: DNA polymerase mu

polν: DNA polymerase nu

PP2A: protein phosphatase 2

PRAS40: proline-rich Akt substrate 40 kDa

PRMT1: protein arginine N-methyltransferase 1

protor1/2: protein observed with rictor 1 and 2

PTEN: phosphatase and tensin homolog

qRT-PCR: quantitative reverse transcription PCR

raptor: regulatory-associated protein of mTOR

RecBCD complex: RecB-RecC-RecD complex

rictor: rapamycin-insensitive companion of mTOR

Rmi1: RecQ-mediated genome instability protein 1

RNA: ribonucleic acid

ROS: reactive oxygen species

RPA: replication protein A

RpoS: RNA polymerase, sigma S (sigma 38) factor

RSK: 40S ribosomal protein S6 kinase

RTK: receptor tyrosine kinase

RuvABC complex: RuvA-RuvB-RuvC complex

S.E.M.: standard error of the mean

S6K: S6 kinase

SDSA: synthesis-dependent strand annealing

Sgs1: slow growth suppressor 1

shRNA: short hairpin RNA

SIM: stress-induced mutagenesis

Sos: son of sevenless

SSBR: single-strand break (SSB) repair

ssDNA: single-stranded DNA

STAT1: signal transducer and activator of transcription 1

STR complex: Sgs1-TOPIIIα-Rmi1 complex

SV40p: simian vacuolating virus 40 (SV40) promoter

TDT: terminal deoxynucleotidyl transferase

TFEB: transcription factor EB

TFIIH: transcription factor II human

Tg: transgene

TGFβR2: transforming growth factor beta (TGFβ) receptor 2

TLS: translesion synthesis

TOPBP1: DNA topoisomerase II binding protein 1

TOPIIIα: DNA topoisomerase 3 alpha

TOR: target of rapamycin

tracrRNA: trans-activating crRNA

tRNA: transfer RNA

TSC1/2: tuberous sclerosis 1/2

UPR: unfolded protein response

UV: ultraviolet

V(D)J recombination: variable (diversity) joining recombination

XBP1: X-box binding protein 1

XP-V: xeroderma pigmentosum variant

XP: xeroderma pigmentosum

XPO1/CRM1: exportin-1

XRCC1/4: X-ray repair cross-complementing protein 1/4

yAP1: yeast AP-1-like transcription factor

γH2AX: phosphorylated histone H2AX

CHAPTER 1: INTRODUCTION

1.1 The interplay between DNA polymerases, repair pathways, and mutation rate

1.1.1 Background

A mutation is defined as a permanent alteration to a nucleotide sequence. Mutations can result from errors created during DNA replication or in response to various types of DNA damage. While mutations can introduce variety for natural selection to act upon, they can also be deleterious. Furthermore, mutations (and the increased mutation rate that generates them) have been shown to play a role in tumor progression for many different types of cancer (*1–5*). To reduce the rate at which mutations are acquired, human cells utilize a variety of DNA polymerases and DNA repair processes to achieve an overall *in vivo* mutation rate lower than 1×10^{-9} mutations per base pair, which means less than 1 error for every billion base pairs copied (Figure 1) (*6*).

There are fifteen different human DNA polymerases, and only a few perform the majority of DNA replication while the rest function in a variety of DNA damage repair and/or tolerance processes. Each polymerase has a specific structure that facilitates its function(s) but also affects its error rate. As a result, most DNA polymerases can be separated into two major groups: 1) the high fidelity DNA polymerases that function in DNA replication and 2) the more error-prone DNA polymerases that function in DNA repair/tolerance pathways but have high mutation rates when replicating on undamaged DNA (*7*). This section will review all the human DNA polymerases and discuss how their structure and function influence their error rates.

Human cells also utilize a number of DNA repair pathways. Mismatch repair (MMR) fixes any DNA polymerase mistakes not caught by proofreading. Translesion synthesis (TLS) allows replication past bulky single-stranded DNA damage, which can later be fixed by base excision repair (BER), nucleotide excision repair (NER), or direct reversal repair. Single-strand breaks (SSBs) can be fixed by single-strand break repair (SSBR) while interstrand crosslinks (ICLs) can be repaired by interstrand crosslink repair. Finally, homologous recombination (HR), non-homologous end joining (NHEJ), and microhomology-mediated end joining (MMEJ) all function to repair double-strand breaks (DSBs) (*8*, *9*). This section will also give an overview of the various DNA repair pathways with a particular focus on MMR.

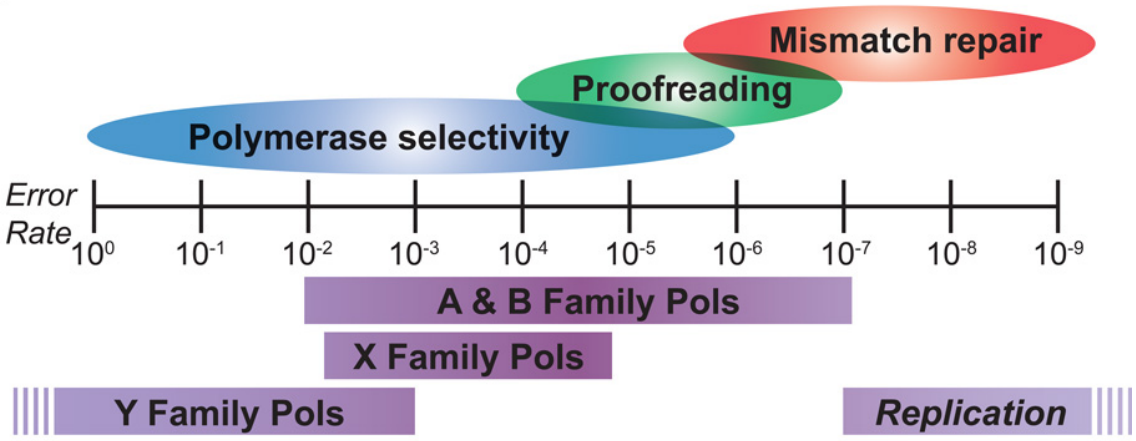

Figure 1. Determinants of replication fidelity.
DNA polymerases replicate DNA *in vitro* with a wide range of error rates depending on their family, and the major contributors to these differences are polymerase selectivity and proofreading. Furthermore, since the *in vitro* error rate of any polymerases is higher that that observed during replication *in vivo*, mismatch repair (MMR) must fix those extra mistakes. In this figure, the relative contributions of polymerase selectivity, proofreading, and MMR to replication fidelity were determined using the mutation rates of systems defective in one or more. Figure adapted from (*6*).

1.1.2 DNA polymerases

Overview of DNA polymerases

Deoxyribonucleic acid (DNA) is composed of two chains of nucleotides bound together by hydrogen bonds to form a double helix structure. Nucleotides consist of a nitrogenous base, deoxyribose sugar, and a single phosphate group and can be divided into purines (guanine and adenine) and pyrimidines (cytosine and thymine). Cytosine and guanine base pair together as do thymine and adenine, and this enables the synthesis of a new DNA molecule using an existing strand as the template (*10*). DNA polymerases are enzymes that synthesize new DNA molecules from a pool of deoxyribonucleoside triphosphates (dNTPs). To initiate this reaction, they require a pre-existing DNA or RNA molecule (called a primer) already base paired to the template strand. This primer provides a free 3' –OH group to which the DNA polymerase can covalently link the 5' α-phosphate of the next dNTP, thereby increasing the DNA molecule by one nucleotide while releasing pyrophosphate (*11*).

Humans utilize fifteen DNA polymerases, which can be divided into four different families using sequence homology (Table 1) (*12*). The A family includes DNA polymerases gamma (polγ), theta (polθ), and nu (polν). The B family consists of DNA polymerases alpha (polα), delta (polδ), epsilon (polε), and zeta (polζ). The X family is made up of DNA polymerases beta (polβ), lambda (polλ), and mu (polμ) as well as template-independent terminal deoxynucleotidyl transferase (TdT). Finally, the Y family contains DNA polymerases eta (polη), iota (polι), and kappa (polκ) plus Rev1.

Table 1. Human DNA polymerases.

Polymerase	Family	Error rate for base substitutions ($\times 10^{-5}$)*	Proofreading?	Function
γ (gamma)	A	1.0	Yes	mtDNA replication
θ (theta)	A	240	No	DNA repair
ν (nu)	A	350	No	DNA repair
α (alpha)	B	9.6	No	DNA replication
δ (delta)	B	≤1.3	Yes	DNA replication
ε (epsilon)	B	≤0.2	Yes	DNA replication
ζ (zeta)	B	110	No	DNA repair
β (beta)	X	67	No	DNA repair
λ (lambda)	X	96	No	DNA repair
μ (mu)	X	100	No	DNA repair
TdT	X	-	No	DNA repair
η (eta)	Y	3,500	No	DNA repair
ι (iota)	Y	72,000	No	DNA repair
κ (kappa)	Y	580	No	DNA repair
Rev1	Y	-	No	DNA repair

*Error rates taken from (*5*, *6*). mtDNA = mitochondrial DNA.

Structural similarities

Although some polymerases consist of a single subunit while others are multi-subunit enzymes, they all share a general conserved architecture that resembles a right hand with thumb, finger, and palm domains (Figure 2). The palm domain contains the catalytic residues required for the DNA polymerization reaction and is highly conserved while the finger and thumb domains are more variable. The finger domain is involved in important interactions with both the incoming dNTP and the template DNA while the thumb domain plays a role in processivity (i.e. the average number of nucleotides added before the polymerase releases the template), translocation, and positioning of the DNA. Some polymerases have additional domains characteristic of their family, which are detailed in each section below (*7*).

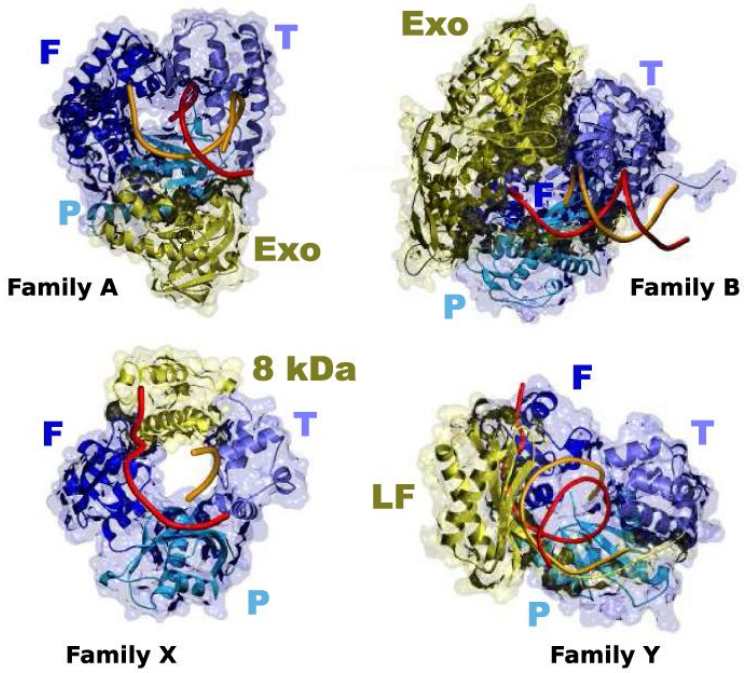

Figure 2. Structural similarities of DNA polymerases from different families. All DNA polymerases have finger (F), palm (P), and thumb (T) subdomains (shown in different shades of blue). Each family also has additional specialized subdomains (shown in yellow). These include the 3′ → 5′ exonuclease (Exo) subdomain seen in the representative members from the A and B families (*Thermus aquaticus* Pol I and RB69 Pol, respectively), the 8 kilodalton (8 kDa) domain seen in the representative X family member (Pol λ), and the little finger (LF) domain seen in the representative Y family member (*Sulfolobus solfataricus* Dpo4). Figure adapted from (*7*).

A family polymerases

polγ, polθ, and polν are members of the A family. polγ is responsible for both the replication and repair of mitochondrial DNA. It is a multi-subunit enzyme with 3' → 5' exonuclease (i.e. proofreading) activity, high processivity, and high fidelity (~10^{-5} mutations per base pair) similar to the replicative B family polymerases (*13*). polγ also has a 5'-deoxyribose-5-phosphate (5'-dRP) lysase activity that is utilized in mitochondrial BER. Due to its importance in the mitochondria, mutations that cause loss of function for polγ are associated with inherited mitochondrial disorders (*14*).

On the other hand, polθ and polν are single subunit enzymes that lack proofreading domains and have low fidelity (~10^{-3} mutations per base pair). Both enzymes have insertions of various sizes in the tip of the thumb subdomain, and as this region is important in DNA binding, it is hypothesized that the insertions contribute to the decreased fidelity observed for polθ and polν (*15*, *16*). polθ has been implicated in somatic hypermutation of immunoglobulin (Ig) genes (*17*) and has also been shown to play a role in various DNA repair processes, including TLS past abasic sites (*16*), short-patch BER (*18*), and MMEJ (*19*). polν's function is still under investigation, but it appears to play a role in ICL repair and in TLS for thymine glycol (*15*, *20*).

B family polymerases

polα, polδ, polε, and polζ are members of the B family. These polymerases are all multi-subunit enzymes with polα, polδ, and polε functioning in DNA replication and polζ in DNA damage repair/tolerance. polα consists of a polymerase subunit, a regulatory subunit, and two primase subunits. It has low processivity but is able to generate the short RNA-DNA hybrid primer used to begin DNA replication. Despite lacking a proofreading domain, it maintains an error rate of ~10^{-4} via high polymerase selectivity (which is explained in further detail below for polδ and polε). The number of errors is further reduced via extrinsic proofreading by polδ (*6*, *21*).

polδ and polε have proofreading activity and therefore function as the main replicative polymerases with polδ replicating the lagging strand and polε the leading strand. Both enzymes are made up of four subunits with POLD1 and POLE serving as the central catalytic subunit for polδ and polε, respectively, and the other three subunits

functioning to increase processivity by interacting with the DNA clamp PCNA and other proteins. These polymerases have a low error rate of $\leq 10^{-5}$ mutations per base pair, which is due to high selectivity against dNTP misincorporation and their intrinsic proofreading abilities. This high selectivity is achieved by having a small active site, which serves two major purposes. First, it limits solvent accessibility, thereby allowing enthalpy-entropy compensation to contribute during the formation of hydrogen bonds between template bases and incoming dNTPs. Second, as the canonical Watson-Crick base pairs have nearly identical sizes, an active site that provides a snug fit for correct base pairs would experience steric clashes in the presence of mismatches. These steric clashes would reduce the rate of phosphodiester bond formation by affecting the binding affinity of the incorrect dNTP and the conformation changes required for catalysis. Despite this high selectivity, misincorporation does occasionally occur, but since a mismatched primer terminus is extended with a lower efficiency than a matched terminus, this creates a delay that allows the intrinsic proofreading capabilities of polδ and polε to function (*6*). Loss of function mutations affecting the proofreading capability of either polδ or polε have been implicated in both inherited and sporadic cancer (*3*).

Like polα, polζ consists of multiple subunits and cannot proofread, but it differs from the other B family members in having much lower nucleotide selectivity and a resulting higher error rate of $\sim 10^{-3}$ mutations per base pair. However, as it is able to efficiently extend a mismatched primer terminus, it plays an important role in the extension step of TLS after initial bypass of the DNA damage by a Y family member (*20*, *22*) and during somatic hypermutation of Ig genes (*23*).

X family polymerases

polβ, polλ, polμ, and TdT are members of the X family. X family polymerases are monomeric and characterized by the presence of an N-terminal 8 kDa DNA-binding domain, which facilitates binding to gapped/nicked substrates. They also contain two helix-hairpin-helix (HhH) motifs that can bind to DNA in a sequence-independent manner. Specifically, the HhH motif present in the 8 kDa domain interacts with the downstream end of the gap while the HhH motif in the finger domain interacts with the upstream end. As a result, these polymerases function in short-patch BER (polβ and polλ) and NHEJ (polλ, polμ, and TdT) (*24*).

BER is a DNA repair process that fixes single bases that have been chemically damaged by excising the base via a damage-specific DNA glycosylase to generate an abasic site that is recognized and cleaved by AP endonuclease-1 (APE1), creating a SSB with 5'-dRP and 3′-OH ends. This 5'-dRP residue is then processed by the 5'-dRP lyase activity of polβ into a 5'-phosphate, and after polβ adds one nucleotide to the 3′-OH, a DNA ligase can seal the two ends. While polλ also has both enzymatic abilities, polβ functions as the key polymerase/5'-dRP lyase during short-patch BER (*20*, *25*, *26*).

NHEJ allows the repair of DSBs resulting either from DNA damage or during V(D)J recombination, and polλ, polμ, and TdT contain an N-terminal BRCT domain that allows them to interact with the other NHEJ proteins occupying the ends of DSBs. polβ lacks this domain and therefore plays no role in NHEJ. polλ and polμ play a role in NHEJ both after DNA damage and during V(D)J recombination while TdT only functions in V(D)J recombination (*24*, *27*).

The error rates of X family polymerases fall between ~10^{-2} to 10^{-5} mutations per base pair. Of the X family members, polβ has the highest fidelity followed by polλ and then polμ (*6*). TdT is a template-independent polymerase that generates stretches of random sequences during V(D)J recombination and thus has the lowest fidelity. This range of fidelities is due to differences in their template requirements and mechanism of catalytic activation. For example, polβ requires an unbroken template strand while polλ can fill a DSB with at least one complementary base pair next to the gap, and polμ requires no complementary template strand nucleotide. Furthermore, polβ is catalytically activated through subdomain motion, similar to A and B family polymerases, but polλ does not require large-scale subdomain movements and is instead activated by template repositioning (*24*).

Y family polymerases

polη, polι, polκ, and Rev1 are members of the Y family. These polymerases lack a proofreading domain but are characterized by an additional "little-finger" domain that makes additional contact with the DNA and is believed to influence processivity, fidelity, and substrate specificity (*28*). They also have a large active site, which facilitates their role in TLS, or replication past bulky DNA damage. The smaller active sites present in polδ and polε prevent them from accommodating the DNA damage, so replication stalling would occur without these TLS polymerases. However, this large active site also results in relaxed nucleotide selectivity and increased solvent accessibility compared to that observed for the replicative polymerases, and when combined with their lack of proofreading ability, this results in a very large error rate (ranging between ~10^{0} to 10^{-3})

when replicating on undamaged DNA. While they all function in TLS, each member of this family is specialized for specific types of DNA damage, and the efficiency and fidelity of the bypass is polymerase-specific (*6*, *20*). In concert with polζ, members of the Y family have also been implicated in somatic hypermutation of Ig genes (*23*).

polη is specialized to bypass cyclobutane pyrimidine dimers (CPDs) and (6,4)-photoproducts resulting from ultraviolet (UV) radiation in a fairly error-free manner (*29*), and loss of function mutations in polη are associated with an increased risk of skin cancer (*2*). polη has also been reported to be able to bypass other types of DNA damage, including 8-oxoguanine, O6-methylguanine, and benzo[a]pyrene adducts, as well as perform the extension step during HR (*20*, *30*). The processivity of polη depends on the DNA structure – it is high when bypassing CPDs and low when replicating on undamaged DNA (*29*). This is likely part of the mechanism through which the risk of polη accessing undamaged DNA *in vivo* is reduced.

polι can also bypass UV-induced lesions (especially in the absence of polη) albeit in a more error-prone manner (*31*). While it serves as a back-up polymerase to polη with regards to UV damage, loss of polι leads to increased sensitivity to oxidative damage as well as increased susceptibility to urethane-induced lung cancers (*32*), suggesting a function in replicating past 8-oxoguanine. polι has a much higher error rate than polη overall, but its fidelity was found to be dependent upon the template nucleotide with higher fidelity shown opposite purines than pyrimidines (*20*). This could explain why polι plays a bigger role in bypassing 8-oxoguanine than UV adducts. Furthermore, polι has been shown to play a role in BER and has 5'-dRP lyase activity (*33*).

polκ functions mostly to replicate past bulky lesions, including minor-groove N_2-deoxyguanine adducts, benzo[a]pyrene adducts, and ICLs. Deficiency of polκ increases cellular sensitivity to both UV and alkylating agents, suggesting it might also bypass UV-induced CPDs in collaboration with polη (*6*, *20*). A role for polκ has also been demonstrated in NER (*34*). polκ has been shown to have greater processivity than the other Y family polymerases due to the presence of a N-clasp that allows near encirclement of DNA and therefore enhances polκ's ability to bind DNA (*35*), but it has a similarly high error rate when replicating on undamaged DNA (*6*, *20*). Furthermore, unlike with polη, overexpression of polκ results in increased genomic instability and cellular mutagenesis, which suggests a different regulatory mechanism (*36*, *37*). Mice deficient in polκ also display a mutator phenotype (*38*), demonstrating the importance of maintaining a specific level of polκ activity.

Finally, Rev1 only has deoxycytidine monophosphate (dCMP) transferase ability, which means it adds cytosine opposite any lesion (*39*). Rev1 does contain a BRCT domain, which is important in protein-protein interactions, and a proposed role for Rev1 is as a scaffold that recruits the other TLS polymerases to damaged DNA rather than as an actual polymerase (*6*, *20*).

1.1.3 Mismatch repair (MMR)

MutS and MutL homologs play major roles in MMR

In bacteria, MutS and MutL play major roles in the initial steps of MMR. Eukaryotic cells contain five MutS homologs (MSH2, MSH3, MSH4, MSH5, and MSH6) and four MutL homologs (MLH1, MLH3, PMS1, and PMS2) (*40*, *41*). MSH4 and MSH5

do not play a role in MMR but instead facilitate crossovers between homologous chromosomes during meiosis (*42*, *43*). MSH2 forms heterodimeric complexes with MSH6 (MutSα) and MSH3 (MutSβ). The MutS complexes function to recognize mismatches with MutSα primarily recognizing mispaired bases and small insertion/deletion loops (IDLs) and MutSβ primarily recognizing large IDLs, but there is some redundancy. MLH1 forms heterodimeric complexes with PMS2 (MutLα), PMS1 (MutLβ), and MLH3 (MutLγ). MutLα plays a greater role in MMR than MutLβ or MutLγ (Figure 3), and its major function appears to be as an endonuclease. MutLα has also been shown to increase mismatch recognition by MutSα and MutSβ (*44*).

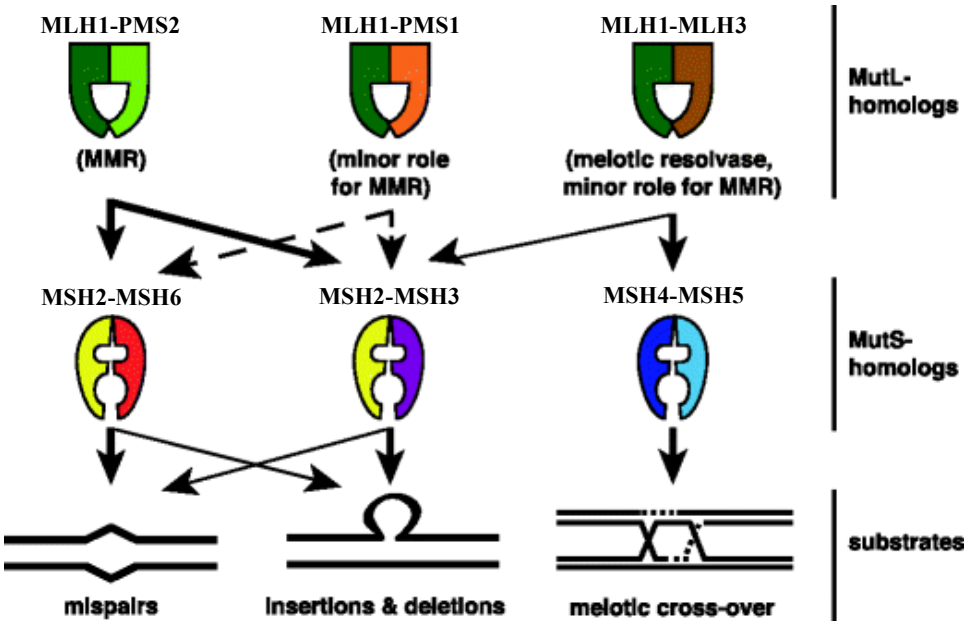

Figure 3. MMR complexes.
Heterodimeric complexes are formed from MutL homologs (MLH1-PMS2, MLH1-PMS1, and MLH1-MLH3) and from MutS homologs (MSH2-MSH6, MSH2-MSH3, and MSH4-MSH5), which play different roles in MMR and/or meiotic crossover. The major interactions and functions of these complexes are indicated by thick arrows and the minor ones by thin arrows. Dashed lines indicate interactions only relevant in specific genetic backgrounds. Figure adapted from (*40*).

Summary of the mechanism

MMR is the process by which mismatches consisting of either mispaired bases or IDLs are recognized, removed, and then replaced by the correct base pair(s) (Figure 4). During the first step, mismatches are recognized by MutSα or MutSβ, and binding to the mismatch induces a conformational change that promotes the recruitment of MutLα. After activation by PCNA, MutLα creates nicks in the nascent DNA strand on both the 5'- and 3'-sides of the mismatch (*45*, *46*). These nicks are recognized by the 5′ → 3′ exonuclease 1 (Exo1), which is capable of digesting single-stranded DNA (ssDNA) starting from an exposed 5'-end. The resulting gap is filled via resynthesis of the correct base pairs by DNA polymerase polδ (or possibly polε) before DNA ligase 1 (Lig1) completes the process by sealing the ends together (*47*).

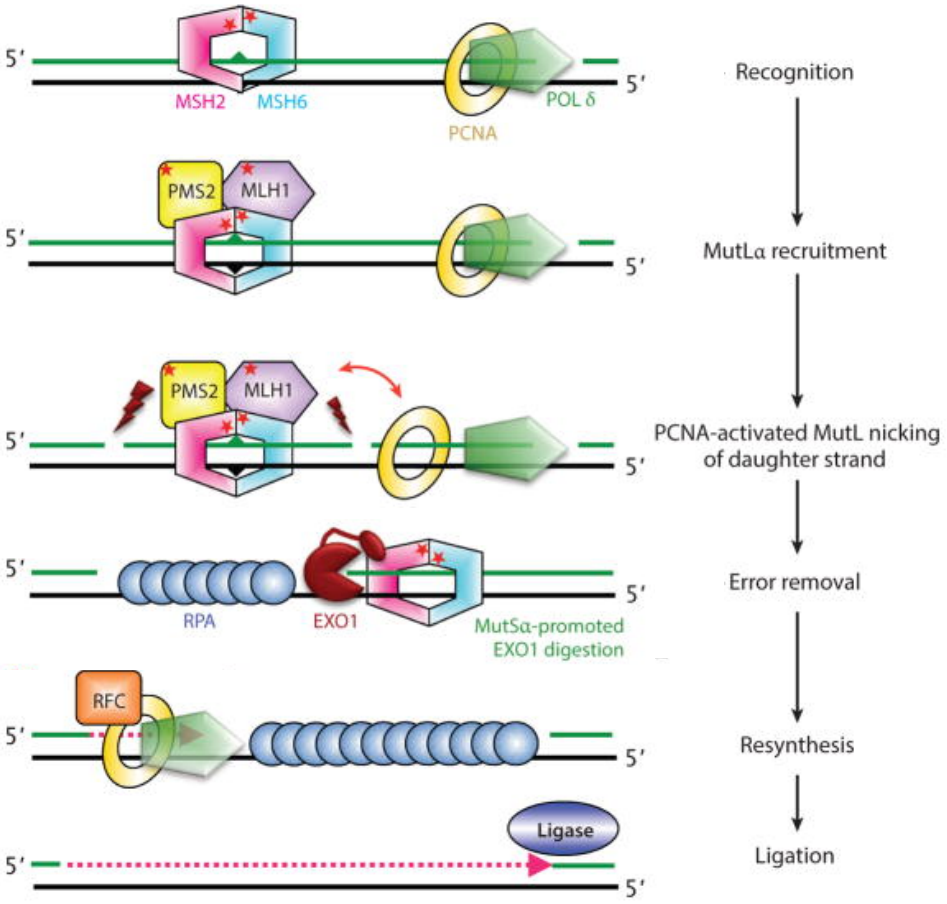

Figure 4. Eukaryotic MMR.
Binding of MutSα (MSH2–MSH6) to a mismatch initiates the MMR pathway and leads to recruitment of MutLα (MLH1-PMS2). Activation of MutLα by PCNA enables it to nick the newly synthesized DNA strand. Exo1 uses these nicks to remove the mismatch, and then a DNA polymerase with PCNA and RFC resynthesizes the correct bases before the ends are ligated together to complete the repair. Figure adapted from (*47*).

Strand discrimination is essential for proper MMR

When performing MMR, cells must be able to distinguish between the template strand (which has the correct sequence) and the newly synthesized strand containing the mismatch, or else they might "fix" the wrong strand and create a permanent mutation. In *Escherichia coli* (*E. coli*), this discrimination utilizes the fact that the nascent strand will not be methylated until after replication completes (*48*). Therefore, by temporally coupling

MMR to DNA replication, cells can take advantage of the short timeframe in which the strands can be distinguished. Eukaryotic cells also couple MMR and DNA replication but do not use DNA methylation for strand discrimination (*49*). Instead, the cell is proposed to use the single-strand gaps and nicks transiently generated by DNA replication to mark the nascent strand, such as those arising from Okazki fragments and ribonucleotide excision repair (*50–52*). Strand discrimination is also influenced by the asymmetrical loading of PCNA because it causes PCNA to interact with MutLα in such an orientation that MutLα preferentially nicks the daughter strand (*46*).

1.1.4 The DNA damage response (DDR)

Types of DNA damage

DNA damage refers to "any modification in the physical and/or chemical structure of DNA resulting in an altered DNA molecule which is different from the original DNA molecule with regard to its physical, chemical, and/or structural properties" (*53*). The source of this modification can be exogenous (ex: environmental factors) or endogenous (ex: produced by normal cell metabolism) in origin, but both can have similar effects on DNA, including direct modification of the DNA and/or induction of structural changes that increase the risk for additional damage, such as strand breaks or mutations (*53*). Different types of DNA damage are summarized in Table 2.

Table 2. Types of DNA damage.

Type	Modification	Direct result	Source(s)*	Functional effect on DNA	Example
Modification of a base	Deamination	Conversion of one base to another	N (spontaneous, enzymes)	Mutation if replicated	Deamination of cytosine into uracil (C:G → T:A)
	Tautomerization	Change in base conformation	N (spontaneous); X (IR)	Mutation if replicated	Thymine-enol pairs with guanine (T:A → C:G)
	Hydrolytic loss of a base	Abasic site	N (spontaneous); X (ROS from IR, heat)	Strand breakage and/or mutation if replicated	Loss of adenine to produce an apurinic site (A:T → any pair)
	Alkylation/ methylation	Changes base size and pairing affinity	N (enzymes); X (various chemicals)	Stalled replication fork and/or mutation if replicated	O6-alkylguanine pairs with thymine (G:C → A:T)
	Oxidation	Increases base size	N (ROS); X (ROS from IR, UV, or various chemicals)	Stalled replication fork and/or mutation if replicated	8-hydroxyguanine
	Addition of a bulky adduct	Increases base size	X (various chemicals)	Stalled replication fork and/or mutation if replicated	Benzo[a]pyrene adducts
	Dimerization	Produces bonds between adjacent bases	X (UV)	Stalled replication fork and/or mutation if replicated	Thymidine dimer
	Cross-linking	Forms a bond between two bases on the same (intrastrand) or different (interstrand) strands	N (ROS); X (ROS, various chemicals)	Distortions to DNA helix, stalled replication fork, and/or mutation if replicated	5'-GC interstrand crosslink (ICL)
DNA break	Single-strand break (SSB)	Break in one strand of DNA	N (ROS); X (IR, UV, various chemicals, heat)	Can cause a DSB if two occur in the same vicinity	-
	Double-strand break (DSB)	Break in both strands of DNA	X (IR)	Chromosomal deletions, translocations, and duplications	-

*N = endogenous; X = exogenous. IR = ionizing radiation. ROS = reactive oxygen species. Information summarized from (*53*).

Overview of the DDR

To combat the threats presented by all the different types of DNA damage, cells have evolved a number of mechanisms collectively referred to as the DNA damage response (DDR). Together these mechanisms sense the DNA damage and then determine whether to temporarily tolerate it via TLS or immediately repair it (and which repair pathway to use). This decision depends on the type of DNA damage and the cell cycle stage it is detected in (*9*). The different mechanisms that make up the DDR (and their specific functions) are listed below:

- Translesion synthesis (TLS): bypass of a damaged base blocking fork progression during DNA replication
- Direct reversal repair: chemical reversal of specific types of alkylated bases
- Base excision repair (BER): repair of damaged/modified bases
- Nucleotide excision repair (NER): repair of helix-distorting base lesions
- Single-strand break repair (SSBR): repair of single-strand breaks
- Homologous recombination (HR), non-homologous end joining (NHEJ), and microhomology-mediated end joining (MMEJ): repair of double-strand breaks
- Interstrand crosslink (ICL) repair: repair of interstrand crosslinks

Key signaling cascades in the DDR

For some types of damage, the damage is sensed, a repair complex immediately forms, and the damage is fixed without the need for elaborate signaling. However, the presence of DSBs or blocked replication can activate a cascade of protein kinases that eventually results in the phosphorylation of relevant downstream substrates that act as

effectors of various cellular processes. Human cells contain three major cascades, and each enables them to stimulate specific repair pathways while also making decisions regarding if the cell cycle just needs to be arrested until the repair is complete or a more permanent action like senescence or apoptosis is warranted. This decision is largely dependent upon cell type-specific factors (*54–56*). The first cascade is initiated by replication stress due to blocked fork progression by a DNA lesion that exposes ssDNA. The ssDNA is recognized by RPA, leading to recruitment of ATR via its partner ATRIP. At the same time, RAD17 facilitates localization of the RAD9-RAD1-HUS1 (9-1-1) complex to the site, and the 9-1-1 complex then interacts with the ATR activator TOPBP1, leading to ATR activation. ATR can then phosphorylate its targets, including Chk1, resulting in replication fork recovery via TLS (*57*). DSBs can initiate the second cascade when they are sensed by the Mre11-RAD50-Nbs1 (MRN) complex, which then recruits ATM. Inactive ATM is sequestered in dimers, and activation occurs via autophosphorylation events that disrupt this dimerization to form monomers, which allows access of the active site to substrates. Active ATM phosphorylates many different substrates, including the histone H2AX and the kinase Chk2, resulting in HR. Phosphorylated H2AX (called γH2AX) functions to recruit/stabilize various proteins/complexes at the DSB, including 53BP1, BRCA1, and the MRN complex, and it can also be used as a marker of DSBs (*58–61*). Although ATR/Chk1 and ATM/Chk2 typically respond to different types of DNA damage, there is some cross-talk between the two pathways (*57*, *62*). The other cascade that can be activated by DSBs occurs mostly during G0/G1 and G2. In this case, the DSB is instead recognized by the Ku70-Ku80 heterodimer, which then recruits DNA-PK_{CS}. This promotes repair via NHEJ (*63*, *64*). A

major effector of all these cascades is p53, which is activated in response to DNA damage. Activated p53 can mediate transcriptional activation of a number of genes whose products play roles in DNA repair, cell cycle arrest, or apoptosis (Figure 5) (*65*). Importantly, defects in the DDR increase cellular sensitivity to DNA damage and also contribute to human diseases, such as cancer (*9*).

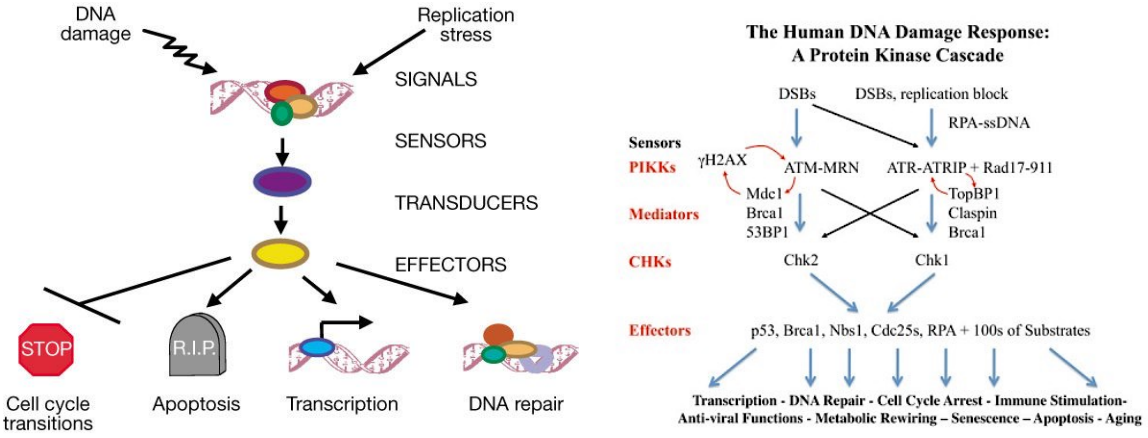

Figure 5. A general outline of the DDR.
The presence of DNA damage is recognized by various sensor proteins. These sensors initiate signaling pathways made of transducers/mediators that regulate effector proteins. These effectors make the decision whether to tolerate or repair the lesion while impacting other cellular processes, including the cell cycle and apoptosis. The image on the left more generally summarizes the roles played by proteins involved in the signaling cascade while the one on the right lists the specific proteins performing those roles. See text for more details. Left figure adapted from (*54*). Right figure adapted from (*61*).

Translesion synthesis (TLS)

As mentioned above, the small active site of the replicative polymerases polδ and polε cannot accommodate DNA larger than the canonical base pairs (*6*). Therefore, damaged bases that are not caught before the start of replication will cause the replication fork to stall and generate replication stress. Blocked fork progression exposes ssDNA due to uncoupling of the helicase and the polymerase, and this ssDNA is recognized by RPA,

leading to activation of the ATR/Chk1 arm of the DDR. This signaling cascade promotes TLS and cell cycle arrest, which gives the cell more time to replicate the problematic regions (*57*). Then, once replication is complete, the damage is fixed by the appropriate repair pathway (*66*). Although members of the A and X families can exhibit TLS activity, the major DNA polymerases that function in TLS are the Y family polymerases (polη, polι, polκ, and Rev1) plus the B family polymerase polζ. polη, polι, and polκ are each highly specialized for specific types of DNA (ex: polη and UV-induced dimers), allowing lesion bypass to occur in a fairly error-free and efficient manner (*29*). Extension from the bypassed lesion can be performed by polζ or the Y family polymerase responsible for the bypass, and which is used appears to depend on the type of damage (*67*). Rev1 is proposed to play a scaffolding role and help bring the different components together (Figure 6) (*68*).

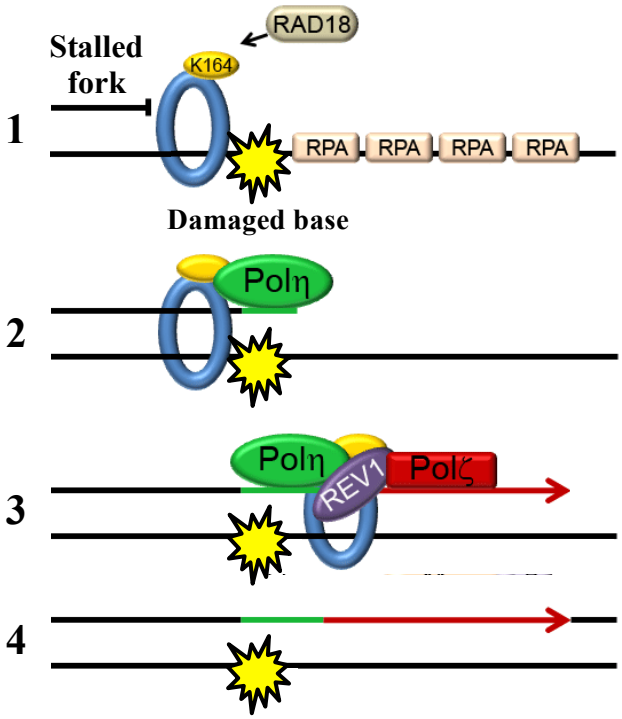

Figure 6. Eukaryotic TLS.
1) A replication fork stalls at a damaged base, causing ssDNA to form via helicase-

polymerase uncoupling. RPA coats the ssDNA and helps recruit RAD18, which functions to mono-ubiquitinate PCNA. 2) Mono-ubiquitination of PCNA promotes its interaction with a Y family polymerase (in this case polη). polη synthesizes directly across from the damaged base. 3) Rev1 helps localize polζ to the site, and then polζ extends from the base replicated by polη. 4) Bypass is complete, and normal replication can resume. Figure adapted from (*68*).

The regulation of TLS is still under investigation, but there is evidence that the ubiquitination status of PCNA plays a major role. For example, Chk1 induces the mono-ubiqutination of PCNA (*57*), and the recruitment of polη to stalled replication forks following UV exposure was shown to depend upon RAD18/RAD6-dependent mono-ubiquitination of PCNA. Both polη and polδ are able to interact with PCNA, but mono-ubiquitinated PCNA has a stronger preference for polη, which promotes the switch from the replicative polymerase to the TLS polymerase (*69*). A similar dependency on mono-ubiquitinated PCNA and RAD18 has also been shown for polκ (*70*) and is likely also true for polι and Rev1 as all the Y family polymerases contain ubiquitin-binding domains (*71*). Rev1 interacts with polη, polι, polκ, and polζ and has been proposed to play a scaffolding role, so regulation of its localization could also affect the localization/activity of the other TLS polymerases (*67*). Furthermore, it is unknown how the correct polymerase for the type of damage is selected. Some models propose that transient association of several polymerases with the DNA lesion occurs sequentially until the best-suited polymerase bypasses it. Therefore, specificity is based on the inherent efficiency of each polymerase for that lesion because the more efficient it is, the higher the probability that it will complete the bypass before being dissociated. While this may play a role, it seems likely that polymerase concentration, PCNA's ubiquitination status, other post-translational modifications, and/or interaction with Rev1 also influence which polymerase is used (*66*).

Direct reversal repair

Unlike BER and NER, direct reversal repair is completely error-free as it does not require breakage of the phosphodiester backbone or DNA resynthesis. However, it is extremely specific and in humans can only be used to correct O- and N-alkylated products. It is suggested that the structural distortions these modification make to DNA are what allows the direct reversal repair enzymes to locate them. O-modifications, such as O6-methylguanine, are removed by a single enzyme called AGT, which transfers the alkyl group from the DNA to itself. This inactivates AGT, making it a single-use enzyme. On the other hand, four members of the ALKBH family can remove N-modifications, such as 1-methylcytosine, and each enzyme can be used to catalyze multiple reactions. ALKBH family members remove N-modifications via oxidative demethylation, which is a multi-step process that involves hydroxylation of the alkyl adduct to create an unstable intermediate that promotes release of the hydroxylated alkyl group and restoration of the original base (*72*).

Base excision repair (BER)

BER is used to repair bases damaged by chemical modification, such as 8-oxoguanine, uracil, and 3-methyladenine. DNA glycosylases are required for the initiation of BER as they serve to first locate the damaged base and then catalyze cleavage of the glycosidic bond linking the damaged base to the DNA backbone. Human cells contain eleven DNA glycosylases (four for the removal of mispaired uracil and thymine, six for oxidative damage, and one for alkylated bases). Glycosylases fall into two classes: monofunctional (which generate an abasic site) and bifunctional (which generate an abasic

site with a 3' nick). Both products (along with naturally occurring abasic sites) are then processed by APE1, which nicks the 5'-side of the abasic site to generate a SSB with 3'-hydroxyl (3'-OH) and 5'-dRP ends. In the case of BER initiated by a monofunctional glycosylase or a naturally occurring abasic site, this 5'-dRP group has to be removed by polβ before DNA polymerization can occur. On the other hand, during BER with a bifunctional glycosylase, the 3' nick causes the entire abasic site to fall off, and polymerization can directly occur. Polymerization can either occur via the synthesis of one base by polβ (short-patch BER) or synthesis of between two and fifteen bases by polδ/polε, which causes strand displacement and requires the endonuclease activity of FEN1 to remove the displaced strand (long-patch BER). The final step in BER is ligation of the 3'-end of the newly synthesized DNA with the 5'-end of the pre-existing DNA, and this is performed by DNA ligase IIIα (Lig3α)/XRCC1 (short-patch BER) or Lig1 (short- and long-patch BER) (*73*, *74*).

Nucleotide excision repair (NER)

NER is also used to repair damaged bases, but these lesions are typically more helix distorting than those repaired by BER, such as CPDs, benzo[a]pyrene-guanine adducts, and intrastrand crosslinks. NER is able to eliminate these structurally unrelated DNA lesions with only six multi-subunit complexes (RPA, XPA, XPC, TFIIH, XPG, and XPF•ERCC1) by performing a "cut and patch" reaction. DNA damage causing local DNA helix destabilization is initially recognized by RPA, XPA, and XPC, and they assemble cooperatively at the site in a random order. The cooperative assembly means that once one damage recognition factor is bound, it greatly promotes the binding of the next and so on.

XPC recruits TFIIH, which uses its helicase activity to unwind the duplex around the lesion. XPC then recruits XPG before leaving, and the complex consisting of RPA, XPA, TFIIH, and XPG is recognized by XPF•ERCC1. XPG and XPF•ERCC1 then make a 3' and 5' incision, respectively, to release a 24 to 32 nucleotide-long oligomer containing the damaged base(s). RPA remains in the gap, and the rest of the complex dissociates. The resulting gap is filled in by polδ, polε, or polκ before Lig1 or Lig3α/XRCC1 completes the repair reaction as in BER (*34*, *75*, *76*).

Single-strand break repair (SSBR)

As SSBs can become DSBs, they must be repaired quickly. Detection of SSBs is performed by PARP1 (or other members of the PARP superfamily). PARP1 is believed to accelerate SSBR by promoting the accumulation and/or stability of SSBR complexes, such as the molecular scaffold XRCC1, at SSBs. SSBs usually have damaged 5'- and/or 3'-ends, which must be restored to 5'-phosphate and 3'-OH groups before gap filling and ligation can occur. Many different enzymes are responsible for the end-processing step as each is specialized for a specific type of damaged end. Gap filling (using polβ, polδ, and/or polε) and ligation (using Lig1 or Lig3α/XRCC1) proceed as during the final steps of BER with both short- and long-patch repair observed (*77*).

The cell cycle determines which DSB repair (DSBR) pathway is used

A major factor that influences whether HR, NHEJ, or MMEJ repairs a specific DSB is the phase of the cell cycle. For example, because HR requires a homologous sequence, which typically takes the form of a sister chromatid, it is primarily active during

mid-S to early G2 phase of the cell cycle. In addition, while NHEJ can occur at any point during the cell cycle, it predominantly occurs in G0/G1 and G2 (i.e. when HR is unavailable). Another important factor is the degree of end resection as NEHJ requires minimal resection, MMEJ a small resection, and HR a large resection. The activity of the nucleases responsible for end resection is affected by CDK-dependent phosphorylation, which provides another way that the cell cycle can affect the DDR (*78*).

Homologous recombination (HR)

The first step of HR involves processing the ends of the DSB via 5'-end resection to generate 3'-overhanging tails. An essential component of the end resection step is the MRN complex, which plays multiple roles. It functions in the initial end resection where Mre11's endonuclease abilities functions to clean up damaged ends, remove any bound Ku protein, and generate an entry site for the proteins involved in the long-range resection. The MRN complex also serves a scaffolding role and helps recruit and promote the activity of Exo1 (*79–81*). Long-range resection is performed by either Exo1 or Dna2, and the resulting ssDNA is quickly bound by RPA. RPA prevents RAD51 from binding, so recombination mediators, such as RAD52, function to exchange RPA and RAD51. The filament consisting of RAD51 and one 3'-overhang can then search for a homologous sequence within the genome via a poorly understood mechanism involving RAD54. Once a homologous sequence is found, the filament invades into the homologous sequence and anneals to its complementary strand to form a transient displacement loop (D-loop). The 3'-OH end of the invading filament is used as a primer for DNA extension, which generates a Holliday junction (HJ), and this extension can be performed by a replicative

polymerase (polδ/polε) or a TLS polymerase (polη/polκ). At this point, HR can proceed via one of two pathways, which are distinguished by the involvement of the second 3'-overhang. In the synthesis-dependent strand annealing (SDSA) pathway, the first 3'-overhang is extended and then released via the action of a helicase. The newly extended 3'-end is now able to anneal to the second 3'-overhang, and DNA synthesis and ligation fill in any remaining single-stranded gaps. The SDSA pathway always produces a non-crossover product. Alternatively, in the classical DSBR pathway, the second 3'-overhang also invades and then replicates to form a second HJ. This double Holliday junction (dHJ) must be either dissolved or resolved. Dissolution results from the decatenase activity of TOPIIIα and helicase activity of Sgs1, which form the STR complex with the DNA-binding protein Rmi1, and always produces non-crossover products. Resolution requires cleavage of the HJs by an endonuclease, and depending on how each HJ is cleaved, crossover or non-crossover products will be formed (*82*, *83*).

Non-homologous end joining (NHEJ)

Unlike HR, NHEJ uses little or no homology and is therefore more inherently error-prone, especially if the DNA requires processing prior to ligation. In NHEJ, DSB ends are recognized by the Ku70-Ku80 heterodimer, which then recruits DNA-PK_{CS} to form the DNA-PK complex. Formation of the DNA-PK complex is associated with a conformational change that makes the DNA ends available. Compatible ends can be ligated by ligase IV in complex with XRCC4 (both of which interact with the DNA-PK complex) while non-compatible ends require further processing before they can be ligated together. Depending on whether the end requires nucleotide removal, nucleotide addition,

and/or the generation of a 3'-OH and 5' phosphate end, nucleases, polymerases (specifically polλ and polμ), and/or PNPK are used for end processing (*84*, *85*).

Microhomology-mediated end joining (MMEJ)

MMEJ is a type of alternative NHEJ that requires between two and twenty base pairs of homology to repair a DSB. MMEJ does not require most of the NHEJ components, and in fact, some steps overlap with HR and other repair pathways. First, PARP1 binds to the DSB ends and recruits CtIP and the MRN complex. CtIP and the MRN complex resect the ends to expose regions of microhomology, which allows annealing of the two ends. Regions of non-homology are removed by the nuclease XPF/ERCC1, and then ssDNA gaps are filled by polθ. polθ is particularly suited to this role due to its ability to stabilize the annealing of two 3'-tails with as little as two basepairs of homology and then use one 3'-tail as a primer and the other as a template. Ligation by Lig1 or Lig3/XRCC1 completes the process (*19*, *85*, *86*).

Interstrand-crosslink (ICL) repair

The mechanism through which ICLs are repaired depends on the phase of the cell cycle. In G0/G1 phase, cells use two rounds of NER in order to remove the ICL without generating a DSB. The first round creates nicks on either side of the ICL on one strand, creating a gap to be filled in. Because the other strand still contains the ICL (and associated excised oligomer), a TLS polymerase is required for the gap-filling step, and evidence suggests that polκ, polζ, and REV1 fulfill this role. The second round of NER

creates nicks on the other strand, excising the ICL and associated oligomers. This gap does not require a specialized polymerase to be filled in (*87*).

In S phase, the ICL repair is directly coupled to DNA replication. Convergence of two replication forks on the ICL generates an X-shaped structure consisting of two leading strands that stall ~20 to 40 base pairs from the ICL and two lagging strands with 5' ends located at a greater and more variable distance from the lesion. Extension of the leading strand of one fork to within a few nucleotides of the ICL is followed by the creation of excisions on either side on the ICL on the parental strand containing the other leading strand. TLS is then used to bypass the lesion on the first parental strand to allow for replication of that DNA molecule to continue. The DSB resulting from excision of the ICL is repaired using HR, and the ICL is eventually fully excised by NER (*88*).

1.2 Constitutive vs. induced mutagenesis in human cancer and bacteria

1.2.1 Background

A mutator is a cell with an increased mutation rate. As was demonstrated in the previous section, the mutation rate of a cell is dependent upon the interplay between the effectiveness of DNA repair and the error rate of DNA replication. Therefore, alterations to either of these processes can generate a mutator phenotype. In addition to the multiple examples of mutator cells arising in bacteria in the lab (*89*) and in nature (*90*, *91*), they have also been shown to play a role in various types of cancer, and examples of this will be provided below.

The fitness of a mutator is dependent upon its environment. For example, competition assays between non-mutators (i.e. cells with a low basal mutation rate) and

constitutive mutators (i.e. cells with a constant high mutation rate) have revealed that the mutators are fitter than the non-mutators under many conditions that provide some level of selection. These conditions include limited glucose (*92*, *93*), treatment with antibiotics (*94*), multiple rounds of selection in the lab (*95*), and colonization of the gut of germ-free mice (*96*). This is an example of second-order selection as the mutator allele is able to hitchhike along with any favorable mutations that it generates (*97*, *98*).

However, when cells are well-adapted (and thus not under selective pressure), most mutations would be either neutral or deleterious, which means a low mutation rate would be advantageous, and mutators would be under negative selection. An alternative to being a constitutive mutator or non-mutator is being an induced mutator (Figure 7). Induced mutators can switch between mutator and non-mutator states in response to their environment (i.e. be a mutator in unfavorable environments and a non-mutator in favorable ones). This prevents the continued accumulation of unnecessary mutations in a well-adapted cell while allowing cells to still be able to increase their variation when maladapted (*99*). This suggests they would be better adapted than both non-mutators and constitutive mutators regardless of the environment. In fact, over 80% of the natural isolates of *E. coli* tested in one study were induced mutators (*100*) compared to previous reports of constitutive mutators making up between 1-15% of *E. coli* and *Salmonella enterica* isolates (*90*, *91*). In both constitutive and induced mutators, the fold-increase in mutation rate compared to a non-mutator varied greatly. The major example of an induced mutator comes from bacteria where *E. coli* have been shown to switch from a low to a high mutation rate in response to stress. That phenomenon called stress-induced mutagenesis (SIM) is covered at the end of this section.

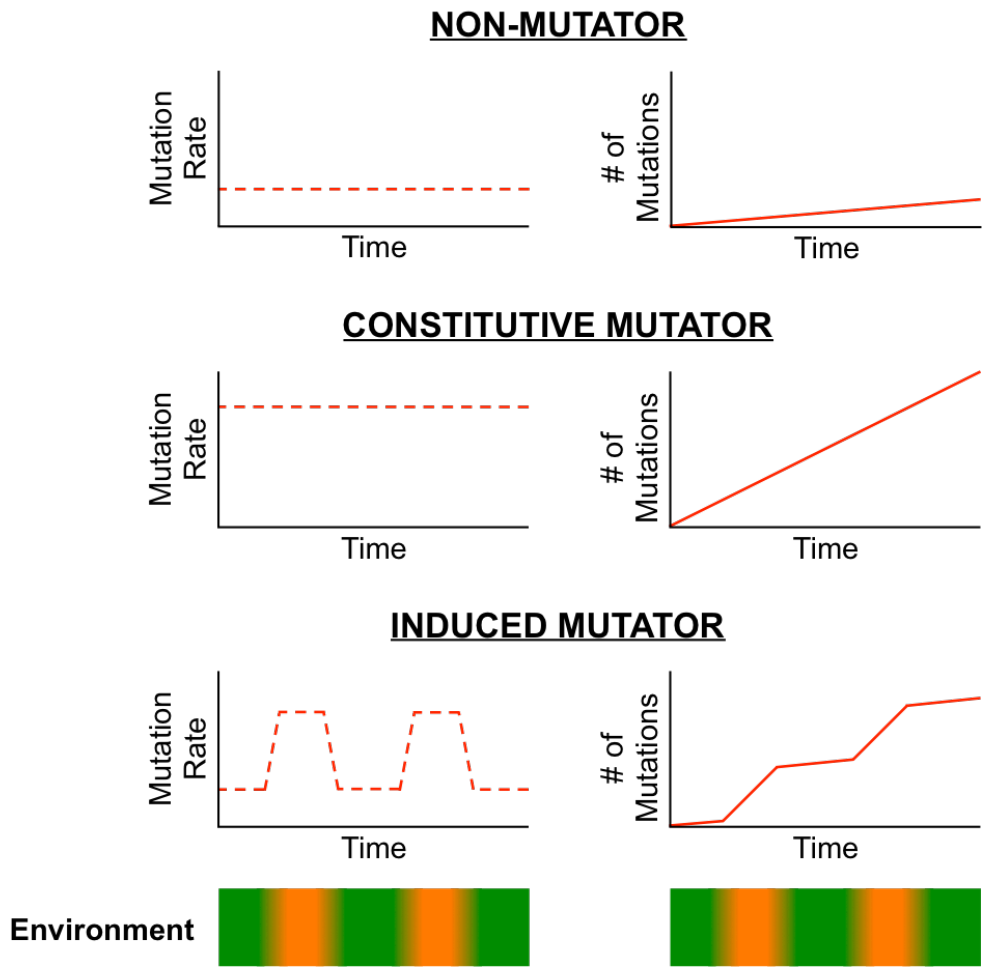

Figure 7. The effects of the environment on the mutation rate and number of mutations for non-mutators, constitutive mutators, and induced mutators.
The mutation rate over time for each phenotype is shown on the left (dashed lines) and the accumulation of mutations over time on the right (solid lines). The colored bars at the bottom represent the environment with green signifying a favorable environment and orange an unfavorable one. In summary, non-mutators have a constant low mutation rate, constitutive mutators have a constant high mutation rate, and induced mutators switch between a low and high mutation rate depending on the environment.

1.2.2 Constitutive mutagenesis in cancer

There have been multiple reports of how alterations to DNA replication and repair processes can contribute to tumor initiation and progression via constitutively increased mutation rates. These alterations can either cause a defect in the repair/tolerance of mutations (ex: loss of MMR or loss of polη) or increase the amount of error-prone DNA

replication that occurs (ex: proofreading domain mutations or overexpression of TLS polymerases). These examples are summarized below.

Loss of MMR and Lynch syndrome-associated colorectal adenomas

MMR plays a key role in maintaining a low mutation rate via the repair of mismatched bases and IDLs. Accordingly, defects in all seven MutL and MutS homologs involved in MMR (MLH1, MLH3, PMS1, PMS2, MSH2, MSH3, and MSH6) have been shown to occur in patients with Lynch syndrome, which predisposes them to a wide variety of tumors including colon and gynecologic cancers (*4*, *101*, *102*). Of these, mutations in MLH1 and MSH2 are the most common (*103–105*) as would be expected since they form a critical part of every MutL and MutS heterodimer, respectively. Furthermore, mutations in PMS2 and MSH6 are more common than mutations in PMS1, MLH3, and MSH3 (*106–109*). This also correlates with their importance to MMR as MLH1-PMS2 and MSH2-MSH6 are the major MMR complexes with the other heterodimers playing more minor roles. A defining characteristic of tumors resulting from defective MMR is microsatellite instability (MSI), which can result in frameshift deletions in cancer-related genes, such as TGFβR2, that contain coding microsatellite repeats (*110*). Defects in MMR are also observed in cases of sporadic cancer, typically via silencing of the *MLH1* gene by promoter hypermethylation, and these tumors also display MSI (*111*).

Loss of polη and xeroderma pigmentosum variant (XP-V)

Xeroderma pigmentosum (XP) is an autosomal recessive disorder in which patients are less able to repair DNA damage, especially in response to UV (*112*, *113*).

These patients exhibit sun sensitivity and a high risk for early development of skin cancer (Figure 8) as well as various internal cancers (*114*, *115*). The increased skin cancer risk is due to defective repair of UV damage while the internal cancers are believed to arise due to defective repair of damage caused by chemical carcinogens from the environment (*116*). The majority of XP patients were found to have deficits in NER, and cell fusion experiments revealed seven different complementation groups (XP-A to XP-G). The genes responsible for NER were eventually discovered and named after their respective complementation group (*117–120*). Cases with normal NER were termed xeroderma pigmentosum variant (XP-V) and later discovered to have defects in DNA synthesis after UV damage (*121*). Over twenty years later, the responsible gene was identified as polη (*2*), which is the major TLS polymerase responsible for bypass of UV lesions.

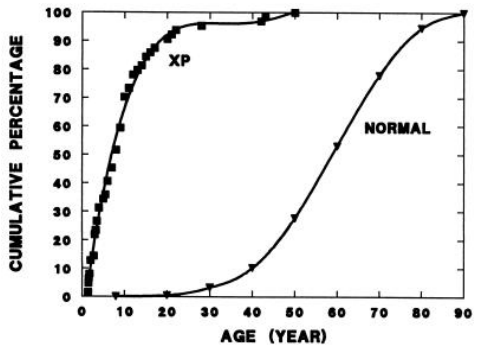

Figure 8. Age of onset in normal and XP skin cancer patients.
The cumulative percentage of patients with skin cancer is plotted versus the age of diagnosis for normal (29,757 samples) and XP (63 samples) populations. Figure adapted from (*122*). Copyright 1997 National Academy of Sciences.

Proofreading domain mutations in polδ/polε and colorectal cancer

Similar to loss of MMR proteins, mutations in the proofreading domain of polδ or polε have been observed in a number of patients with familial and sporadic colorectal

cancer, but instead of MSI, these tumors have a large number of base substitutions (*3*, *123*, *124*). Proofreading domain mutations have also been observed in patients with endometrial cancer (both polδ and polε) (*125*, *126*) and glioma (polε only) (*127*). Inactivation of the proofreading domain of a replicative polymerase by a germline or somatic mutation would dramatically increase its error rate as the polymerase would have to rely solely on polymerase selectivity to ensure the correct base was added. Interestingly, many patients with these mutations develop colorectal adenomas that rarely progress to malignant carcinoma, a phenomenon that is also observed in some Lynch syndrome patients (*3*). Endometrial cancers and gliomas with these mutations have been shown to have a better prognosis as well (*126*, *127*). This suggests that while a high mutation rate promotes the initiation of cancer, maintaining a high mutation rate can be inhibitory towards further progression of the disease. This matches the predicted long-term fitness of a constitutive mutator. In addition, some patients have concurrent proofreading domain mutations and loss of MMR (*128*), and this has been demonstrated *in vitro* to dramatically increase the mutation rate compared to either alone (*129*). Finally, it is interesting to note that this provides further support for the idea that different repair pathways are more important in specific cancers. Data with MMR loss and polδ/polε mutations demonstrates the importance of replication errors and coupled repair of base pair-level mutations to colorectal cancer in contrast to breast/ovarian cancer and melanoma in which DSBR (ex: BRCA1/2) and NER/UV TLS (ex: XP genes/polη) play an significant role in predisposition, respectively. This could be due to the sources of DNA damage each cell of origin is normally exposed to and/or the susceptibility of relevant oncogenes and tumor suppressors to specific mechanisms of mutagenesis (*3*, *110*, *116*, *130*).

Overexpression of TLS polymerases and cancer

polι and polκ have also been implicated in cancer; however, unlike polη, they are not mutated but rather overexpressed. Overexpression of polι has been implicated in bladder cancer, breast cancer, and glioma as well as esophageal cancer, where its expression levels positively correlate with lymph node metastasis/clinical stage (*131–135*). Overexpression of polκ, on the other hand, has been identified in both lung cancer and glioma (*132*, *136*). Furthermore, polκ overexpression in glioblastoma cells increases resistance to the DNA-damaging agent temozolomide (*137*). While the exact mechanism for how overexpression of TLS polymerases contributes to cancer is unknown, it is likely due to increased mutagenesis. Overexpression of polκ has been demonstrated to be mutagenic (*37*), and any of those mutations could contribute to cancer initiation and/or progression. In addition, polη has not been shown to be overexpressed in cancer (*132*), which is interesting since unlike polκ, polη does not cause increased mutagenesis when overexpressed (*36*).

1.2.3 Induced mutator: stress-induced mutagenesis (SIM) in *E. coli*

Decades worth of work have revealed that *E. coli* use a mechanism referred to as SIM to temporarily increase their mutation rate during periods of stress (*138–141*). This permits cells to accelerate adaptive evolution when maladapted to their environment but then once rare advantageous mutations are acquired, return to a low mutation rate. At its most basic level, SIM in bacteria occurs via to a switch from high fidelity to error-prone

DSBR, and this switch is controlled by the RpoS stress response. For SIM to occur, cells must meet the following requirements:

Requirement #1: creation of a DSB

An essential requirement for SIM is a DSB. TraI is a single-strand endonuclease that creates single-strand nicks at the F origin of transfer, and these nicks can become the required DSBs (*99*). A small percentage of the required DSBs also occur spontaneously (*142*). Furthermore, work by Ponder *et al* that substituted the double-strand endonuclease I-SceI for TraI revealed that by controlling where the DSBs occurred, they were able to determine where the highest number of mutations would arise (*140*).

Requirement #2: repair of the DSB via HR

Another requirement for SIM is repair of a DSB by HR. In bacteria, DSBs are recognized by a complex composed of RecB, RecC, and RecD (called RecBCD). The RecBCD complex processes the ends of the DSB using its helicase and exonuclease activity, and then RecA binds to the ssDNA. Similar to human RAD51, bacterial RecA forms a nucleoprotein filament on the DSB end that promotes strand invasion of a homologous sequence. It also facilitates the auto-proteolytic cleavage of the LexA transcriptional repressor, and this relieves LexA's repression on the expression of SOS genes (*99*, *143*, *144*). After strand invasion, DNA extension occurs (in either a high fidelity or error-prone manner), and then the RuvA-RuvB-RuvC (RuvABC) complex cleaves the resulting HJs. Inactivation of these genes results in a ≥10-fold decrease in stress-induced mutants (*99*, *145*, *146*).

Requirement #3: SOS response

The third requirement for SIM is activation of the SOS response, which is similar to the DDR in humans. LexA negatively regulates expression of the SOS genes by binding to a 20-bp consensus sequence called the SOS box in the operator region of those genes. The affinity of LexA for each particular site determines at what level the genes are expressed under repression conditions. As mentioned above, processing of DSB ends activates RecA, so RecA can then relieve LexA's repression by promoting its self-cleavage (*99*, *139*). This upregulates ~40 genes; although work has demonstrated that the sole purpose served by activation of the SOS response during SIM is transcriptional upregulation of the error-prone DNA polymerase DinB (*99*, *147*).

Requirement #4: RpoS response

Bacteria use sigma factors to initiate transcription of specific genes by enabling RNA polymerase to bind to their promoters. Environmental conditions control which sigma factor is used and thus which genes are expressed. RpoS (or σ^S) is the stationary phase/starvation sigma factor that is responsible for controlling the general stress response. It is nearly absent in rapidly growing cells, but entry into the stationary phase or exposure to stress, such as starvation, strongly induces its activity. While there is no direct homolog in humans, RpoS is hypothesized to be analogous to the stress sensor mTOR. Data has shown that up to 10% of *E. coli* genes are under direct or indirect control of RpoS; although the majority are induced by some stresses but not others (*148*). Like the SOS response, RpoS is able to upregulate expression of DinB, but it also is required to license

the use of DinB in error-prone HR (*140*). The exact mechanism by which this occurs is unknown but could potentially involve RpoS-controlled expression of factor(s) that permit DinB use (*99*, *149*, *150*).

Requirement #5: DinB

Pol III is responsible for high fidelity HR, but in response to stress, the majority of error-prone HR is performed by the Y family DNA polymerase DinB, the closest bacterial ortholog of human polκ, with Pol II and Pol V shown to be responsible for the rest (*141*, *151*, *152*). Like the human Y family polymerases, DinB normally catalyzes TLS in a relatively error-free manner but is highly mutagenic when replicating on undamaged DNA. DinB is transcriptionally upregulated ~10-fold by the SOS response and ~2-fold by the RpoS response, and it is also licensed to replicate on undamaged DNA via an unknown mechanism mediated by RpoS (*99*, *153*, *154*).

Overview of the mechanism

As stated above, the major requirements for bacterial SIM are a DSB, repair by HR, activation of the SOS response, activation of the RpoS general stress response, and upregulation/activation of the error-prone DNA polymerase DinB. These requirements come together via the following mechanism. Under optimal growth conditions, a DSB would activate the SOS response but not RpoS, leading to high fidelity HR using Pol III. However, DSBs that occur during stressful conditions would activate the SOS response while the stress would activate RpoS. Together the SOS and RpoS responses would increase expression of DinB, and then RpoS would also license it to perform error-prone

HR, thereby increasing the mutation rate of the cell. Once the stressful condition is resolved, HR would return to its high fidelity mechanism (Figure 9) (*99*, *139–141*, *147*, *149*, *150*, *153*).

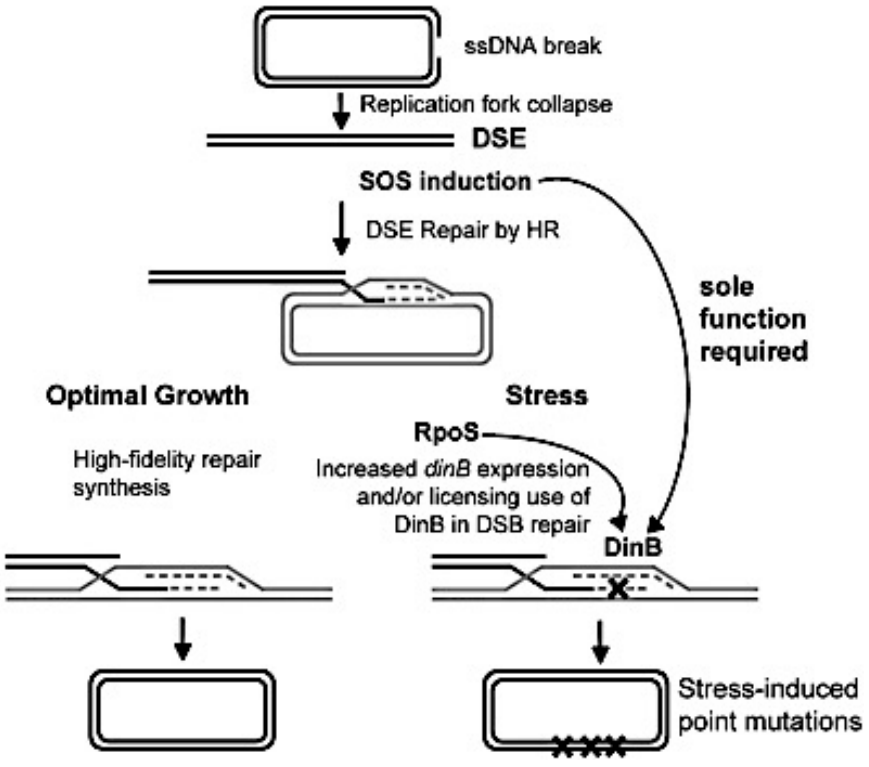

Figure 9. Mechanism of bacterial SIM.
Summary of the mechanism by which bacteria can temporarily increase their mutation rates in response to stress. Parallel lines represent dsDNA, dashed lines indicate newly synthesized DNA strands, and X's mark mutations. See text for more details. Figure adapted from (*147*).

Role of MMR in SIM

In addition to activating the error-prone DNA polymerase DinB, stress has also been shown to limit MMR, which allows the mutations generated by DinB to be inherited. During stationary phase and starvation, the levels of the MMR proteins MutS and MutH decline with MutS becoming barely detectable. This decrease is regulated by RpoS (*155*).

On the other hand, MutL levels remain constant in both stationary phase and carbon-starved cells compared to exponentially growing ones. Despite this, it appears that MutL levels are the actual limiting factor for MMR during conditions of stress since overexpression of MutL, but not MutS, reduces the number of stress-induced mutations (*156*, *157*). It is therefore proposed that the high numbers of mutations produced by DinB-mediated DSBR are able to saturate the MMR machinery (and specifically MutL) (*99*).

1.2.4 Human parallels to the pathways of bacterial SIM

Parallel pathways exist in humans for all the major pathways that function in bacterial SIM: HR, SOS response/DDR, RpoS response/PI3K-mTOR pathway, and MMR. The roles each pathway plays in SIM, the bacterial proteins responsible for each role, and the equivalent protein(s) in the human pathway are summarized in Table 3, and further details can be found in the following sections:

- HR: Section 1.2.3 (bacteria), Section 1.1.4 (human)
- SOS response: Section 1.2.3 (bacteria)
- DDR: Section 1.1.4 (human)
- RpoS response; Section 1.2.3 (bacteria)
- PI3K-mTOR pathway: Section 1.3.4 (human)
- MMR: Section 1.2.3 (bacteria), Section 1.1.3 (human)

Table 3. Proteins/pathways involved in bacterial SIM and their human equivalents.

Bacterial pathway	Function during SIM (responsible protein/complex)	Human equivalent(s)	Reference(s)
HR	Recognizes DSB ends and resects them to produce 3'-overhangs *(RecBCD complex)*	MRN complex (recognition) + Exo1/Dna2 (resection)	(*78*, *79*, *149*, *154*, *155*)
	Promotes strand invasion by the 3'-overhang into a homologous sequence *(RecA)*	RAD51	
	Error-prone DNA extension to form HJs *(DinB)*	polκ (and other Y-family polymerases)	
	High fidelity DNA extension to form HJs *(Pol III)*	polδ/polε	
	Cleaves HJs *(RuvABC complex)*	Endonuclease	
SOS response	Initiates activation of DSBR by HR *(RecA)*	MRN complex	(*61*, *143*, *156*)
	Regulates the expression/activity of many downstream targets (especially DinB) that promote DSBR by HR (*LexA)*	ATM (as part of the DDR)	
RpoS response	Senses and then responds to starvation (and other stresses) to promote expression and licensing of DinB for HR *(RpoS)*	mTOR (as part of the PI3K-mTOR signaling pathway)	(*157–160*)
MMR	Recognizes mismatches and IDLs *(MutS)*	MutSα and MutSβ complexes	(*40*, *161*)
	Mediates protein-protein interactions during recognition, discrimination, and strand removal *(MutL)*	MutLα complex (and to a lesser extent, MutLβ and MutLγ complexes)	
	Discriminates between DNA strands and creates a nick in the nascent strand *(MutH)*		

1.3 Melanoma

1.3.1 Overview of the disease

Melanoma is a type of skin cancer arising from melanocytes, which are neural crest-derived cells that produce pigment in the skin (*166*). The disease is characterized by striking heterogeneity (*167*) and goes through radial and then vertical growth phases before eventually metastasizing (*168*). Metastatic melanoma is particularly deadly with a 3-year survival rate of 58% even when treated with combination immunotherapies (*169*).

Although melanoma risk has been linked to UV exposure (*2*, *170*), it is now understood that cutaneous melanomas fall into two major categories: chronically sun damaged (CSD) and non-CSD. CSD melanomas arise on skin from the head and neck (regions with a higher degree of cumulative exposure to UV) of older individuals (>55 years of age), have a high mutational burden, and are associated with $BRAF^{non\text{-}V600E}$, NRAS, NF1, and KIT mutations. Non-CSD melanomas, on the other hand, affect intermittently sun-exposed areas (ex: trunk and proximal extremities) of younger individuals (<55 years of age), have a moderate mutational burden, and predominantly have a $BRAF^{V600E}$ mutation (*171*). As demonstrated by the most commonly mutated genes, the MAPK pathway is central to melanoma, and activation of this pathway plays a critical role in the proliferation and survival of melanoma cells (*172*, *173*).

1.3.2 MAPK pathway

Overview of the pathway

Mitogen-activated protein kinases (MAPKs) are serinine-threonine kinases that can phosphorylate themselves or their substrates, which are often other MAPKs. They are

organized into cascades consisting of MAPKs, MAP2Ks (MAPK kinases), and MAP3Ks (MAP2K kinases). MAPKs and MAP2Ks are activated by a simple phosphorylation-dependent mechanism while MAP3Ks typically require multiple steps, including relief of autoinhibition, dimerization, and transphosphorylation. Once active, the MAP3K phosphorylates the MAP2K, which in turn phosphorylates the MAPK. The MAPK then phosphorylates multiple substrates to regulate important cellular processes such as proliferation, stress responses, and apoptosis. Negative regulation of these cascades is performed by phosphatases that remove the activating phosphates from the MAPK proteins and their substrates (*174*).

Human utilize four canonical MAPK signaling cascades, which are classified by the last MAPK family member in each cascade: 1) ERK1/2, 2) JNK1/2/3, 3) p38-MAPK, and 4) ERK5 (Figure 10). Each cascade typically responds to a specific type of signal (i.e. growth factors, stress, and/or pro-inflammatory signals), but crosstalk between the MAPK cascades and with other signaling pathways does occur. Typically, this crosstalk is restricted to the upper tier proteins while the lower tiers are used to provide specificity (*174*).

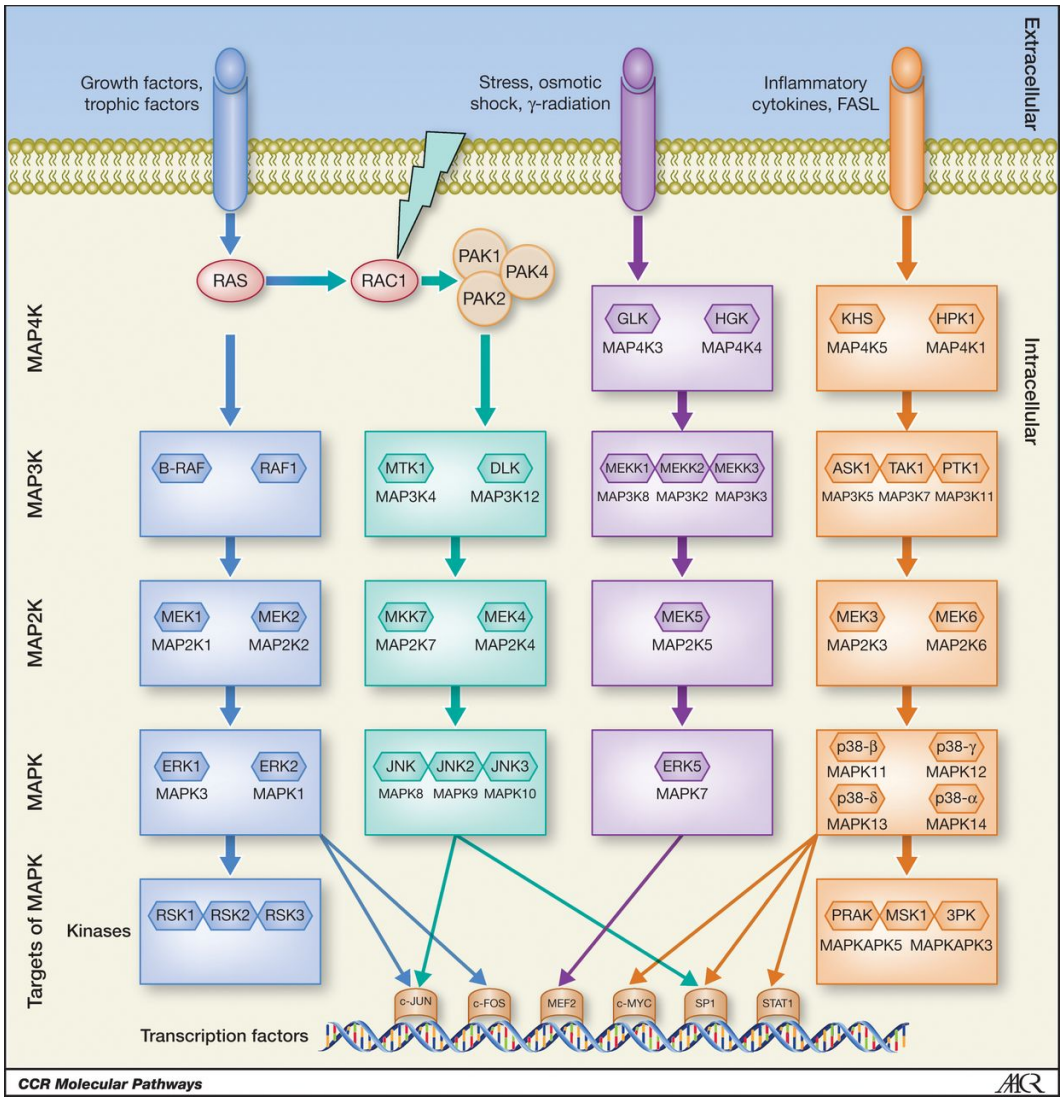

Figure 10. Overview of the 4 canonical MAPK signaling pathways.
The MAPK pathways function to transmit an external signal through the cell to effector proteins that can alter cellular functions like proliferation and survival. See text for further details. Figure adapted from (*174*).

The ERK1/2 signaling cascade is initiated by ligand-induced dimerization of receptor tyrosine kinases (RTKs) like EGFR, as this promotes their activation and subsequent autophosphorylation. These phosphorylated residues serve as binding sites for proteins including Grb2. Grb2 can then recruit Sos, which is a guanine nucleotide exchange factor (GEF) for Ras. Once at the plasma membrane, Sos can interact with Ras

and stimulate the exchange of guanosine diphosphate (GDP) for guanosine triphosphate (GTP). This exchange activates Ras and allows it to bind to and activate the MAP3K BRAF (or sometimes RAF-1, which is also known as CRAF). Activated BRAF can then phosphorylate the MAP2Ks MEK1 and MEK2. The only targets of MEK1/2 are ERK1 and ERK2, and activated ERK1/2 phosphorylates various substrates, including the transcription factors FOS, p53, and Elk1, thereby affecting cellular processes such as proliferation and survival. For example, activation of ERK1/2 has been demonstrated to be essential in efficient progression from G1-to S-phase of the cell cycle (*174*, *175*).

Stress stimuli (ex: UV, DNA damage, and inflammation) can directly activate the G-protein RAC1 to initiate the JNK1/2/3 signaling cascade. Activation of RAC1 promotes its interaction with members of the PAK family, which are MAP4Ks (MAP3K kinases). This enables PAK1/2/4 to phosphorylate and activate MAP3Ks, such as MAP3K4 and MAP3K12. Twelve other MAP3Ks have also been linked to the JNK1/2/3 cascade. The activated MAP3Ks phosphorylate MKK4 (MAP2K4) and MKK7 (MAP2K7), which in turn phosphorylate JNK1, JNK2, and JNK3. Substrates of the JNK proteins include the transcription factors JUN, JUND, and p53. Similar to the ERK1/2 pathway, the JNK1/2/3 cascade plays a important in regulating cell proliferation (*174*, *175*).

In the p38-MAPK signaling cascade, the activating signal can come in the form of inflammatory cytokines and/or environmental stress. The numerous MAP3Ks that function in this pathway are tissue- and stimulus-specific, and RAC1, G-protein coupled receptors (GPCRs), and/or MAP4Ks have been implicated in their activation. The MAP2Ks in this cascade are MEK3 and MEK6, and they are both highly specific for the three p38 MAPKs (p38-α, p38-β, p38-γ, and p38-δ), which are tissue-specific and have

different target substrates, including the transcription factors p53, STAT1, and NF- κB as well as cytoskeletal proteins and other kinases. The p38-MAPK cascade has been implicated in cell cycle checkpoint control in certain cell types and has also been shown to increase angiogenesis in response to hypoxia (*174*, *175*).

Finally, the ERK5 signaling cascade is activated by growth factors, cellular stress, and inflammatory cytokines. The major MAP3Ks are MAP3K2 and MAP3K3, which specifically phosphorylate MEK5. MEK5 is the only protein able to activate ERK5, and ERK5's substrates can ultimately affect angiogenesis, apoptosis, cell differentiation, and proliferation (*174*, *175*).

BRAF^{V600E} mutations and melanoma

Mutations leading to constitutive activation of the MAPK pathway are extremely common in melanoma, especially in Ras and BRAF (*176*, *177*). About 50–70% of melanoma cell lines and tumors have activating mutations in BRAF, and of those, over 90% consist of a substitution of valine to glutamic acid at amino acid 600 (BRAF^{V660E}) (*178–180*). Interestingly, the missense mutation responsible for this substitution is a thymine-to-adenine transversion, which is not a classic UV-signature mutation (*171*).

Targeted inhibitors in melanoma

Initial attempts to treat cancer utilized chemotherapies, which target rapidly dividing cells and thus hit cancer cells but also various wild-type cell populations in the patient, so toxic side effects and narrow therapeutic windows have greatly limited their efficacy. As a result, researchers turned their attention to the development of targeted

inhibitors, which are designed to selectively target the driver mutation/pathway of a particular cancer. In $BRAF^{V600E}$-mutant melanoma, that first led to the creation of inhibitors against MEK. MEK1 and MEK2 are the major (if not only) downstream effectors of $BRAF^{V600E}$-mediated transformation, and studies with cell lines *in vitro* and xenografts *in vivo* revealed that mutant BRAF was associated with enhanced sensitivity to MEK inhibitors (*181*). Use of MEK inhibitors in clinical trials resulted in a number of partial responses (and even some complete responses), but like with chemotherapy, there were also a number of dose-limiting side effects, including rash, diarrhea, and visual disturbances (*182*, *183*). These likely resulted from inhibition of MAPK signaling in non-cancerous cells.

Another promising advance in treating $BRAF^{V600E}$-mutant melanoma came from the development of an inhibitor specific for mutant BRAF called vemurafenib (or PLX4032) (*184*). This drug has been shown to have the same inhibitory effects on $BRAF^{V600E}$-mutant cells *in vitro* as MEK inhibitors, but it does not inhibit MAPK signaling in cells with wild-type BRAF, suggesting a better therapeutic index could be achieved (*185*). Clinical trials with PLX4032 revealed complete or partial tumor regression in the majority of patients with $BRAF^{V600E}$-mutant melanoma without most of the side effects seen with MEK inhibitors (*186–188*).

However, treatment with either inhibitor alone typically results in the development of resistance. Combination therapies of MEK and BRAF inhibitors together have been shown to delay the emergence of resistance (*189*). Furthermore, recent advances in immunotherapy, which is designed to stimulate the immune system to kill the cancer cells, have been shown to be particularly effective in treating melanoma (*169*, *190*).

BRAF inhibition and endoplasmic reticulum (ER) stress

BRAF inhibitors such as PLX4032 can induce cell stress prior to overt death of the melanoma cell, which can occur via the ER stress pathway (*191*) and is associated with stress-induced senescence (*192*). This is because when activated, the ERK1/2 signaling cascade promotes proliferation and prevents apoptosis, and this is lost when $BRAF^{V600E}$ is inhibited (*175*). Treatment with PLX4032 causes ER stress via depletion of ER calcium levels, which leads to an accumulation of unfolded/misfolded proteins in the ER and activation of the unfolded protein response (UPR), and suppression of the ER chaperone GRP78, which further intensifies the response (*191*).

Other inducers of ER stress include glucose starvation and several drugs (ex: tunicamycin, thapsigargin, and brefeldin A), which all also activate the UPR. Three different sensors can trigger the UPR: ATF6, PERK, and IRE1, which are all normally inhibited by GRP78. Binding of unfolded/misfolded proteins to GRP78 releases the sensors, enabling them to activate key downstream UPR proteins such as ATF4, CHOP, and XBP1. Depending on the length of the signal, this can then upregulate expression of UPR genes, reduce global protein synthesis, and eventually cause apoptosis (Figure 11) (*193*). The decrease in protein synthesis occurs at least in part via inhibition of Akt/mTOR (*194*, *195*).

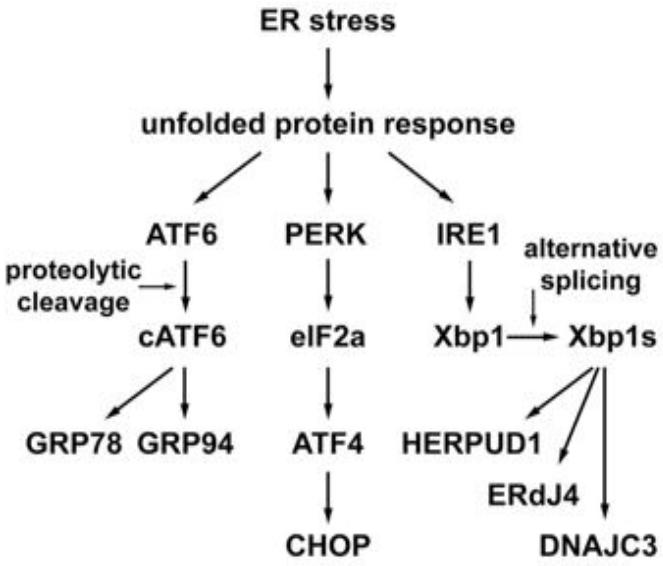

Figure 11. Overview of ER stress/the UPR.
BRAF inhibition, glucose starvation, and several other stressors can trigger ER stress, thereby activating UPR master regulators. Signaling through these proteins can upregulate expression of UPR and apoptotic genes and decrease translation. Figure adapted from (*196*). Copyright by Karin Eigner *et al* (Scientific Reports) / CC BY 4.0.

1.3.3 Drug resistance

Overview of drug resistance

Drug resistance presents a major challenge faced in the "War on Cancer" as extremely effective drugs can be rendered effectively useless by a single mutation or change in gene expression in the cancer cell. This is true for both chemotherapies and targeted inhibitors. These alterations can affect the drug target directly, another member of the same pathway, or a member of an alternative pathway. Other resistance mechanisms include increased drug efflux, increased activation of DNA damage repair, epigenetic changes, and effects from the tumor microenvironment (*197*).

Pre-existing vs. acquired drug resistance mutations

Mutations that confer drug resistance can either be pre-existing (i.e. present at the start of the treatment) or acquired (i.e. gained during the course of the treatment) (Figure 12). Pre-existing mutations would be generated as part of normal tumor heterogeneity, likely making up only a proportion of the entire tumor, but under the strong selective forces faced by the tumor upon exposure to the drug, cells with the pre-existing resistance mutation would be able to survive and proliferate while those without it would die (*198*). Alternatively, a tumor without any pre-existing resistance mutations could be exposed to the drug. In that case, additional genetic heterogeneity would need to be generated during treatment with the drug. Initially, most of the cells would die except for a population of "persister" cells. Persister cells utilize reversible mechanisms of drug tolerance to temporarily survive a stressful environment until an acquired resistance mutation can emerge. Similar to a pre-existing resistance mutation, any acquired resistance mutation can result in increased survival and expansion of the population harboring it (*198*, *199*). Persister cells have been shown to occur in both bacterial populations and human tumors and to be activated via stress responses (*200–204*). Overall, the major difference between the two mechanisms is the timing at which resistance becomes detectable (i.e. the number of resistant cells surpasses a threshold of detection). Tumors with pre-existing resistance mutations would be expected to reach that threshold much faster than tumors that have to acquire a resistance mutation. Furthermore, the greater the proportion of the original tumor made up by cells with the pre-existing resistance mutation, the less time that should be required before the resistant tumor is detectable (*205*).

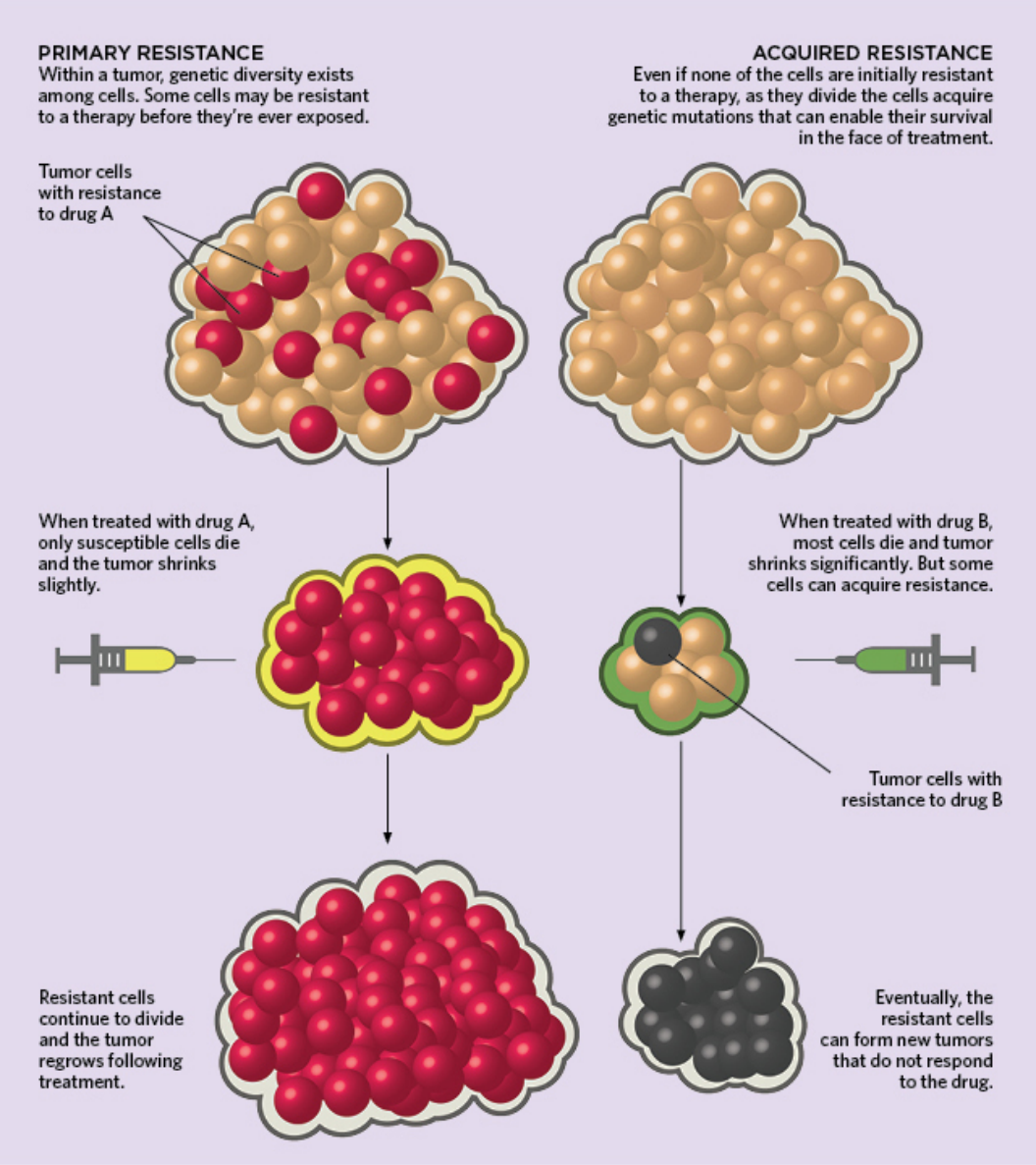

Figure 12. Pre-existing (primary) vs. acquired resistance mutations.
LEFT: This tumor already contains cells with resistance to drug A (indicated by red cells) prior to treatment with that drug. Treatment with drug A causes the susceptible cells to die, leaving behind the resistant cells to reform the tumor. RIGHT: This tumor does not have any pre-existing resistance mutations, so treatment with drug B causes the tumor to shrink. However, some cells are able to persist long enough to acquire a resistance mutation (indicated by black cells), and these resistant cells will reform the tumor. Figure adapted from (*206*). Copyright by Nirja Desai.

While there are many examples of pre-existing resistance mutations (*207–212*), it is harder to obtain definitive proof of acquired resistance mutations. For example, the

major method to demonstrate a mutation was pre-existing is to show it was present in biopsied cells collected prior to treatment as well as those collected after resistance emerges. On the other hand, if a mutation is not present in the pretreatment sample, it could be either 1) an acquired mutation or 2) pre-existing but present in the population at too low of a frequency for detection by that method (*213*). That said, there are a number of human studies where the responsible resistance mutations could not be detected in pretreatment samples (*214–219*) as well as *in vitro* studies in chronic myeloid leukemia (CML), non-small cell lung cancer, and colorectal cancer cell lines that proved the acquisition of resistance mutations in cells experiencing drug stress is feasible (*203*, *204*, *220*, *221*). Finally, a computational model of the development of resistance to imatinib in CML demonstrated that the probability of having a pre-existing resistance mutation increases with disease progression due to the resulting increased number of cells (*205*), suggesting that the time of treatment influences whether pre-existing or acquired resistance mutations are more likely to be important.

Although pre-existing and acquired resistance mutations can have the same final consequence (i.e. relapse of the disease), the distinction is important due to the different implications for disease treatment. Pre-existing mutations will be present prior to starting treatment, so stronger inhibitors, combination therapies, and/or innovative dosing schedules are required to eliminate those cells. Acquired mutations, alternatively, will not exist at the start of treatment, so a preventative strategy that blocks resistance mutations from developing might be more effective (*198*).

Examples of resistance to PLX4032

A number of mechanisms of resistance against PLX4032 in melanoma have been identified using different methods. Resistance can result from a cell-intrinsic genetic (ex: activating mutations in MEK) or epigenetic (ex: overexpression of Cot) alteration or even a cell-extrinsic effect by the microenvironment (ex: secretion of HGF by fibroblasts) (Table 4). Furthermore, the majority of these mechanisms bypass $BRAF^{V600E}$ entirely using either other MAP3Ks or another pro-survival signaling pathway. Interestingly, unlike with many other targeted inhibitors, secondary mutations in $BRAF^{V600E}$ that would confer resistance have not be observed in patient tumors, which further supports the bias towards $BRAF^{V600E}$ bypass (*222*, *223*).

Table 4. Examples of resistance to PLX4032.

Example	Mechanism of resistance	References
Overexpression of $BRAF^{V600E}$	Reactivation of $BRAF^{V600E}$	(*223*)
Alternative splicing of $BRAF^{V600E}$		(*224*)
Activating Ras mutations	Activates Ras, which signals to MEK via CRAF	(*222*)
Loss of NF1		(*225*)
Overexpression of Cot	Alternative MAP3Ks that can bypass BRAF to activate MEK	(*226*)
Overexpression of CRAF		(*226*)
Activating MEK1/2 mutations	BRAF-independent activation of MEK	(*219*, *227*, *228*)
Amplification of MITF	Restores an oncogenic transcriptional output of the MAPK pathway	(*212*)
Upregulation of PDGFRβ	Activates the PI3K-mTOR pathway to promote growth/survival	(*222*)
Upregulation of IGF1R		(*229*)
Loss of PTEN		(*230*)
Secretion of HGF by fibroblasts	Activates both the ERK1/2 (via CRAF) and PI3K-mTOR pathways	(*231*)
Matrix-derived integrin β1 and FAK signaling	Promotes BRAF-independent ERK activation and cell survival	(*232*)

1.3.4 Interaction between the MAPK and PI3K-mTOR pathways

Overview of mTOR and the PI3K-mTOR pathway

mTOR (mammalian/mechanistic target of rapamycin) is the mammalian ortholog of yeast TOR, which was identified as the target of rapamycin, a drug with broad anti-proliferative effects (*233*, *234*). It is a member of the phosphoinositide 3-kinase (PI3K)-related kinase family and functions as a serine/threonine protein kinase. It is the catalytic subunit of two different complexes: mTOR complexes 1 and 2 (mTORC1 and mTORC2), which are made of six and seven components, respectively. Due to differences in subunits, these complexes differ in their sensitivity to rapamycin (mTORC1 has high sensitivity while mTORC2 is insensitive), upstream inputs, and downstream outputs (Figure 13). Overall, because mTOR responds to diverse cues and impacts most major cellular functions, it plays a vital role in regulating a wide number of cellular behaviors (*235*).

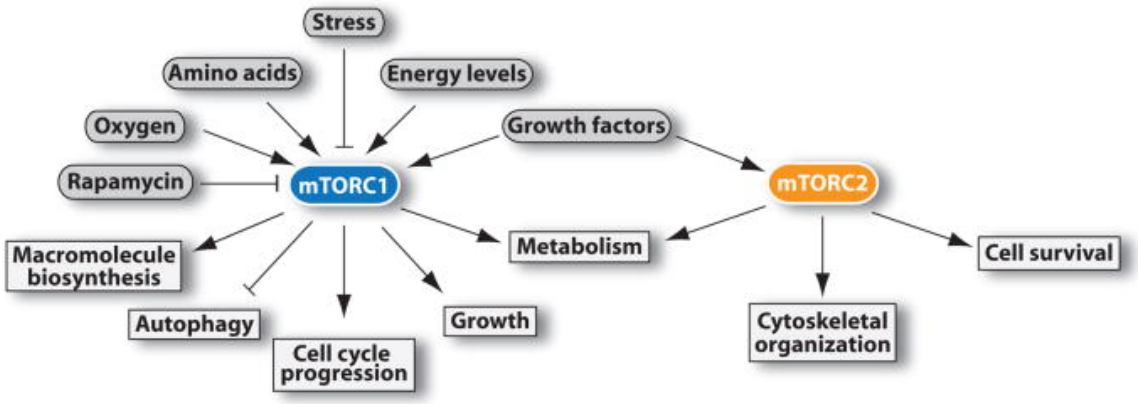

Figure 13. Overview of mTORC1 and mTORC2.
mTOR forms the catalytic core of two distinct complexes called mTORC1 and mTORC2, which respond to different stimuli and affect different downstream pathway (although there is some overlap). Both complexes share the following components: mLST8, DEPTOR and the Tti1/Tel2complex in addition to mTOR. The unique components of mTORC1 are raptor and PRAS40 while only mTORC2 contains rictor, mSin1, and protor1/2. Figure adapted from (*235*).

mTORC1 is activated by multiple intracellular and extracellular cues (oxygen, amino acids, energy levels, and growth factors) and inhibited by stress. When activated, it promotes cell cycle progression, growth, and many different metabolic pathways while inhibiting autophagy (*235*). A key upstream regulator of mTORC1 is the TSC1/2 heterodimer, which functions as a GTPase-activating protein (GAP) for the GTPase Rheb (*236*, *237*). Since GTP-bound Rheb stimulates mTOR's kinase ability, TSC1/2 inhibits mTORC1 by stimulating the catalysis of active Rheb-GTP to inactive Rheb-GDP. Therefore, in order to activate mTORC1, the majority of its inputs must first inactivate TSC1/2. Stresses, on the other hand, function to increase the GAP activity of TSC1/2 (*235*). One growth factor that activates mTORC1 is IGF1. Binding of IGF1 to its RTK (called IGF1R) activates PI3K, which can then phosphorylate phosphatidylinositol (4,5) bisphosphate (PIP_2) into phosphatidylinositol (3,4,5) trisphosphate (PIP_3). PIP_3 is able to recruit PDK1/2, which can then activate protein kinase B (PKB). PI3K is antagonized by the activity of PTEN, which catalyzes the conversion from PIP_3 to PIP_2 (*235*, *238*). Active PKB, which is also known as Akt, is able to phosphorylate the TSC1/2 complex, thereby inactivating it and consequently activating mTORC1 (*239*, *240*). Akt also phosphorylates the inhibitory mTORC1 component PRAS40, causing it to dissociate from the rest of the complex (*235*, *241*, *242*).

Activated mTORC1 can phosphorylate a number of downstream substrates, including the regulators of translation 4E-BP1 and S6 kinase (S6K). Phosphorylation of 4E-BP1 is inhibitory and contributes to the initiation of cap-dependent translation while phosphorylation of S6K is activating. S6K can then phosphorylate a number of different downstream targets, including the ribosomal protein S6 (*243–246*). Phosphorylation of

other mTORC1 substrates allows it to have far-reaching effects on most pathways in the cell (Figure 14) (*235*).

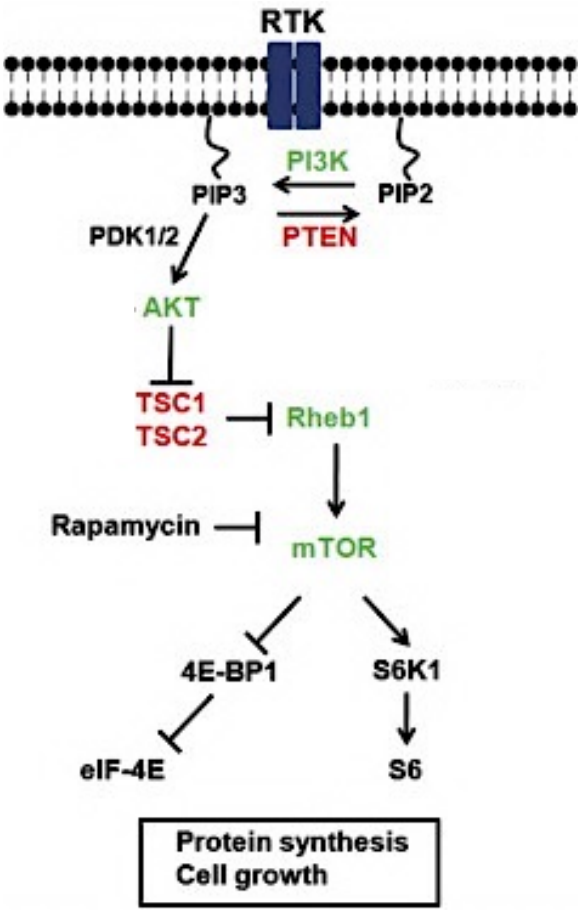

Figure 14. Overview of the PI3K-mTOR pathway.
Growth factors can lead to the activation of mTORC1 via the PI3K-mTOR pathway, and this can have effects on cellular processes, such as protein synthesis and growth. See text for more details. Figure adapted from (*247*).

The mTORC2 complex, on the other hand, mostly responds to growth factor signaling and regulates metabolism, cytoskeletal organization, and cell survival (*235*, *248*, *249*). It does so by phosphorylating several members of the AGC subfamily of kinases, which includes Akt. mTORC2 phosphorylates Akt at a site required for its maximal

activation. Defects in phosphorylation at this site prevent the phosphorylation of some but not all Akt targets; for example, phosphorylation of TSC2 is not affected (*250*, *251*). Other effectors of mTORC2 include Rho GTPases and paxilin, which allow it to affect the actin cytoskeleton (*235*).

Interaction between the ERK1/2 signaling cascade and the PI3K-mTOR pathway

The ERK1/2 signaling cascade and the PI3K-mTOR pathway are the major regulators of cell survival, proliferation, differentiation, and metabolism (*252*). As a result, there is much crosstalk (i.e. regulation of an upstream component by another pathway) and pathway integration (i.e. two pathways directly acting on the same downstream protein or complex) between the two. Crosstalk between the ERK1/2 signaling cascade and the PI3K-mTOR pathway can be negative (cross-inhibition) or positive (cross-activation) (Figure 15). The major mechanism through which the ERK1/2 signaling cascade inhibits the PI3K-mTOR pathway is via phosphorylation of GAB by ERK1/2. This prevents the interaction between the activated RTK and PI3K, which is mediated by GAB, and therefore prevents further activation of the PI3K-mTOR pathway (*252*, *253*). Conversely, the major mechanism through which the PI3K-mTOR pathway inhibits the ERK1/2 signaling cascade is via phosphorylation of RAF by Akt. This phosphorylation occurs at inhibitory sites that are also recognized by 14-3-3 dimers, which sequesters auto-inhibited RAF away from both its activator Ras and its downstream targets MEK1/2 (*254*, *255*).

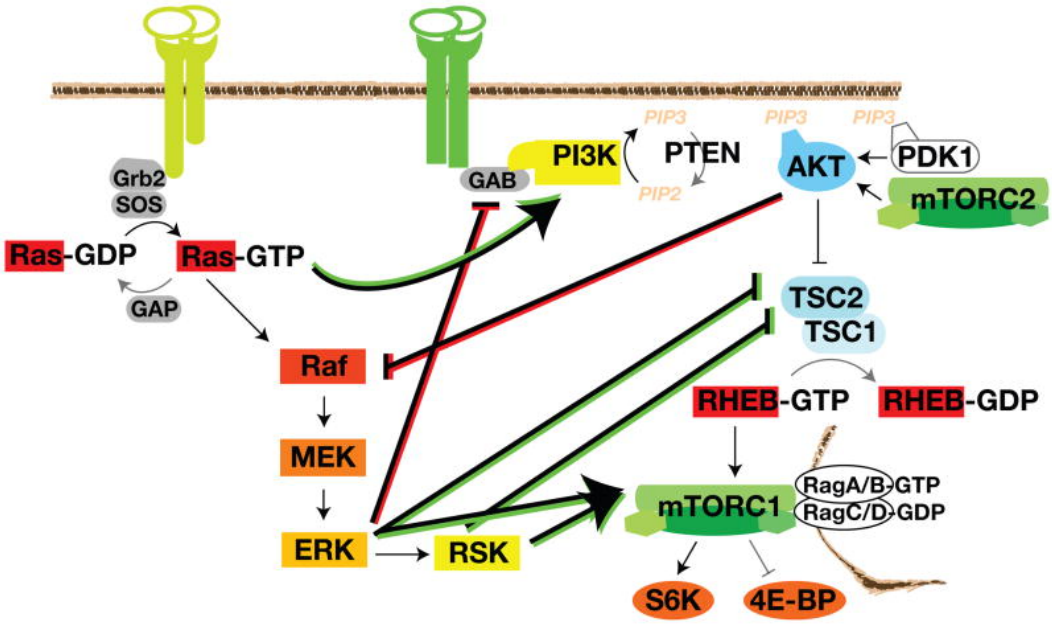

Figure 15. Crosstalk between the MAPK and PI3K-mTOR signaling pathways. Crosstalk between the ERK1/2 MAPK signaling cascade and the PI3K-mTOR pathway can take the form of either cross-inhibition (red lines) or cross-activation (green lines). Arrows are used to indicate activation while blunt-ended lines represent inhibition. See text for more details. Figure adapted from (*252*).

There are multiple mechanisms through which cross-activation occurs. For example, ERK and its downstream substrate RSK can increase mTORC1 activity in two different ways. First, they can phosphorylate TSC2. Similar to phosphorylation by Akt, this inhibits TSC2's GAP ability, thereby increasing the levels of Rheb-GTP, and Rheb-GTP can in turn activate mTORC1 (*256*). Additionally, ERK can directly phosphorylate the mTORC1 component raptor, which activates the complex (*257*). Another example of cross-activation is the activation of PI3K by Ras-GTP (*258*, *259*). Finally, many of the MAPK scaffolding proteins have also been shown to interact with components of the PI3K-mTOR pathway, and this colocalization could promote the above crosstalk (*252*).

The ERK1/2 signaling cascade and PI3K-mTOR pathways also share many downstream substrates, which allows integration of the two pathways to together control

cell survival, proliferation, differentiation, and metabolism. For example, forkhead box O (FOXO) family members, such as FOXO3A, function as transcription factors that activate quiescence and apoptotic gene expression programs. To prevent this, ERK and Akt both phosphorylate FOXO3A at different sites. Phosphorylation by ERK promotes ubiquitination and subsequent degradation of FOXO3A (*260*). Phosphorylation by Akt, on the other hand, induces the cytoplasmic sequestration of FOXO3A by 14-3-3 (*261*). Another example is both RSK (downstream of ERK) and S6K (downstream of mTORC1) can phosphorylate Mad1. Mad1 can function as a heterodimer with c-Myc that negatively regulates growth and survival gene expression programs. c-Myc can also function in another heterodimer with Max to positively regulate the same programs, so the balance between c-Myc-Mad1 complexes and c-Myc-Max complexes determines the cellular outcome. Phosphorylation of Mad1 by RSK or S6K promotes its degradation and pushes the balance towards the pro-growth/pro-survival c-Myc-Max complex (*262*).

1.3.5 Models of melanoma

Human melanoma cell lines

Multiple different human melanoma cells lines have been developed over the years, including A375 and SK-MEL28. Both have the $BRAF^{V600E}$ mutation. The A375 cell line was derived from the malignant melanoma of a 54-year-old female in the early 1970s as part of an attempt to establish cell lines from 200 tumors of different cancer types by cultivating them i*n vitro*. During this initial study, it was shown to continually propagate for at least one year, form colonies in normal monolayers and agar, and form a rapidly growing tumor that resembled a non-pigmented melanoma in anti-thymocyte

serum-treated mice. It was one of the first melanoma cell lines deposited into ATCC (*263*). The SK-MEL28 cell line was derived from the malignant melanoma of a 51-year-old man in 1975 at Memorial Sloan Kettering Cancer Center (*264*). It was later shown to produce tumors after subcutaneous injection into nude mice (*265*).

A transgenic zebrafish model of melanoma

A zebrafish model of melanoma was developed in 2005 in the lab of Leonard Zon (Figure 16). To create this model, a construct expressing mutant $BRAF^{V600E}$ under the melanocyte-specific promoter *mitfa* was injected into zebrafish embryos with a homozygous missense mutation (Met214Lys) in exon 7 of the *p53* gene ($p53^{-/-}$), and melanomas were observed in these fish with a latency of about 4-12 months (*266*). The resulting melanomas were shown to be similar to human melanomas at histological, functional, and genomic levels (*266–268*). Furthermore, expression of $BRAF^{V600E}$ in a p53 wild-type background resulted in benign nevi rather than tumors (*266*), which is similar to the observation that many moles in humans have $BRAF^{V600E}$, and a secondary hit is required for actual melanoma formation (*269*).

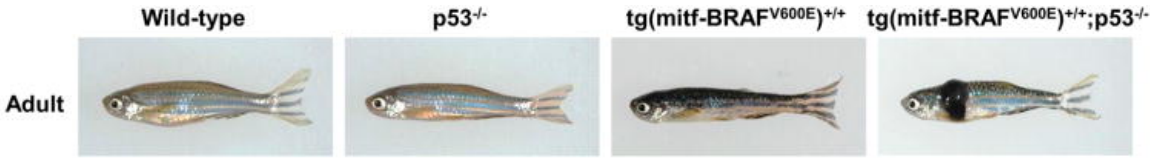

Figure 16. A transgenic zebrafish model of melanoma.
Expression of mutant $BRAF^{V600E}$ using the melanocyte-specific *mitfa* promoter causes the formation of nevi in p53 wild-type zebrafish and melanoma in p53 mutant zebrafish. Figure adapted from (*268*).

1.4 Regulation of subcellular localization

1.4.1 Background

Nuclear vs. cytoplasmic localization

Unlike bacteria, human cells have a nucleus. The presence of a nuclear envelope creates an additional level of regulation that can be used to determine which proteins can access the DNA and under what circumstances. While smaller molecules can diffuse directly through the nuclear membrane, most proteins (larger than ~40 kD) require the help of the nuclear import and export complexes (*270*). This section will first summarize what is known about the subcellular localization of the Y family polymerases before focusing on nuclear import and export more broadly.

Current knowledge regarding the localization of Y family DNA polymerases

The Y family polymerases are assumed to be localized exclusively in the nucleus (i.e. the site of DNA and thus of TLS and the DNA repair pathways). The nuclear localization is presumed to be diffuse under normal conditions and in foci colocalized with PCNA in response to DNA damage. Support for the nuclear localization of the Y family polymerases came from studies using the overexpression of enhanced GFP (eGFP)-polymerase fusion proteins to determine their localization in cells with or without DNA damage. Furthermore, these studies were also able to demonstrate that deletion of the predicted nuclear localization signal/nuclear import domain for polη, polι, and polκ resulted in a cytoplasmic localization of its eGFP-polymerase fusion protein (*271–275*). However, reports from the late 1950s/early 1960s hinted at a cytoplasmic localization of at least some DNA polymerases during at least some phases of the cell cycle. Unfortunately,

because of the limited technology available at that time, they were unable to determine which polymerase(s) they were detecting in the cytoplasm (*276–278*), but it does suggest that the localization of the Y family DNA polymerases might be more complex than originally assumed.

1.4.2 The nuclear pore complex (NPC)

The nucleus of a eukaryotic cell is enclosed by a nuclear envelope consisting of two membranes that separate the nucleoplasm (and associated DNA) from the surrounding cytoplasm. In order for transport to occur between the cytoplasm and the nucleus, holes in the nuclear envelope are required. NPCs form these channels in the nuclear envelope by fusing the inner and outer membranes. NPCs are composed of subcomplexes of nucleoporins (NUPs) that form the cytoplasmic, inner pore, and nuclear rings as well as cytoplasmic filaments and the nuclear basket (Figure 17). Most of the NUPs play structural roles, but NUPs within the central pore region contain phenylalanine- and glycine-rich repeats (FG-NUPs) that allow them to interact with the nuclear transport receptors (NTRs) and facilitate their passage (with or without cargo) through the NPCs. Cytoplasmic filaments function in the termination of export reactions and funneling of import cargo into NPCs. The function of the nuclear basket is still a matter of debate, but it is believed to exclude heterochromatin from the NPC entrance to prevent transport blockage. Overall, NPCs enable the nuclear import, export, and shuttling of RNAs and proteins to occur in a highly specific and regulated manner (*279*, *280*). There are no motors in the NPCs that power this movement between the nucleus and the cytoplasm; rather it occurs via facilitated diffusion that is directional due to Ran GTPase (*281*).

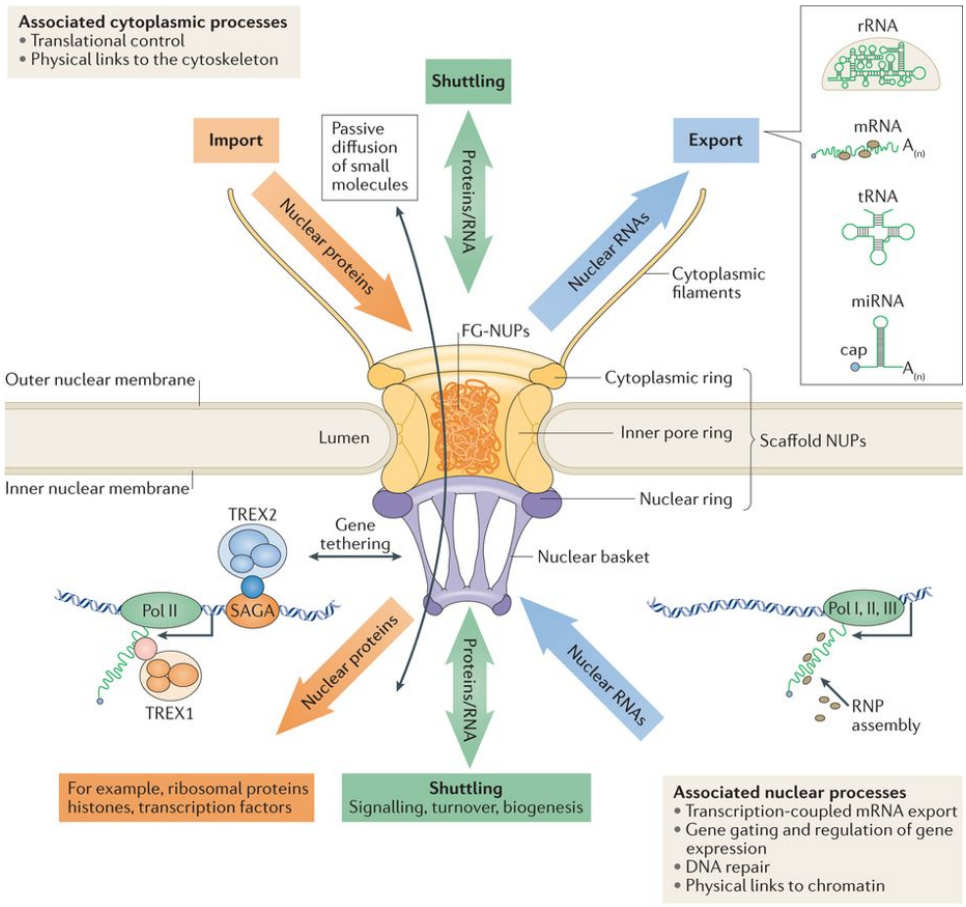

Figure 17. Molecular architecture and functions of nuclear pores.
Nuclear pores are holes in the nuclear envelope through which proteins and RNAs can enter and leave the nucleus. NPCs are made up of 3 rings (cytoplasmic, inner pore, and nuclear) as well as cytoplasmic filaments and the nuclear basket. FG-NUPs that line the central channel provide specificity to transport through the pore. Small molecules are able to diffuse freely in and out of the nucleus, but the export of RNAs, import of nuclear proteins, and bi-directional shuttling of proteins and RNAs are all mediated by NTRs. Figure adapted from (*279*).

1.4.3 The role of Ran in nuclear import and export

Ran is a member of the Ras superfamily of GTPases, meaning it cycles between GDP- and GTP-bound states. RanGEF catalyzes the replacement of GDP with GTP while RanGAP activates the GTPase activity of Ran to convert GTP into GDP. The major function of Ran in nuclear import and export is to provide directional information to

importins and exportins, respectively (*282*). Importins and exportins are members of the karyopherin family of NTRs, and both can form complexes with Ran-GTP. The major difference is that for importins the binding of Ran-GTP and the binding of cargo are mutually exclusive while for exportins the binding of cargo requires the binding of Ran-GTP. Therefore, importins bind cargo where Ran-GTP is low and release it where Ran-GTP is high while the reverse is true for exportins. This means that by keeping the levels of Ran-GTP high in the nucleus and low in the cytoplasm, cells can provide directionality to nuclear import and export. The mechanism through which this is achieved is by restricting RanGEF (which promotes Ran-GTP) to the nucleus and RanGAP (which promotes Ran-GDP) to the cytoplasm. NTF2 functions to return Ran-GDP to the nucleus after its creation in the cytoplasm (*281*).

1.4.4 Nuclear import

Importins and the nuclear localization signal (NLS)

Importins are the members of the karyopherin family that function solely in nuclear import. They do so by recognizing NLSs on cargo proteins and then mediating their transport through NPCs via interactions with FG-NUPs (*283*). Some importins require an adaptor while others do not. The major import NTR importin-β can function either alone or with the adaptor importin-α. Human cells have a large number of importins as well as non-related NTRs responsible for import, but only some have been implicated in nuclear import. Furthermore, much is still unresolved regarding selectivity for cargos, redundancy, and if distinct cargo can bind to multiple importins (*281*, *284*). Importazole is an inhibitor specific for importin-β that likely prevents its function by altering its

interaction with Ran-GTP as cells treated with importazole do not release their importin-β-bound cargo (*285*). NLSs were first discovered in the early 1980s as short amino acid sequences that were necessary and sufficient for nuclear import but not required for nuclear retention (*286*, *287*). NLSs can be classified based on their amino acid sequence (Table 5). Typically, classical NLSs require importin-α while non-classical NLSs can bind directly to importin-β, but there are exceptions to this rule (*284*). polη and polκ both have functional bipartite NLSs (*271*, *274*) while polι has a nuclear import domain but no clearly identifiable NLS (*272*).

Table 5. Examples of NLSs.

Class	Subclass	Sequence features	Example(s)
Classical	Monopartite	Short sequence containing a single cluster of basic amino acids that is often proceeded by a proline	SV40 large T antigen (*287*): P**KKKRK**V
			c-Myc (*288*): PAA**KR**V**K**LD
	Bipartite	Two interdependent clusters of basic amino acids separated by a flexible spacer	Nucleoplasmin (*289*): **KR**PAATKKAGQA**KKKK**
			Rpr4 (*290*): **KR**WKVDIGGKQHAVLM LGSVNLPGGIL**RRK**
Non-classical		Lack a contiguous stretch of basic amino acids	PLSCR1 (*291*): GKISKHWTGI
			Influenza virus NP (*292*): SQGTKRSYEQM

Overview of the nuclear import mechanism

The four major steps of nuclear import are 1) recognition of the NLS by the importin(s), 2) translocation of the complex into the nucleus via a NPC, 3) release of the cargo, and 4) importin recycling (Figure 18). More specifically, in the cytoplasm, a complex forms between the cargo, importin-α, and importin-β. This complex travels via

an NPC to the nucleus, where there are high levels of Ran-GTP. Ran-GTP binds to importin-β, causing release of the cargo (which is now officially imported) as well as importin-α. The importin-β/Ran-GTP complex returns to the cytoplasm where it encounters RanGAP, which mediates GTP hydrolysis to create Ran-GDP. Importin-β has a much weaker interaction with Ran-GDP than Ran-GTP, so it dissociates and is now ready to form a new import complex. Meanwhile, the export carrier CAS, which requires Ran-GTP for its function, binds importin-α. The complex of importin-α, CAS, and Ran-GTP leaves the nucleus for the cytoplasm where it also encounters RanGAP. GTP hydrolysis causes the complex to dissociate, releasing importin-α. CAS can return to the nucleus on its own (*281*, *293*).

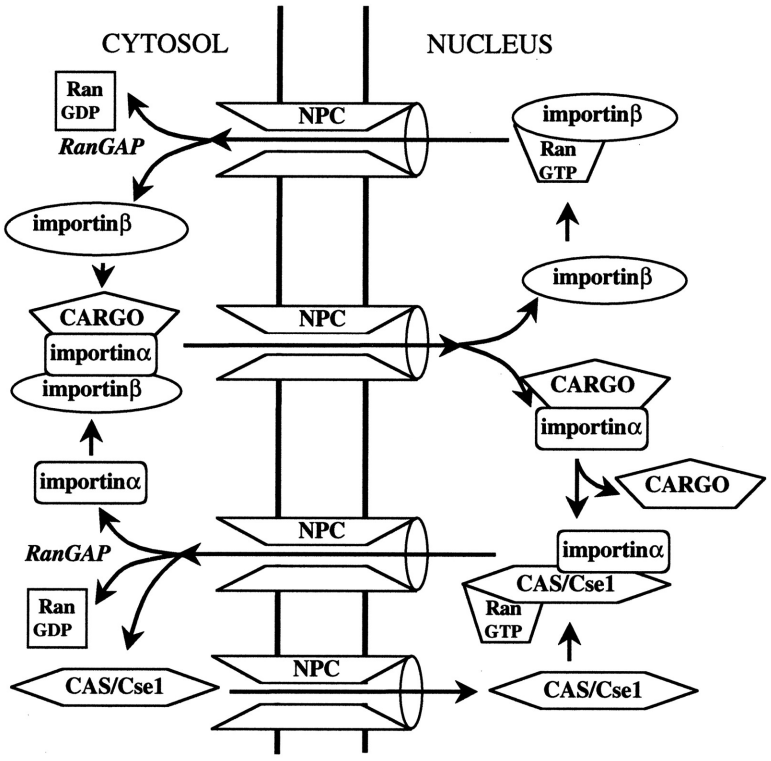

Figure 18. Mechanism of nuclear import by the importin-α/importin-β pathway.
This figure shows a mechanism for nuclear import involving importin-α and importin-β

as well as how both importins are returned to the cytoplasm. See text for details. Figure adapted from (*281*).

1.4.5. Nuclear export

Exportins and the nuclear export signal (NES)

Exportins are the members of the karyopherin family that function solely in nuclear export. They do so by recognizing NESs on cargo proteins and then mediating their transport through NPCs via interactions with FG-NUPs. The major exportin is exportin-1 (XPO1/CRM1) (*281*, *294*). Leptomycin B is a highly specific inhibitor of exportin-1 (*295*). NESs were first discovered in the mid-1990s and consist of a short motif rich in leucine. The prototypical NES is LxxxLxxLxL (where L is leucine and x represents any amino acid but preferentially one that is charged, polar, or small), but the spacing can be somewhat variable and other hydrophobic amino acids (such as valine, isoleucine, methionine, and phenylalanine) can substitute for some of the leucines (*284*, *296*). Moreover, non-canonical NESs exist, such as the NES for the transcription factor NFAT (IVAAINALTT), making it hard to determine if a protein contains an NES (*281*, *297*). polη, polι, and polκ do not have a known NES.

Overview of the nuclear export mechanism

Similar to nuclear import, the four major steps of nuclear export are 1) recognition of the NES by the exportin, 2) translocation of the complex out to the cytoplasm via a NPC, 3) release of the cargo, and 4) exportin recycling (Figure 19). On its own, exportin-1 has low affinity for both Ran-GTP and most NES cargos, but together they form a stable complex. Formation of this complex is promoted by cofactors (such as RanBP3) that

increase NES binding, stimulate RanGEF, and inhibit binding of unloaded exportin-1 to the NPC. Once formed, the complex exits the nucleus where it encounters RanGAP. RanGAP promotes GTP hydrolysis to produce Ran-GDP and subsequent release of the cargo (which is now officially exported). exportin-1 can then return to the nucleus on its own (*281*).

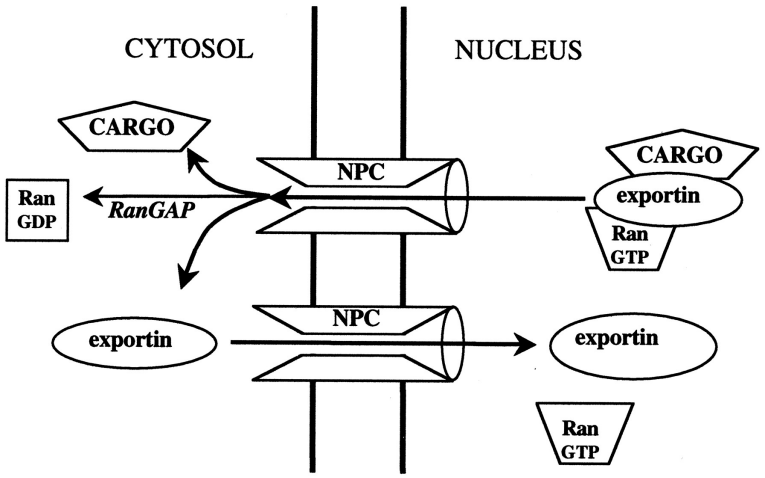

Figure 19. Mechanism of nuclear export.
This figure shows a mechanism for nuclear export involving any exportin as well as how it is returned to the nucleus after. See text for details. Figure adapted from (*281*).

1.4.6 Regulation of nuclear import and export

Regulation of the interaction between cargo and NTRs

One mechanism through which cells can control nuclear import and export is by masking (or unmasking) a NLS or NES through post-translational modifications (ex: phosphorylation) and/or binding by other proteins (such as 14-3-3) (*298*, *299*). Examples of this are described below:

1) Phosphorylation of the protein Pho4 at two sites promotes recognition by its exportin (Msn5) while phosphorylation at a site in its NLS inhibits binding to

its importin. It is unknown if phosphorylation at the first two sites induces a conformational change that reveals the Msn5 binding site or if Msn5 can recognize the actual phosphate groups (*300–302*).

2) Phosphorylation of the cell cycle protein Cdc25c creates a 14-3-3 binding site that obscures the nearby NLS but has no effect on the more distant NES, enabling cytoplasmic localization (*303*, *304*).
3) Binding of 14-3-3 to hTERT in a phosphorylation-independent manner conceals a nearby NES and prevents binding by exportin-1 (*305*).
4) Binding of HIV-Rev by tRNA molecules inhibits the nuclear import of HIV-Rev by preventing its interaction with importin-β (*306*).
5) Phosphorylation of NFAT by protein kinase A creates 14-3-3 binding sites that obscure NFAT's NLS and sequester it in the cytoplasm (*307*). Alternatively, calcium can promote nuclear accumulation of NFAT by promoting its interaction with calcineurin, which both dephosphorylates NFAT and masks its NES (*308*, *309*).
6) When inactive, the N- and C-termini of ERK5 interact, concealing a bipartite NLS and creating a NES. Phosphorylation of ERK5 by MEK5 disrupts the interaction between the two termini, thereby silencing the NES and exposing the NLS (*310*).
7) One or both NLSs of NF-κB is masked when bound by IκB family members, thereby inhibiting its nuclear localization and ability to activate transcription of target genes. Interestingly, IκBβ binds to both NLSs, leading to complete

cytoplasmic localization while IκBα only binds to one NLS, resulting in dynamic shuttling between the cytoplasm and the nucleus (*311*).

8) Oxidation of cysteine residues within the NES of the transcription factor yAP1 blocks interaction with exportin-1, allowing yAP1 to localize to the nucleus (*312*).
9) RNA helicase A contains a bi-directional nuclear transport domain (NTD) consisting of a NLS and a NES. Methylation of an arginine in the NTD of RNA helicase A by PRMT1 is required for its nuclear import. It is proposed that methylation blocks the binding of an unknown cytoplasmic retention factor and exposes the NLS for recognition by importin-β (*313*).
10) Efficient nuclear import of PTEN requires mono-ubiquitination of two different lysine although the exact mechanism has yet to be determined as PTEN does not have a recognizable NLS (*314*).

Alternatively, the formation of complexes can induce conformational changes that either hide or create NLSs or NESs. Interactions between the NLSs and NESs on different proteins in a complex can also influence localization (*298*, *299*). Examples of this are described below:

1) Homodimerization of STAT1 induced by phosphorylation causes a structural rearrangement that exposes a dimer-specific NLS (dsNLS) that is recognized by importin-α (*315*).
2) In the absence of IκBα, NF-κB localizes to the nucleus, but when bound by IκBα, it is predominantly cytoplasmic. This is because the NES of IκBα

can overcome the NLSs of NF-κB, allowing IκBα to serve as a nuclear export chaperone for NF-κB (*316*).

3) NF-κB consists of a heterodimer composed of p50 (NLS only) and RelA (NLS and NES). In the absence of IκBα, expression of only p50 results in nuclear localization while RelA expressed alone localizes in the cytoplasm. However, co-expression of p50 and RelA in the absence of IκBα results in nuclear localization of both proteins. Possible explanations for these observations are that formation of the RelA-p50 heterodimer results in a conformational change that hides RelA's NES or that since the heterodimer has a greater ratio of NLSs to NESs than RelA (2:1 instead of 1:1), the NLSs can exert a greater effect (*317*).
4) Three NLSs and one NES are located in the tetramerization domain of p53. In a p53 monomer, these sites are all exposed, and p53 shifts into the nucleus. If p53 remains a monomer, it will then be rapidly exported back out. However, if activation signals (such as stress) induce the formation of a p53 tetramer, then all the NESs are masked and unable to be recognized by the export machinery (*318*).

Regulation of nuclear transport by the PI3K-mTOR pathway

Members of the PI3K-mTOR pathway have been shown to regulate the nuclear import and/or export of various targets using similar mechanisms to those described above. For example, phosphorylation of FOXO transcription factors by Akt and of the transcription factor EB (TFEB) by mTORC1 has been shown to promote their cytoplasmic

retention since the phosphorylated sites can be recognized by members of the 14-3-3 family, which hides their NLS. FOXO proteins function to activate quiescence and apoptotic gene expression programs while TFEB drives expression of genes related to autophagy, so phosphorylation of these factors by Akt/mTORC1 promotes survival and proliferation (*319–322*). PI3K-mTOR signaling has also been shown to prevent nuclear accumulation of GSK3β such that inhibition of this pathway in response to amino acid deprivation leads to a robust increase in nuclear GSK3β (*323*, *324*). Another example is that mTORC promotes sequestration of NF-κB in the cytoplasm by binding to IKKα, which prevents IKKα from being able to dissociate IκB from the NLS(s) of NF-κB (*325*). Finally, inactivation of mTOR has been demonstrated to increase the nuclear localization of STAT1, but the exact mechanism still requires further investigation (*326*). A similar effect is observed in yeast exposed to stress (such as starvation) where inactivation of TOR (the yeast ortholog of mTOR) promotes the nuclear accumulation of the stress response transcription factors Msn2/4 (*327*, *328*) while inhibition of TOR by nitrogen limitation triggers the nuclear import of the transcription factor GLN3, which activates the nitrogen discrimination pathway. Activated TOR normally phosphorylates GLN3 to promote its association with the cytoplasmic protein URE2, so inhibition of TOR results in nuclear localization of GLN3 by stimulating dephosphorylation of GLN3 by the phosphatase PP2A (*329*). Furthermore, nutrient deprivation results in the nuclear localization of the chaperone Ssa4p (*330*).

In addition to the direct effects on cargo proteins, both the ERK1/2 signaling cascade and the PI3K-mTOR pathway have been shown to regulate nuclear transport by modulating the Ran gradient. This is achieved via the phosphorylation of RanBP3 by RSK

(ERK1/2) or Akt (PI3K-mTOR). RanBP3 can interact with exportin-1 to promote cargo loading and nuclear export, but it is also involved in formation of the Ran gradient. Phosphorylation of RanBP3 is believed to increase its affinity for Ran and to help regulate activity of the RanGEF (*331*). Another Ran binding protein RanBP2 has also been linked to the PI3K-mTOR pathway. Association of mTOR with RanBP2 mediates nuclear import of ribosomal proteins by importin-β via a process that requires its kinase activity (*332*). Overall, many links between the PI3K-mTOR pathway and nuclear transport have already been established, but there is still much more to be discovered.

CHAPTER 2: THE REGULATION OF POLK IN RESPONSE TO STRESS

2.1 Introduction

Errors in DNA replication can lead to increased mutation rates that contribute to cancer pathogenesis. An example of this is somatic or germline mutations in the proofreading domain of polδ or polε that lead to tumors with markedly increased numbers of point mutations (*3*, *125*, *127*). Aside from these two main replicative polymerases, a number of other DNA polymerases have been identified that may contribute to cancer initiation or progression (*20*). For example, inactivation of polη is associated with XP-V, which predisposes patients to UV-induced skin cancers (*2*). Additionally, polι is upregulated in esophageal squamous cell cancer, and its expression levels positively correlate with lymph node metastasis/clinical stage (*134*).

The roles of other DNA polymerases in this process are less well understood but likely could contribute to tumor progression. One such polymerase is polκ, which is a member of the Y family of DNA polymerases that plays an essential role in the DNA damage tolerance process of TLS (*159*, *333*). Several previous studies have shown that overexpression of polκ can contribute to tumorigenesis and drug resistance in cancer (*132*, *136*, *137*, *334*). For example, overexpression of polκ in glioblastoma cells increases resistance to the DNA-damaging agent temozolomide (*137*), and it has also been found to be significantly overexpressed in lung cancer (*136*).

polκ can replicate DNA in both an error-free and error-prone manner during TLS (*335*). It can bypass thymine glycols in a relatively error-free manner (*336*), whereas it bypasses N-2-acetylaminofluorene adducts in a more error-prone manner (*337*). When

replicating on undamaged DNA, polκ has a markedly high error rate due to a relatively large active site and lack of a proofreading domain (*338*). Using *in vitro* assays, it has been shown to have an error rate as high as 1 error per 200 base pairs when replicating on undamaged DNA (*339*). For this reason, it is considered an "error-prone" polymerase that can introduce untargeted mutations while either acting directly at the replication fork or filling in post-replication gaps (*340*). The range of errors introduced by polκ span virtually all substitutions, although to differing degrees (with a high rate of T→G substitutions), as well as a preponderance of deletions (*338*). The error rate is substantially higher than those found for the replicative polymerases polδ and polε.

Because dysregulated polκ can be mutagenic at high levels, it is important that cells limit both its expression and access to DNA. In bacteria, this regulation is enacted via the SOS/DNA damage response along with the RpoS/starvation stress response (*99*, *140*). In work spanning several decades, it has been observed that *E. coli* can temporarily increase their mutation rate during periods of stress using a mechanism called SIM (*138*–*141*). This hypermutation is enacted as part of DSBR, which becomes mutagenic due to the activity of DinB (*153*), the *E. coli* ortholog of human polκ. This mutagenic process is regulated at three levels (*141*): 1) a DSB (*142*, *341*), 2) activation of the SOS DNA damage response (*139*), and 3) activation of the generalized sigma S (RpoS) stress response (*140*). The SOS response, when coupled with this stress response, allows first for upregulation of DinB (*147*) and then subsequent usage of this error-prone polymerase for mutagenic repair, which results in the base substitutions and indels that are commonly observed (*140*). It is likely that deficiencies in MMR contribute to this process since overexpression of MutL inhibits mutagenesis in stationary phase but not during growth

(*156*), whereas both MutS and MutH are downregulated in part by the stress response RpoS pathway (*155*).

In contrast to the work in *E. coli*, the mechanisms regulating the expression and localization of polκ in mammalian cells remain poorly understood. In normal human tissues, polκ is widely expressed at the mRNA level (*342*), whereas in the mouse, it is highly enriched in the adrenal cortex and testis (*343*). In the mouse, protein expression using a peptide-generated antibody was noted in adrenal cortex, pachytene cells in meiosis I, post-meiotic spermatids, and some epithelial cells in the lung and stomach (*343*). At the cellular level, studies using overexpression of eGFP-polκ fusion proteins have demonstrated that polκ is strongly enriched in the nucleus (*273*, *274*). However, antibody staining of endogenous polκ protein using antibodies generated with either a peptide fragment or full-length protein have shown variable expression in the cytoplasm as well as the nucleus (*343*). Analysis of the polκ promoter has shown consensus binding sites for Sp1 and CREB, both of which have been reported to transcriptionally activate its expression (*344*, *345*).

Although recent observations demonstrate that polκ is mutagenic and can promote tumorigenesis and drug resistance (*132*, *136*, *137*, *334*), it is unknown what regulates its expression in cancer. Ectopic expression of polκ allows it to become part of the replication machinery, even in the absence of external stress, indicating that high levels of it alone may be sufficient to induce new mutations (*273*). This has important clinical implications since dysregulation of polκ expression could therefore contribute to tumorigenic phenotypes by affecting its normal subcellular localization. In this chapter, we demonstrate that deprivation of oncogenic signaling in melanoma, lung, and breast cancer

cell lines upregulates polκ and confines it to the nucleus. A similar nuclear enrichment is also observed in response to glucose starvation. These pathways converge on mTOR, a central regulator of nutrient status in the cell (*235*) that may be analogous to the generalized stress factor RpoS in *E. coli* (*141*). When cells are unstressed and have intact mTOR signaling, polκ is primarily present in the cytoplasm; when cells are stressed or mTOR is inhibited, polκ shifts primarily to the nucleus, suggesting that the cell can dynamically regulate polκ in response to cell stress. In line with this, we find that polκ can be rapidly exported back out of the nucleus via the nuclear export machinery, implying that cells may normally use nuclear export to prevent excess mutagenesis. In summary, our data suggest a mechanism by which mammalian cancer cells regulate the levels and localization of the error-prone DNA polymerase polκ in response to stress.

2.2 Results

2.2.1 MAPK inhibition upregulates polκ mRNA expression

Given the role of stress in upregulating DinB/pol IV in *E. coli*, we first asked whether cell stress regulated polκ expression in cancer. We reasoned that drugs blocking oncogenic drivers would induce cell cycle arrest and ultimately apoptosis and would represent an extreme form of cell stress. Small molecules targeting the MAPK pathway have been developed, some of which are being clinically used to treat melanoma patients (*183*, *188*, *346*), and these inhibitors can induce cell stress prior to overt death of the cancer cell (*191*). Based on this, we first asked whether inhibition of the MAPK pathway could induce polκ expression in melanoma.

To assess this, we treated the $BRAF^{V600E}$ mutant A375 human melanoma cell line with the $BRAF^{V600E}$ inhibitor PLX4032 (vemurafenib) (*188*) and measured the levels of polκ as well as the other Y family DNA polymerases (polη, polι, and Rev1) by qRT-PCR at 24 hours post exposure. This revealed upregulated expression of all four polymerases but especially polκ (Figure 20A). We tested additional timepoints and discovered that polκ mRNA levels peak at 24 hours and are sustained thereafter (Figure 20B). Because BRAF activates downstream MEK/ERK signaling, we also examined whether downstream inhibitors would elicit similar effects. In two different $BRAF^{V600E}$ mutant melanoma cell lines (A375 and SK-MEL28), we found that MEK and ERK inhibitors (*183*, *346*) produced an upregulation of polκ and the other Y family polymerases similar to that seen after BRAF inhibition (Figure 20, C to F). polκ showed the greatest upregulation overall, and since it is the closest human ortholog to DinB (*159*), we decided to focus primarily on it going forward.

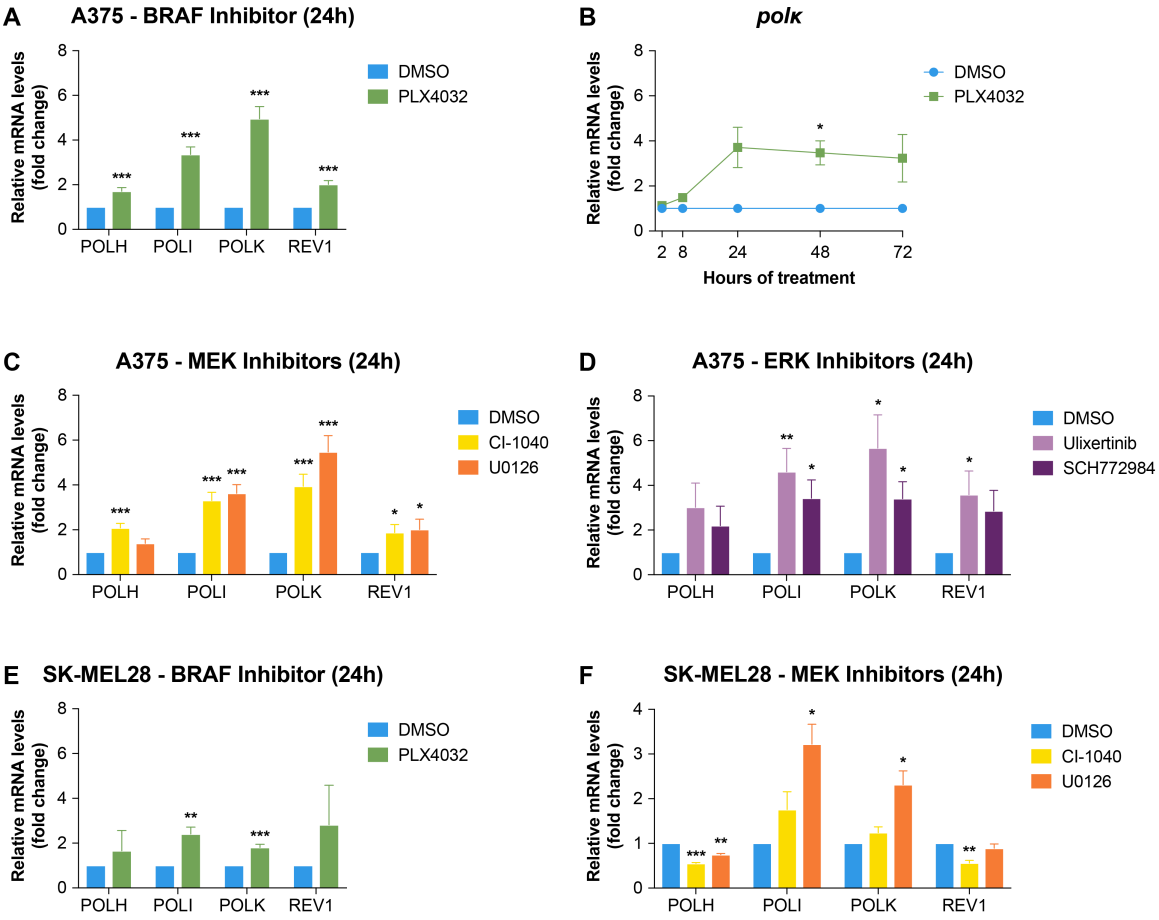

Figure 20. Treatment of melanoma cells with BRAF or other MAPK inhibitors increases mRNA levels of Y family polymerases in multiple melanoma cell lines. **(A)** qRT-PCR to detect the expression of polη, polι, polκ, and Rev1 relative to the DMSO control was performed on A375 cells treated with DMSO or 5 μM PLX4032 for 24 hours (n=30 experiments). **(B)** qRT-PCR to detect the mRNA expression of polκ relative to the DMSO control was performed on A375 cells treated with DMSO or 5 μM PLX4032 for 2, 8, 24, 48, or 72 hours (n=3 experiments). **(C)** qRT-PCR to detect the expression of polη, polι, polκ, and Rev1 relative to the DMSO control was performed on A375 cells treated with DMSO or MEK inhibitors (10 μM CI-1040, 10 μM U0126) for 24 hours (n=16 experiments). **(D)** qRT-PCR to detect the expression of polη, polι, polκ, and Rev1 relative to the DMSO control was performed on A375 cells treated with DMSO or ERK inhibitors (1 μM Ulixertinib, 1 μM SCH772984) for 24 hours (n=9 experiments). **(E)** qRT-PCR to detect the expression of polη, polι, polκ, and Rev1 relative to the DMSO control was performed on SK-MEL28 cells treated with DMSO or 5 μM PLX4032 for 24 hours (n=9 experiments). **(F)** qRT-PCR to detect the expression of polη, polι, polκ, and Rev1 relative to the DMSO control was performed on SK-MEL28 cells treated with DMSO or MEK inhibitors (10 μM CI-1040, 10 μM U0126) for 24 hours (n=4 experiments). All graphs are represented as mean ± S.E.M. Statistical analysis was performed using paired two-tailed t-tests (*P < 0.05, **P < 0.01, ***P < 0.001).

We then began investigating the transcription factor responsible for the observed increase in polκ mRNA levels. Previous studies have revealed roles for the transcription factors CREB, p53, Sp1, and HSF1 in the regulation of polκ levels in human and mouse cells exposed to DNA-damaging reagents, such as benzo[a]pyrene diol epoxide and UV (*343–345*) while p53 has also been shown to be important in the constitutive expression of polκ (*343*).

CREB plays a role in the regulation of many different genes involved in DNA repair, including BRCA1 and polβ (*347*, *348*). CREB becomes activated after phosphorylation at serine-133, and this has been shown to occur in response to a wide variety of stimuli, including both growth factors and stress signals (*349*, *350*). In addition, overexpression of CREB has been implicated in the progression of melanoma (*351*). Because activation of CREB has been previously linked to upregulation of polκ mRNA (*344*, *345*), we decided to investigate if BRAF inhibition could activate CREB by performing ELISAs to determine the levels of total and phosphorylated CREB. However, several timepoints all revealed no significant difference in the amount of activated CREB between the DMSO- and PLX4032-treated samples (Figure 21). On the other hand, treatment with the positive control forskolin, which activates adenylyl cyclase and therefore increases levels of cyclic adenosine monophosphate (cAMP) (*352*), resulted in a robust increase in phospho-CREB as expected (data not shown).

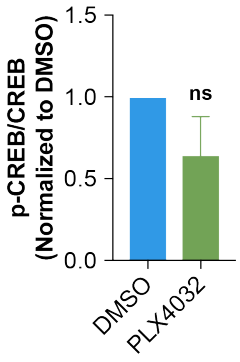

Figure 21. BRAF inhibition does not activate CREB.
ELISAs for CREB and phospho-CREB (p-CREB) were performed on A375 cells treated with DMSO or PLX4032 for 30 minutes. The bar graphs shows the quantification of the results relative to DMSO from 2 experiments and is represented as mean ± S.E.M. Statistical analysis was performed using paired two-tailed t-tests (ns = non-significant, *P < 0.05, **P < 0.01, ***P < 0.001).

We next focused our attention on the potential role of the DDR protein p53 (*65*) in regulating the expression of polκ in response to MAPK inhibition. PLX4032 has been previously shown to increase the levels of p53 protein via reduction of Usp5's deubiquitination activity (*353*), and when we treated our A375 cells with PLX4032 for 2-24 hours, we observed an increase in p53 levels as well (Figure 22, A and B). Therefore, we decided to use shRNA-mediated knockdown (*354*) to determine if p53 played a role in the transcription of polκ. After validating knockdown by two different doxycycline (dox)-inducible p53 shRNAs (Figure 22C), we first asked if p53 played a role in the constitutive expression of polκ. Consistent with this role, we observed a decrease in polκ mRNA levels after p53 knockdown compared to the sh-Ctrl sample (Figure 22D). However, when we followed up our p53 knockdown by treating the cells with DMSO or PLX4032, we observed a similar level of PLX4032-induced upregulation of polκ for both the sh-Ctrl and sh-p53 cells (Figure 22E). This suggests that while p53 functions in the constitutive

expression of polκ, it is not responsible for the observed upregulation after BRAF inhibition. Our data is actually in contradiction with previous studies that showed 1) while p53 plays a role in both constitutive and UV-induced expression of polκ in mice, a similar effect had not been observed in humans (*343*) and 2) polκ expression in lung cancer is actually negatively regulated by p53 (*355*). We are unsure of where the discrepancy in results comes from, but it is potentially due to differences in the cell lines used in each study (melanoma vs. lung and colorectal cancer). In summary, the transcription factor responsible for the mRNA upregulation of polκ remains unclear and awaits further study.

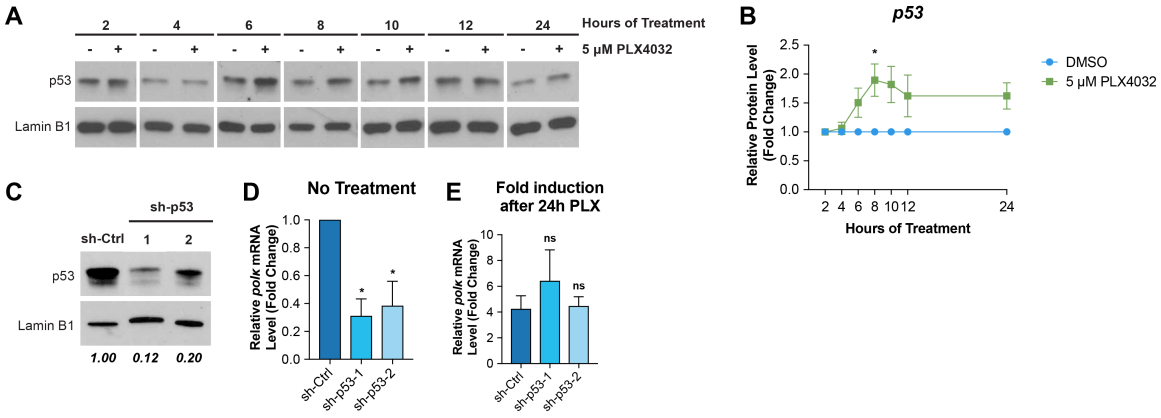

Figure 22. p53 functions as a transcription factor for polκ, but it is not responsible for polκ upregulation after BRAF inhibition.
(A-B) Western blot analysis for p53 was performed on A375 cells treated with DMSO (-) or 5 μM PLX4032 (+) for 2, 4, 6, 8, 10, 12, or 24 hours. Representative blot shown in (A), and quantification of 4-6 experiments relative to the DMSO control shown in (B). Lamin B1 was used as the loading control. **(C)** Western blot analysis for p53 was performed on A375 cells containing a control shRNA (sh-Ctrl) or an shRNA against p53 (sh-p53-1 or sh-p53-2) after treatment with 1 μg/ml dox for 6 days. Lamin B1 served as the loading control. The number underneath each lane represents the levels of p53 relative to the sh-Ctrl. **(D)** qRT-PCR to detect the expression of polκ relative to the sh-Ctrl sample was performed on A375 cells containing a control shRNA (sh-Ctrl) or an shRNA against p53 (sh-p53-1 or sh-p53-2) after treatment with 1 μg/ml dox for 6 days (n=3 experiments). **(E)** qRT-PCR to detect the expression of polκ relative to the DMSO control was performed on A375 cells containing a control shRNA (sh-Ctrl) or an shRNA against p53 (sh-p53-1 or sh-p53-2) after treatment with 1 μg/ml dox for 6 days followed by treatment with DMSO or 5 μM PLX4032 + 1 μg/ml dox for 24 hours (n=2

experiments). Only the 5 μM PLX4032 samples are shown. All graphs are represented as mean ± S.E.M. Statistical analysis was performed using paired two-tailed t-tests (ns = non-significant, *P < 0.05, **P < 0.01, ***P < 0.001).

2.2.2 MAPK inhibition changes the subcellular localization of polκ protein

We next examined expression of polκ at the protein level under similar conditions. We utilized an antibody raised against full-length human polκ protein and verified its specificity using shRNA-mediated knockdown and overexpression of polκ (Figure 23).

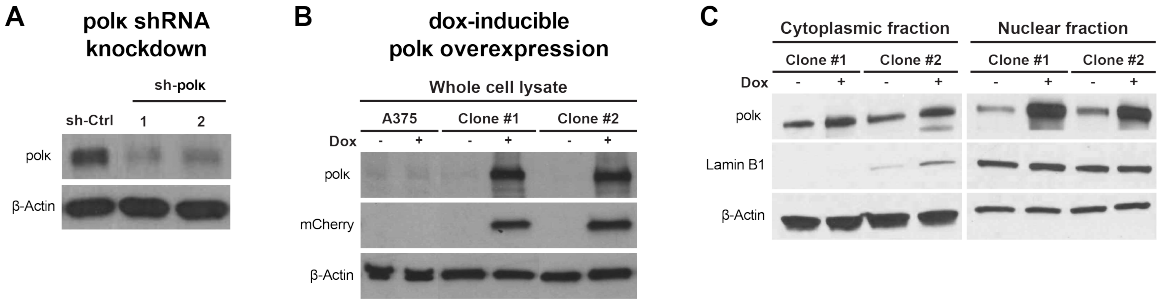

Figure 23. Validation of the polκ antibody.
(A) Western blot analysis for polκ was performed on A375 cells containing a control shRNA (sh-Ctrl) or an shRNA against polκ (sh-polκ-1 or sh-polκ-2) after treatment with 1 μg/ml dox for 1 month. β-actin served as the loading control. **(B)** Western blot analysis for polκ and mCherry was performed on whole cell lysates of control A375 cells or 2 different clones of A375 cells containing a dox-inducible polκ overexpression construct (Clone #1 and Clone #2) treated with media with (Dox+) or without (Dox-) 1 μg/ml dox for 24 hours. β-actin served as the loading control. **(C)** Western blot analysis for polκ was performed on cytoplasmic and nuclear fractions of 2 different clones of A375 cells containing a dox-inducible polκ overexpression construct (Clone #1 and Clone #2) treated with media with (Dox+) or without (Dox-) 1 μg/ml dox for 96 hours. Lamin B1 was used to show isolation of the nuclear fraction, and β-actin served as the loading control.

Although polκ has been largely reported to be localized in the nucleus when overexpressed as an eGFP-tagged fusion protein (*273*, *274*), we surprisingly found that the Western blot using an antibody raised against the full-length protein showed that endogenous polκ was expressed in both cytoplasmic and nuclear fractions (Figure 24A).

This expression pattern is similar to that of the related family member polη, where both cytoplasmic and nuclear expression is seen (Human Protein Atlas (*356*)). While treatment with vemurafenib did not change overall protein levels of polκ, it instead induced a specific increase in nuclear polκ and corresponding decrease in cytoplasmic polκ (Figure 24, A to C). We confirmed this redistribution using immunofluorescence, where acute exposure to PLX4032 induced a shift of polκ from the cytoplasm to the nucleus (Figure 24, D and E). In addition, we found that MEK and ERK inhibitors produced a similar shift of polκ to the nucleus in both A375 and SK-MEL28 cells (Figure 24, F to J). Cytoplasmic localization of a DNA polymerase that can shift from the cytoplasm to the nucleus has been reported previously (*276–278*), suggesting that this mode of regulation might be relevant for polκ under physiologic conditions.

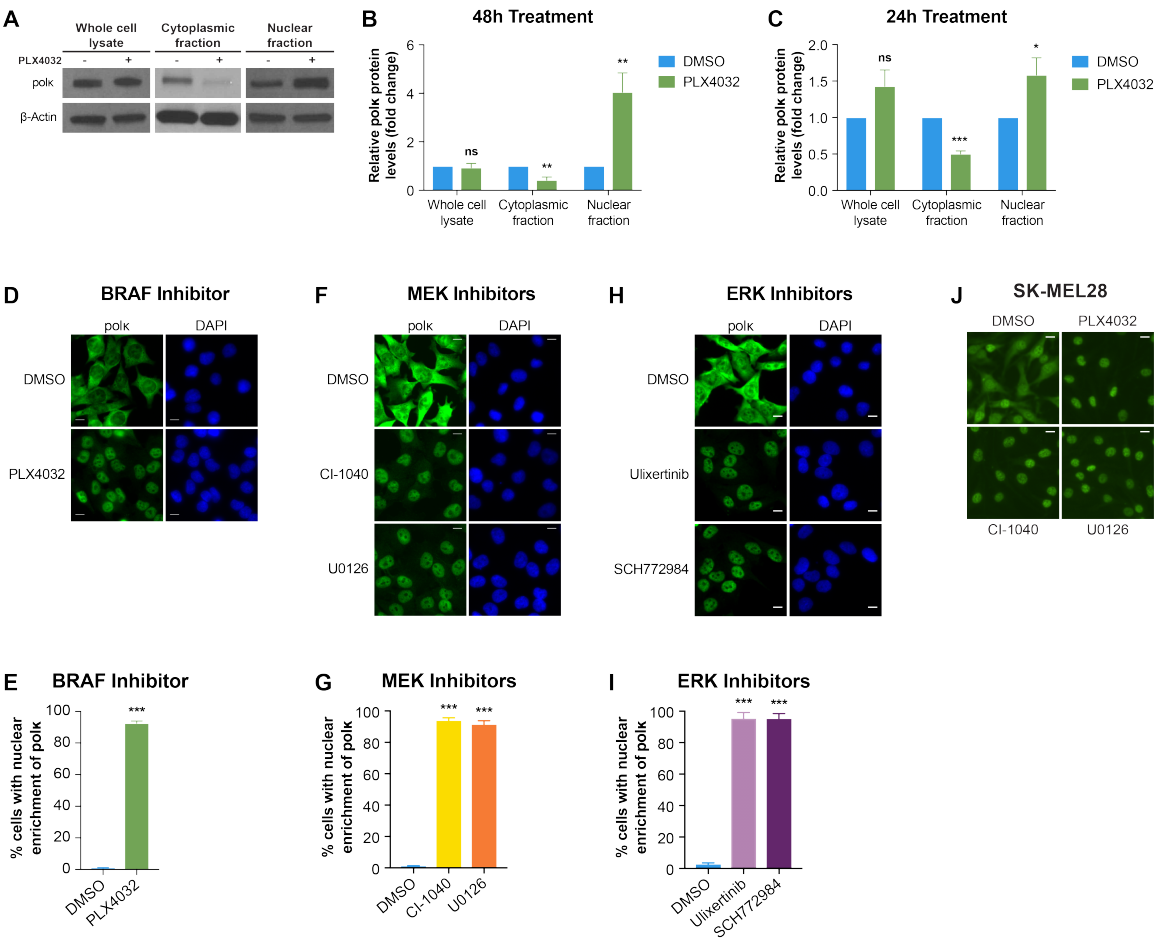

Figure 24. Treatment of melanoma cells with BRAF or other MAPK inhibitors modulates polκ's subcellular localization.

(A-B) Western blot analysis for polκ was performed on A375 cells treated with DMSO (-) or 5 μM PLX4032 (+) for 48 hours. Representative blot shown in (A), and quantification of 5-8 experiments relative to the DMSO control shown in (B). β-actin was used as the loading control. **(C)** Western blot analysis for polκ was performed on A375 cells treated with DMSO or 5 μM PLX4032 for 24 hours. The bar graph shows quantification of the results relative to the DMSO control from 9-17 experiments. β-actin was used as the loading control. **(D-E)** Immunofluorescence staining for polκ was performed on A375 cells treated with DMSO or 5 μM PLX4032 for 24 hours. Representative images shown in (D), and quantification of the percentage of cells with nuclear enrichment of polκ shown in (E). At least 2500 cells were counted for each sample across 22 fields of view. **(F-G)** Immunofluorescence staining for polκ was performed on A375 cells treated with DMSO or MEK inhibitors (10 μM CI-1040, 10 μM U0126) for 24 hours. Representative images shown in (F), and quantification of the percentage of cells with nuclear enrichment of polκ shown in (G). At least 1000 cells were counted for each sample across 18 fields of view. **(H-I)** Immunofluorescence staining for polκ was performed on A375 cells treated with DMSO or ERK inhibitors (1 μM Ulixertinib, 1 μM SCH772984) for 24 hours. Representative images shown in (H), and quantification of the percentage of cells with nuclear enrichment of polκ shown in

(I). At least 250 cells were counted for each sample across 6 fields of view. **(J)** Immunofluorescence staining for polκ was performed on SK-MEL28 cells treated with DMSO, 5 μM PLX4032, or MEK inhibitors (10 μM CI-1040, 10 μM U0126) for 24 hours. All graphs are represented as mean ± S.E.M. Statistical analysis was performed using paired two-tailed t-tests (ns = non-significant, *P < 0.05, **P < 0.01, ***P < 0.001). All scale bars 10 μm.

BRAF inhibition is known to cause cell cycle arrest (*184*), so to ensure that these effects were not simply due to inhibition of the cell cycle, we treated A375 cells with either the CDK4/6 inhibitor PD0332991 (*357*) or PLX4032 and then assessed the cell cycle using flow cytometry and polκ localization using immunofluorescence. As expected, both of these interventions led to a near complete G1 arrest (Figure 25A); however, treatment with the CDK4/6 inhibitor resulted in little to no nuclear polκ (Figure 25, B and C), suggesting it is specific to inhibition of the MAPK pathway. Given the potential importance of the cytoplasmic to nuclear shift of polκ, we investigated several potential mechanisms for this shift.

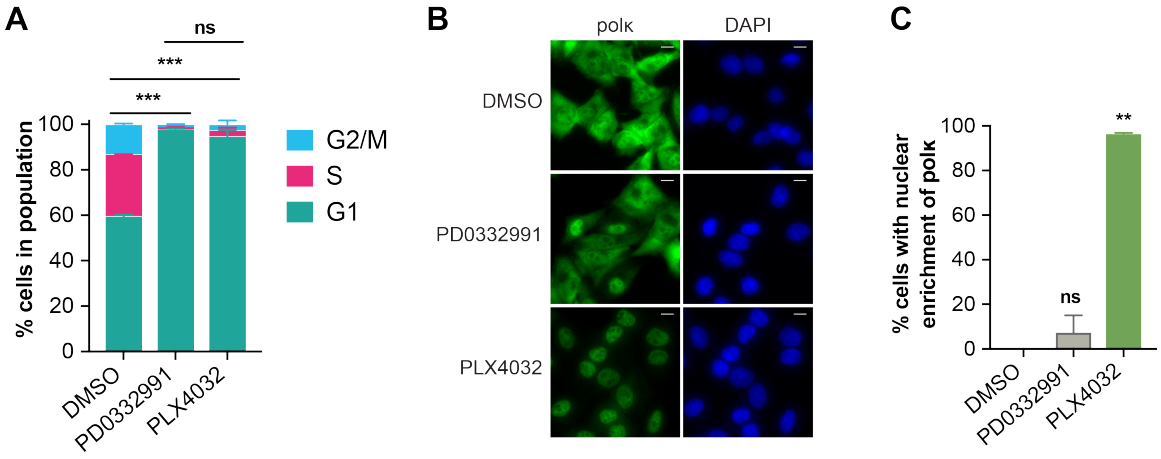

Figure 25. Cell cycle inhibition is not responsible for the shift in polκ's subcellular localization.
(A) Cell cycle profiles were measured by flow cytometry after treating A375 cells with DMSO, 0.5 μM PD0332991, or 5 μM PLX4032 for 24 hours. The bar graph shows the distribution of cells in different phases of the cell cycle. **(B-C)** Immunofluorescence

staining for polκ was performed on A375 cells treated with DMSO, 0.5 μM PD0332991, or 5 μM PLX4032 for 24 hours. Representative images shown in (B), and quantification of the percentage of cells with nuclear enrichment of polκ shown in (C). At least 40 cells were counted for each sample across 2 fields of view. All graphs are represented as mean ± S.E.M. Statistical analysis was performed using chi-square tests (A) or paired two-tailed t-tests (C) (ns = non-significant, *P < 0.05, **P < 0.01, ***P < 0.001). All scale bars 10 μm.

2.2.3 The DNA damage response pathway does not play a role in the subcellular localization of polκ in response to MAPK inhibition

The induction of DinB in bacteria relies upon two systems: the SOS/DNA damage response and the RpoS-controlled general/starvation stress response. We reasoned that the nuclear localization of polκ in response to MAPK inhibition might act through one of these two mechanisms. To test this, we treated A375 melanoma cells with vemurafenib and then checked for markers of DDR activation (*358*), including gamma H2AX (γH2AX), 53BP1, phosphorylated Chk1 (p-Chk1), and phosphorylated Chk2 (p-Chk2) but saw no induction of any of these markers (Figure 26).

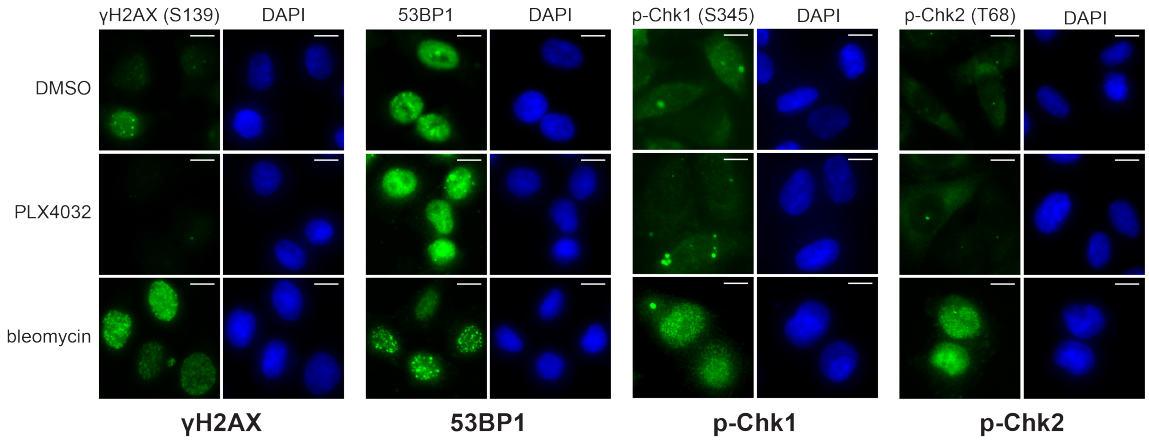

Figure 26. Activation of the DDR is not observed after BRAF inhibition.
Immunofluorescence staining for γH2AX, 53BP1, p-Chk1, and p-Chk2 was performed on A375 cells treated with DMSO, 5 μM PLX4032, or 10 μM bleomycin for 6 hours. All scale bars 10 μm.

Although we showed p53 was not responsible for the observed increase in polκ mRNA, it is upregulated in response to BRAF inhibition (Figure 22, A and B), so we decided to test if it was responsible for the observed subcellular shift in polκ protein. Using the same dox-inducible p53 shRNAs (Figure 22C), we tested whether knockdown of p53 would prevent the shift but failed to see any change in the nuclear localization of polκ after treatment with DMSO or PLX4032 (Figure 27). These data indicate that MAPK inhibition strongly induces polκ's nuclear localization even in the absence of DDR activation.

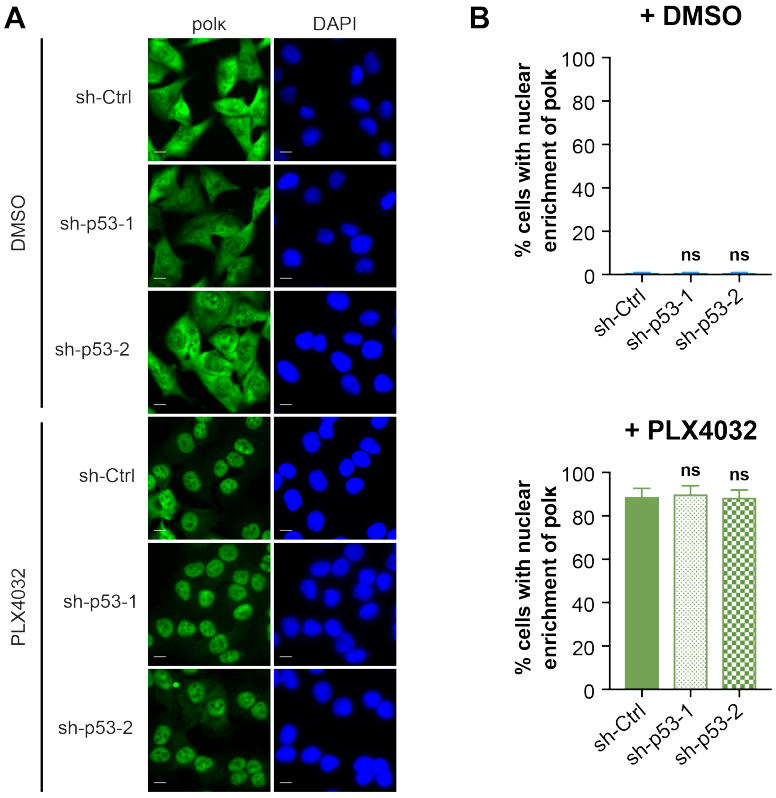

Figure 27. Loss of p53 has no effect on the subcellular shift of polκ.
(A-B) Immunofluorescence staining for polκ was performed on A375 cells containing a control shRNA (sh-Ctrl) or an shRNA against p53 (sh-p53-1 or sh-p53-2) treated with 1 μg/ml dox for 8 days and then with 1 μg/ml dox + DMSO or 5 μM PLX4032 for an

additional 24 hours. Representative images shown in (A), and quantification of the percentage of cells with nuclear enrichment of polκ shown in (B). At least 50 cells were counted for each sample across 2 fields of view. All graphs are represented as mean ± S.E.M. Statistical analysis was performed using paired two-tailed t-tests (ns = non-significant, *P < 0.05, **P < 0.01, ***P < 0.001). All scale bars 10 μm.

2.2.4 Glucose starvation and ER stress phenocopy the effects on the subcellular localization of polκ

We next turned to the starvation/stress response, the other major inducer of SIM in bacteria. *E. coli* require the RpoS starvation/stress response for DinB's upregulation and activation during SIM (*99*, *140*), so we assessed whether we could observe a similar effect on polκ in starved cells. To test this idea, we examined the effect of nutrient deprivation on polκ's localization by growing A375 cells in a variety of media conditions in which we selectively removed serum, glucose, or glutamine and measured polκ's localization by immunofluorescence. Whereas we found that both glutamine and serum deprivation had small effects on the nuclear localization of polκ, glucose starvation resulted in a highly significant induction of nuclear polκ (Figure 28). Because glucose is a major carbon source for rapidly growing cancer cells, this may be analogous to the starvation response induced in *E. coli* by deprivation of lactose, which is an important carbon source for bacteria.

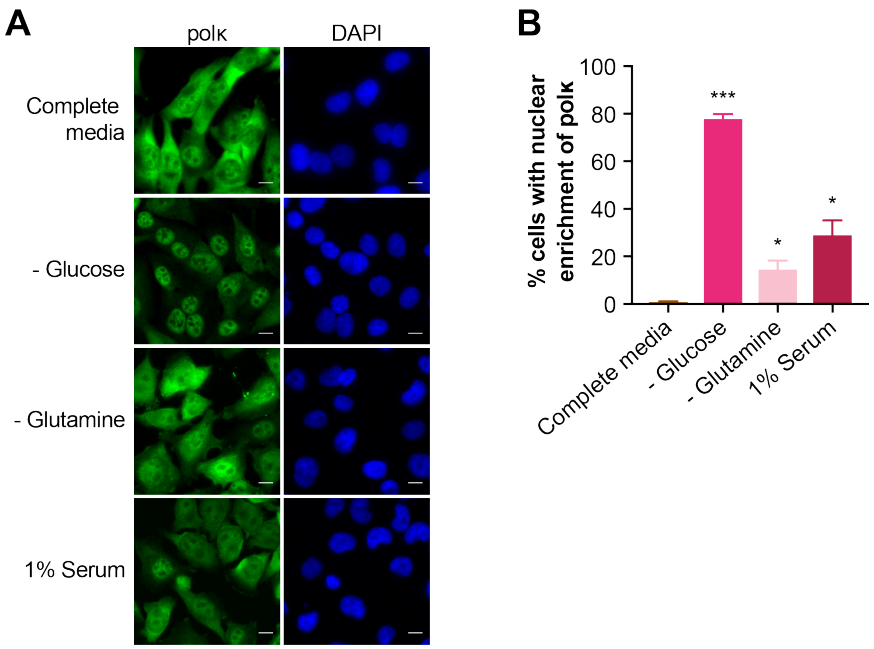

Figure 28. Glucose starvation modulates polκ's subcellular localization as well.
(A-B) Immunofluorescence staining for polκ was performed on A375 cells treated with complete media (25 mM glucose, 6 mM glutamine, and 10% FBS), media – glucose (0 mM glucose, 6 mM glutamine, and 10% FBS), media – glutamine (25 mM glucose, 0 mM glutamine, and 10% FBS), or media with 1% serum (25 mM glucose, 6 mM glutamine, and 1% FBS) for 48 hours. Representative images shown in (A), and quantification of the percentage of cells with nuclear enrichment of polκ shown in (B). At least 150 cells were counted for each sample across 4 fields of view. All graphs are represented as mean ± S.E.M. Statistical analysis was performed using paired two-tailed t-tests (*$P < 0.05$, **$P < 0.01$, ***$P < 0.001$). All scale bars 10 μm.

We also tested whether ER stress, a common cell stress state, could similarly mimic this effect. Both glucose starvation and BRAF inhibition have been demonstrated to activate ER stress/the UPR (*191*, *193*, *359*, *360*), and we observed a similar induction in the expression of two UPR genes (ATF4 and CHOP) in A375 cells treated with PLX4032 (Figure 29, A and B). Furthermore, we also found that multiple ER stress activators (*193*) (i.e. brefeldin A, thapsigargin, tunicamycin) induced similar, if not identical, increases in nuclear polκ (Figure 29, C and D). This suggested to us that induction of ER stress could

potentially function downstream of stressors like MAPK inhibition and glucose starvation to mediate the shift of polκ from the cytoplasm into the nucleus.

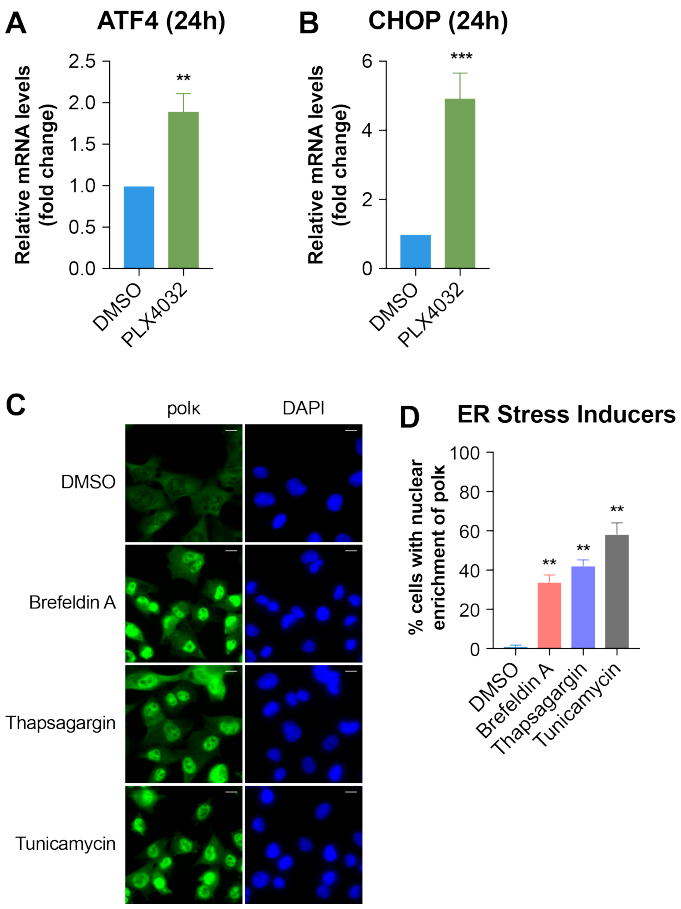

Figure 29. BRAF inhibition induces ER stress, and other inducers of ER stress also cause the shift.
(A) qRT-PCR to detect the expression of ATF4 relative to the DMSO control was performed on A375 cells treated with DMSO or 5 μM PLX4032 for 24 hours (n=11 experiments). **(B)** qRT-PCR to detect the expression of CHOP relative to the DMSO control was performed on A375 cells treated with DMSO or 5 μM PLX4032 for 24 hours (n=11 experiments). **(C-D)** Immunofluorescence staining for polκ was performed on A375 cells treated with DMSO, 5 μg/ml brefeldin A, 7.5 μM thapsigargin, or 10 μg/ml tunicamycin for 24 hours. Representative images shown in (C), and quantification of the percentage of cells with nuclear enrichment of polκ shown in (D). At least 100 cells were counted for each sample across 4 fields of view. All graphs are represented as mean ± S.E.M. Statistical analysis was performed using paired two-tailed t-tests (*$P < 0.05$, **$P < 0.01$, ***$P < 0.001$). All scale bars 10 μm.

2.2.5 mTOR inhibition rapidly induces polκ nuclear accumulation

We next turned to the pathways downstream of these effects. mTOR is the major downstream sensor of nutrient status, growth factor signaling, and cell stress (*235*) and can be thought of as analogous to the RpoS stress/starvation response required for bacterial SIM (*140*, *164*). In addition, multiple connections exist between the MAPK pathway (*252*, *256*, *257*, *259*), glucose starvation (*235*, *361–365*), and ER stress (*194*, *195*, *360*, *366*, *367*) and the PI3K-mTOR pathway. Based on this, we reasoned that the effects of MAPK inhibition and glucose starvation on polκ might be mediated via mTOR.

We first tested whether MAPK inhibition dampened downstream mTOR signaling in melanoma. We treated A375 cells with a BRAF inhibitor for 24 hours and then measured mTOR pathway activation using Western blot analysis to determine levels of phosphorylated Akt (p-Akt), phosphorylated S6 (p-S6), and phosphorylated 4E-BP1 (p-4E-BP1). We observed decreases in both p-S6 and p-4E-BP1 (which are targets of mTORC1) but not p-Akt (which is a target of mTORC2) (Figure 30, A and B) (*235*, *243*, *248*). We were able to verify these results using immunofluorescence against p-S6, which also revealed a potent decrease in p-S6 levels after treatment with PLX4032 (Figure 30, C and D). Furthermore, this inversely correlated with the shift of polκ to the nucleus: cells with the lowest level of p-S6 had the highest levels of nuclear polκ (Figure 30E). We also observed the decrease in p-S6 when using MEK or ERK inhibitors (Figure 30, F and G).

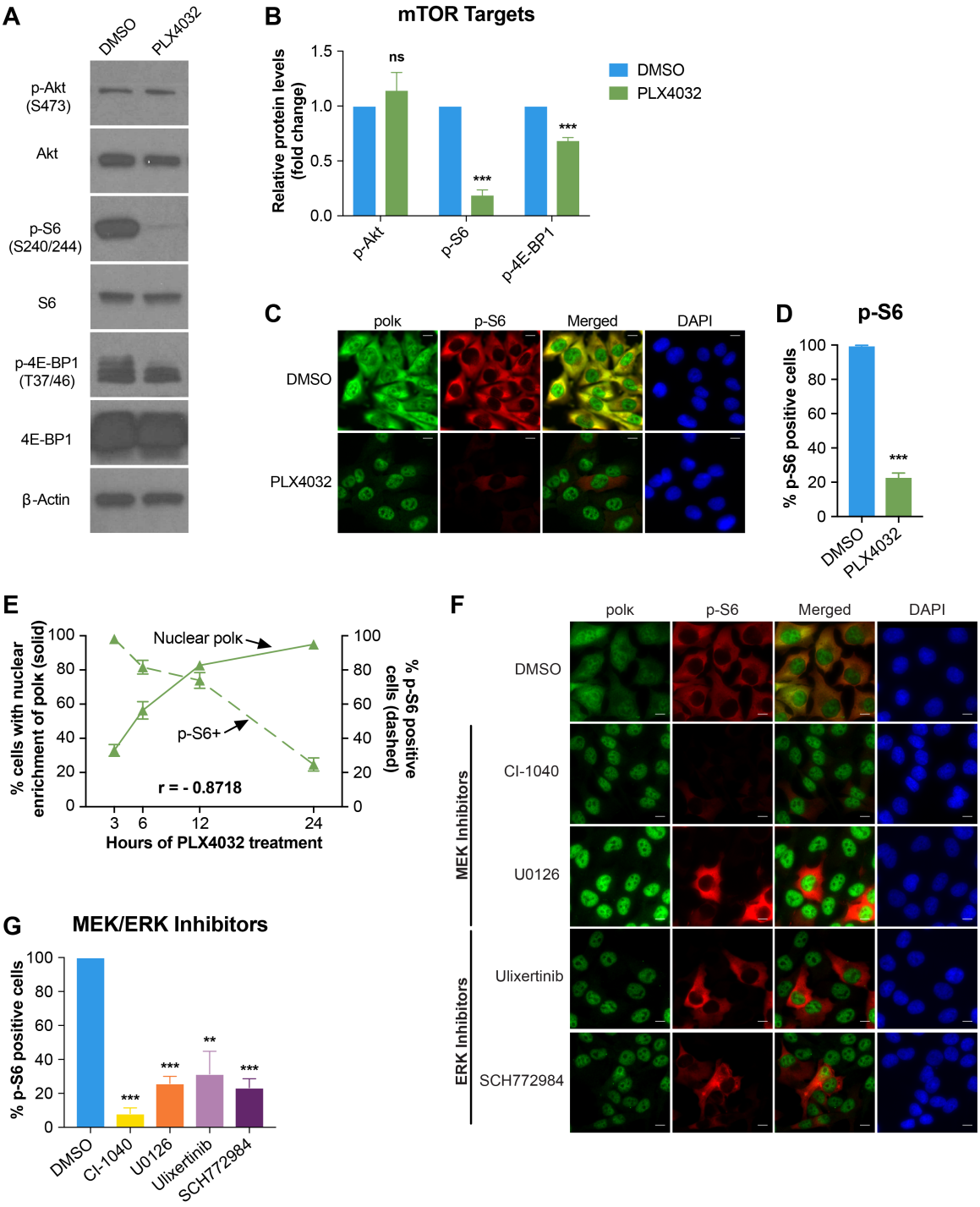

Figure 30. MAPK inhibition decreases the levels of phospho-S6 and other targets of mTOR.

(A-B) Western blot analysis for Akt, S6, and 4E-BP1 (phosphorylated and total) was performed on A375 cells treated with DMSO or 5 μM PLX4032 for 24 hours. Representative blot shown in (A), and quantification of 5-7 experiments relative to the DMSO control shown in (B). β-actin was used as the loading control. **(C-D)**

Immunofluorescence staining for polκ and phospho-S6 (p-S6, S240/244) was performed on A375 cells treated with DMSO or 5 μM PLX4032 for 24 hours. Representative images shown in (C), and quantification of the percentage of cells with p-S6 shown in (D). At least 400 cells were counted for each sample across 8 fields of view. **(E)** Immunofluorescence staining for polκ and p-S6 was performed on A375 cells treated with 5 μM PLX4032 for 3, 6, 12, or 24 hours. The graph shows the percentage of cells with nuclear enrichment of polκ (left axis, solid line) and the percentage of cells with p-S6 (right axis, dashed line). At least 150 cells were counted for each sample across 4-8 fields of view. The Pearson correlation coefficient (r) was calculated for the percentage of cells with nuclear enrichment of polκ vs. the percentage of cells with p-S6. **(F-G)** Immunofluorescence staining for polκ and p-S6 was performed on A375 cells treated with DMSO, MEK inhibitors (10 μM CI-1040, 10 μM U0126), or ERK inhibitors (1 μM Ulixertinib, 1 μM SCH772984) for 24 hours. Representative images shown in (F), and quantification of the percentage of cells with p-S6 shown in (G). At least 150 cells were counted for each sample across 4 fields of view. All graphs are represented as mean ± S.E.M. Statistical analysis for all bar graphs was performed using paired two-tailed t-tests (ns = non-significant, *P < 0.05, **P < 0.01, ***P < 0.001). All scale bars 10 μm.

These observations prompted us to then test whether inhibitors of the PI3K-mTOR pathway itself would lead to an effect on polκ that was similar to either glucose deprivation or MAPK inhibition. We treated A375 melanoma cells with several inhibitors of the PI3K-mTOR pathway, including mTOR inhibitors (rapamycin or PP242) and a PI3K inhibitor (LY29002). We found that these inhibitors potently induced nuclear polκ to a level comparable to that seen with the BRAF/MEK/ERK inhibitors (Figure 31, A and B), but it occurred much more rapidly. Whereas the MAPK inhibitors took ~24 hours for full induction of nuclear polκ, the mTOR pathway inhibitors could do this in as little as ~3.5 to 6 hours. As with PLX4032, the decrease in p-S6 was inversely correlated with the increase in cells with nuclear polκ after treatment with rapamycin (Figure 31C) or the other inhibitors (data not shown). Finally, since S6 is directly phosphorylated by mTOR's downstream target S6K (*235*, *243*), we tested the effects of the S6K inhibitor PF-4708671 and found it also leads to robust nuclear accumulation of polκ (Figure 31, D and E). Overall, these studies provide a connection between stressors like BRAF

inhibition/glucose starvation, ER stress, and mTOR inhibition, demonstrating part of a potential mechanism through which cellular stress could influence polκ's subcellular localization.

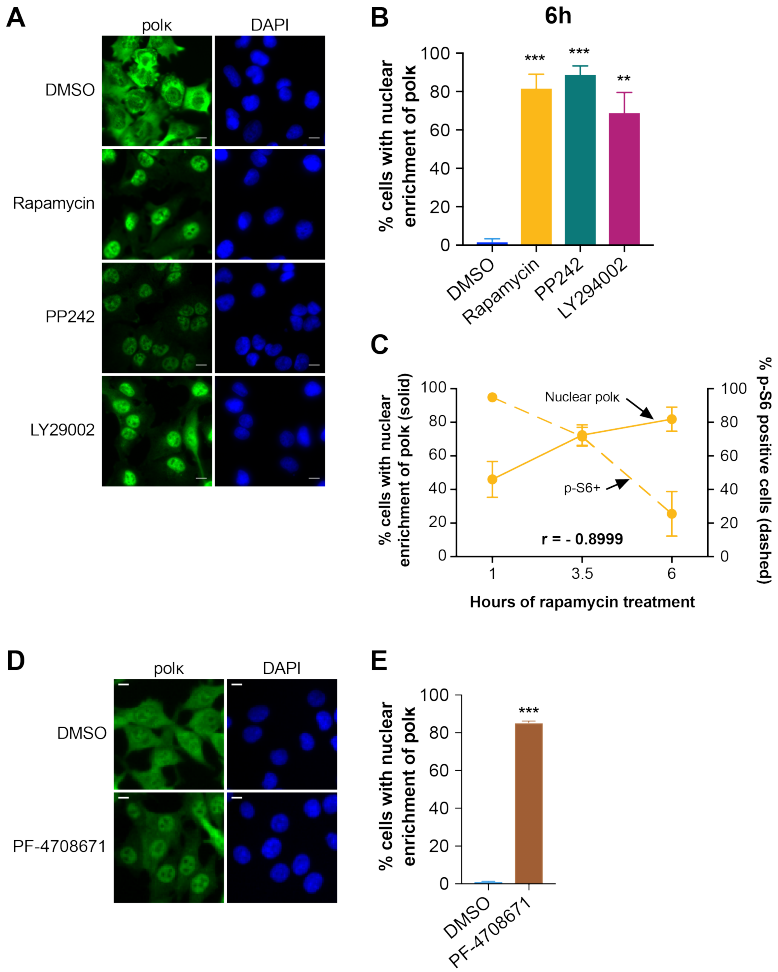

Figure 31. mTOR signaling regulates polκ's subcellular localization.
(A-B) Immunofluorescence staining for polκ was performed on A375 cells treated with DMSO, 0.5 μM rapamycin, 5 μM PP242, or 30 μM LY294002 for 6 hours. Representative images shown in (A), and quantification of the percentage of cells with nuclear enrichment of polκ shown in (B). At least 200 cells were counted for each sample across 8-12 fields of view. **(C)** Immunofluorescence staining for polκ and p-S6 was performed on A375 cells treated with 0.5 μM rapamycin for 1, 3.5, or 6 hours. The bar graph shows the percentage of cells with nuclear enrichment of polκ (left axis, solid line) and the percentage of cells with p-S6, (right axis, dashed line). At least 100 cells were counted for each sample across 4-12 fields of view. The Pearson correlation coefficient (r) was calculated for the percentage of cells with nuclear enrichment of polκ vs. the

percentage of cells with p-S6. **(D-E)** Immunofluorescence staining for polκ was performed on A375 cells treated with 10 μM PF-4708671 for 24 hours. Representative images shown in (D), and quantification of the percentage of cells with nuclear enrichment of polκ shown in (E). At least 6000 cells were counted for each sample across 16 fields of view. All graphs are represented as mean ± S.E.M. Statistical analysis of all bar graphs was performed using paired two-tailed t-tests (*$P < 0.05$, **$P < 0.01$, ***$P < 0.001$). All scale bars 10 μm.

2.2.6 polκ dysregulation occurs in other cancer types exposed to targeted inhibitors

We next wished to determine if the observed effects on polκ were specific to melanoma/the BRAF pathway or if they could be applied more broadly. To test this, we examined polκ mRNA levels and subcellular localization in breast and lung cancer cell lines, which harbor unique oncogenic dependencies that differ from melanoma. PC-9 lung cancer cells harbor activating mutations in EGFR and are critically dependent upon that growth factor signaling pathway. We treated PC-9 cells with either the EGFR inhibitor erlotinib (*368*) or the $BRAF^{V600E}$ inhibitor PLX4032 (which we would expect to have no effect as these cells contain wild-type BRAF) and then measured the expression of polκ and determined its localization. Both high and low doses of erlotinib caused induction of polκ mRNA and a shift of polκ to the nucleus in the PC-9 cells, but as expected, this effect was not seen with PLX4032 (Figure 32A and Figure 33, A and B). Analogous to what we observed for melanoma, this shift of polκ to the nucleus was accompanied by a loss of p-S6 in the lung cancer cells (Figure 33, A and C). A similar effect was seen in a breast cancer cell line. SK-BR3 cells, which overexpress the HER2 oncogene, were treated with the HER2 inhibitor lapatinib (*369*) or the $BRAF^{V600E}$ inhibitor PLX4032. Lapatinib caused a marked induction of polκ expression, nuclear accumulation of polκ, and suppression of p-S6 (Figure 32B and Figure 33, D to F), an effect that was not seen with PLX4032 as

expected. These results demonstrate that the observed effects on polκ are specific to the driver oncogene, and that they are generalizable to multiple cancer types.

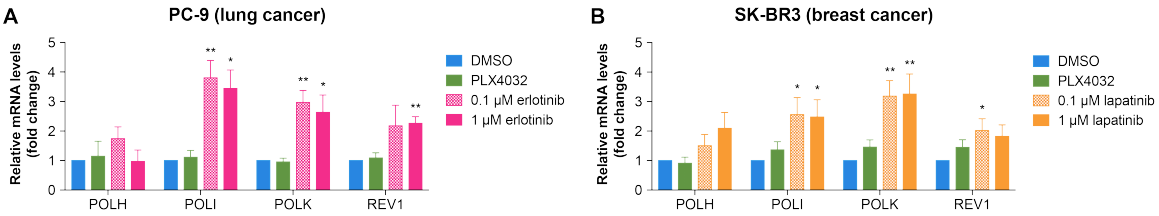

Figure 32. The effects on polκ mRNA levels are driver gene specific across tumor types.
(A) qRT-PCR to detect the expression of polη, polι, polκ, and Rev1 relative to the DMSO control was performed on the PC-9 human lung adenocarcinoma cell line treated with DMSO, 5 μM PLX4032, or erlotinib (0.1 μM or 1 μM) for 24 hours (n=6 experiments). **(B)** qRT-PCR to detect the expression of polη, polι, polκ, and Rev1 relative to the DMSO control was performed on the SK-BR3 human breast adenocarcinoma cell line treated with DMSO, 5 μM PLX4032, or lapatinib (0.1 μM or 1 μM) for 24 hours (n=9 experiments). All graphs are represented as mean ± S.E.M. Statistical analysis was performed using paired two-tailed t-tests (*$P < 0.05$, **$P < 0.01$, ***$P < 0.001$).

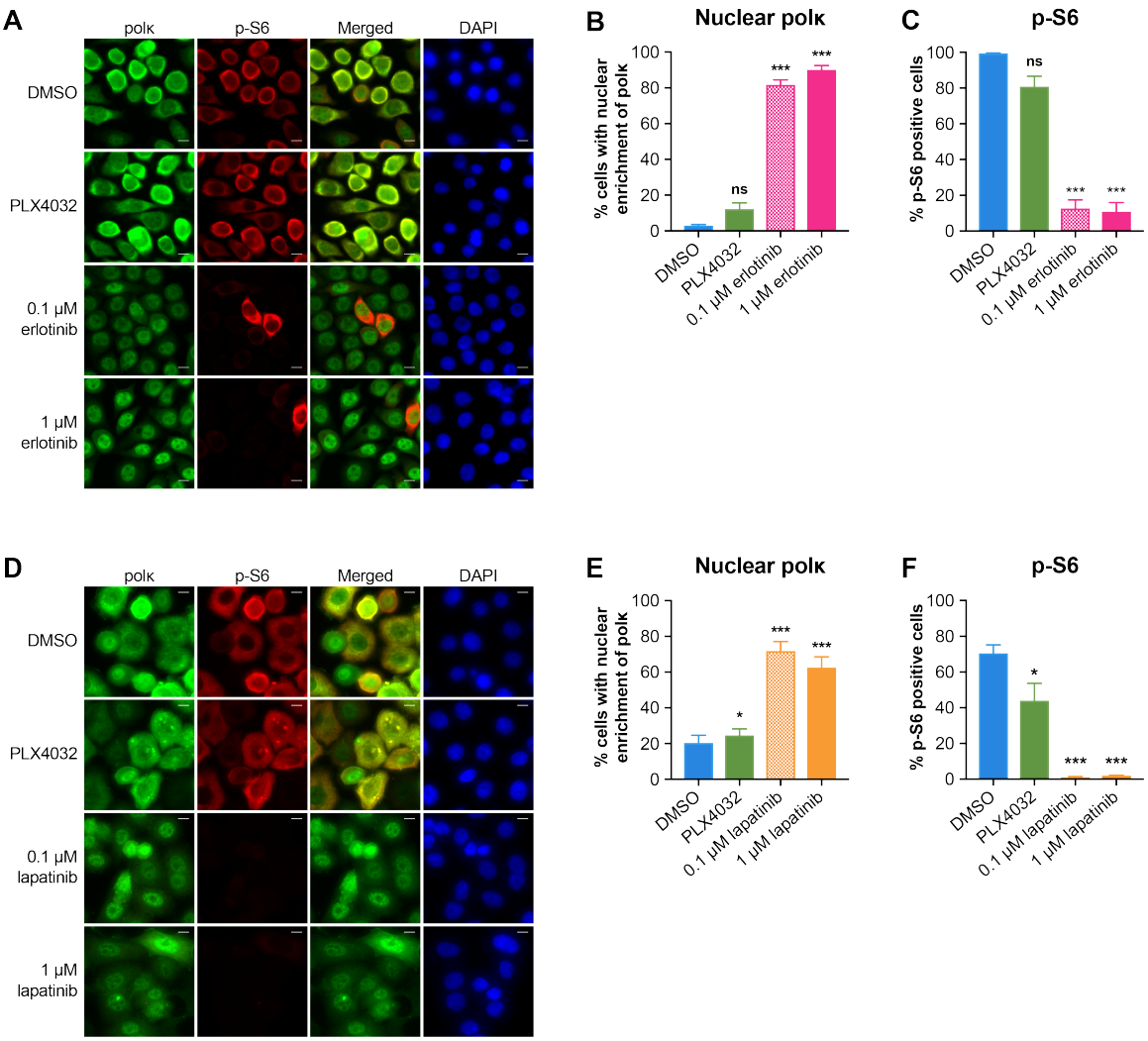

Figure 33. The effects on polκ's localization and p-S6 levels are driver gene specific across tumor types.

(A-C) Immunofluorescence staining for polκ and p-S6 was performed on PC-9 cells treated with DMSO, 5 μM PLX4032, or erlotinib (0.1 μM or 1 μM) for 24 hours. Representative images shown in (A), quantification of the percentage of cells with nuclear enrichment of polκ shown in (B), and quantification of the percentage of cells with p-S6 shown in (C). At least 100 cells were counted for each sample across 4 fields of view. **(D-F)** Immunofluorescence staining for polκ and p-S6 was performed on SK-BR3 cells treated with DMSO, 5 μM PLX4032, or lapatinib (0.1 μM or 1 μM) for 24 hours. Representative images shown in (D), quantification of the percentage of cells with nuclear enrichment of polκ shown in (E), and quantification of the percentage of cells with p-S6 shown in (F). At least 200 cells were counted for each sample across 7 fields of view. All graphs are represented as mean ± S.E.M. Statistical analysis was performed using paired two-tailed t-tests (ns = non-significant, *$P < 0.05$, **$P < 0.01$, ***$P < 0.001$). All scale bars 10 μm.

2.2.7 Exportin-1 plays a role in regulating the subcellular localization of polκ

This data led us to ask what mechanisms the cells may use to control cytoplasmic versus nuclear localization of polκ. A previous analysis demonstrated that full-length polκ contains a bipartite NLS towards its 3' end (*274*, *342*), and computational analysis (*370*) also indicates a likely NES. Deletion of the NLS region results in the protein completely localizing to the cytoplasm (*274*), which suggested to us that the localization results we saw above might be controlled by the nuclear import and/or export machinery. To test this, we utilized inhibitors of the major import (importin-β) or export (exportin-1) factor and tested whether they affected the shift of polκ in response to BRAF inhibition in melanoma cells. We found that importazole, which inhibits importin-β (*285*), had little effect on polκ localization when combined with PLX4032 (Figure 34) or PI3K/mTOR inhibitors (data not shown). This suggests polκ utilizes a different nuclear transport protein for its import, and further work is required to determine which one is responsible.

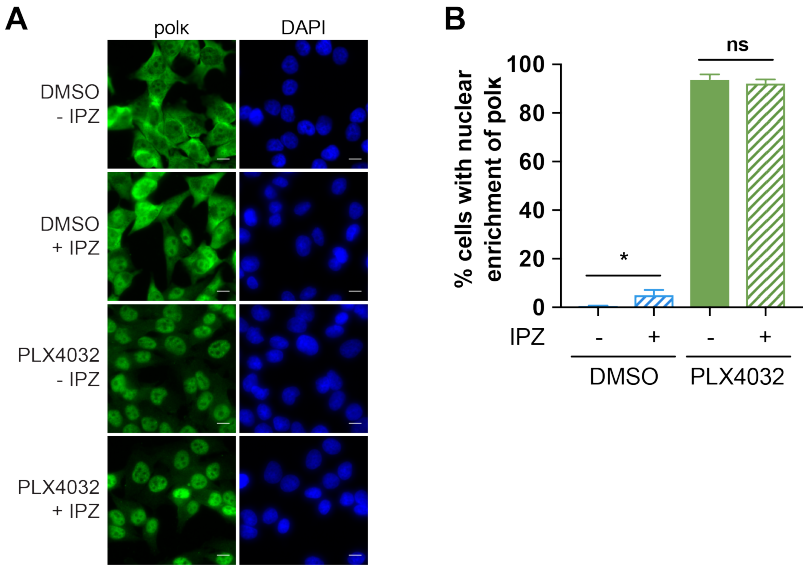

Figure 34. Inhibiting importin-β does not prevent the nuclear shift of polκ.
(A-B) Immunofluorescence staining for polκ was performed on A375 cells treated with

DMSO or 5 μM PLX4032 ± 20 μM importazole (IPZ) for 24 hours. Representative images shown in (A), and quantification of the percentage of cells with nuclear enrichment of polκ shown in (B). At least 350 cells were counted for each sample across 8 fields of view. All graphs are represented as mean ± S.E.M. Statistical analysis was performed using paired two-tailed t-tests (ns = non-significant, *P < 0.05, **P < 0.01, ***P < 0.001). All scale bars 10 μm.

In contrast, co-treatment with leptomycin B, which inhibits exportin-1 (*295*), accelerated the rate at which polκ localized to the nucleus: whereas 3 hours of PLX4032 typically only leads to ~30% induction of nuclear polκ, in the presence of leptomycin B, this increased to 60% (Figure 35, A to C). In addition, we noted that leptomycin B alone (even in the absence of PLX4032) induced a small but significant increase in nuclear polκ, indicating that polκ normally cycles between the cytoplasm and nucleus, and the BRAF/mTOR inhibitors likely act to prevent nuclear export of polκ. To further test the contribution of the nuclear export machinery, we performed washout experiments. A375 cells were treated with PLX4032 (to induce nuclear polκ) and then after 24 hours, the drug was washed away (Figure 35D). After washout and replacement with DMSO, polκ relocates to the cytoplasm within 24 hours, demonstrating the responsiveness of the system to changes in cellular conditions. However, if leptomycin B is added after PLX4032 washout instead, polκ remains present in the nucleus (Figure 35, E and F). This data indicates that oncogenic signaling regulates the nuclear localization of polκ (at least in part) through the export machinery.

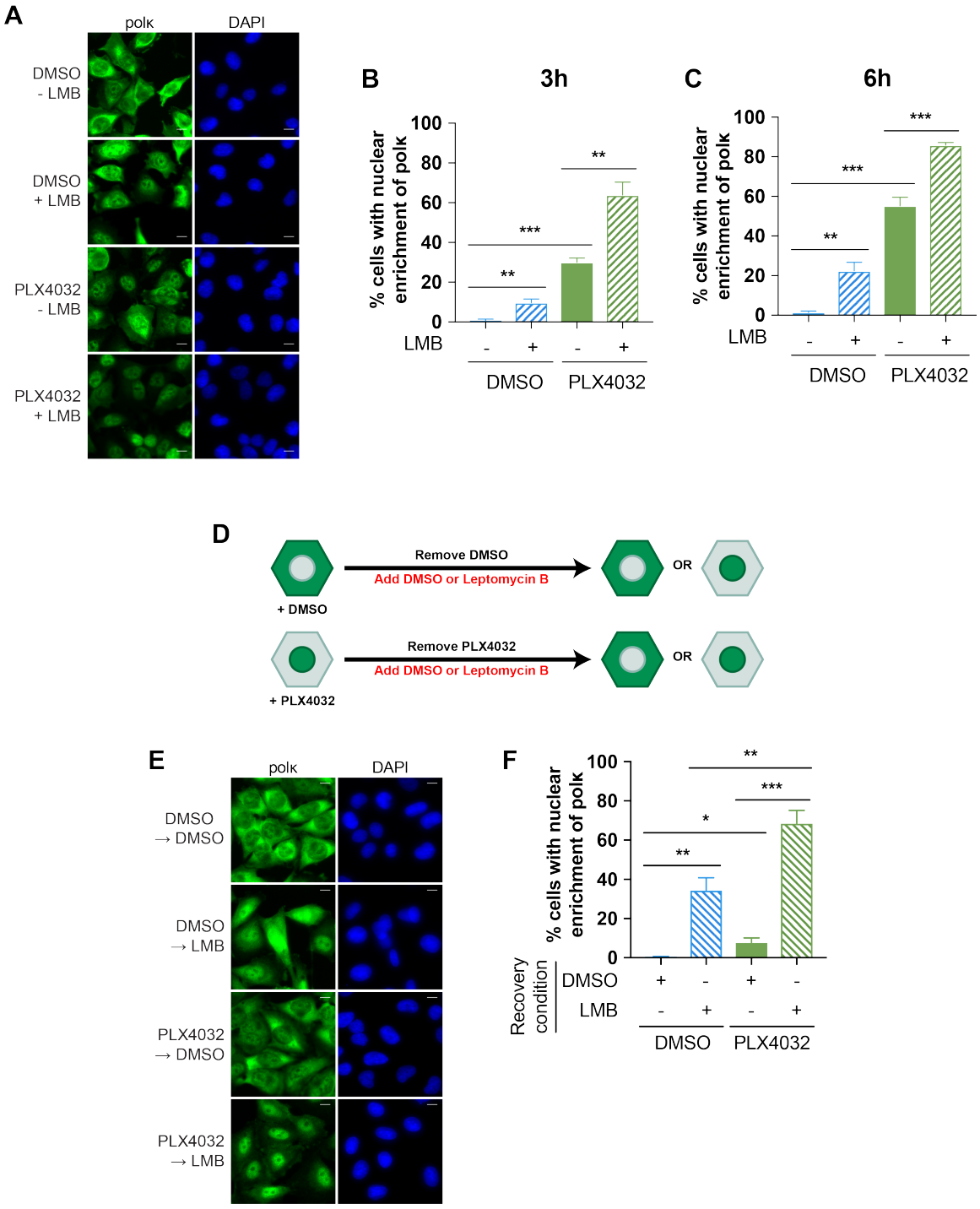

Figure 35. Exportin-1 plays a role in the subcellular localization of polκ.
(A-C) Immunofluorescence staining for polκ was performed on A375 cells treated with DMSO or 5 μM PLX4032 ± 20 μM leptomycin B (LMB) for 3 or 6 hours. Representative images after 6 hours shown in (A), and quantification of the percentage of cells with nuclear enrichment of polκ shown in (B) and (C). At least 100 cells were counted for each sample across 4-8 fields of view. **(D)** Schema detailing the experiment design for

the washout assay. **(E-F)** Immunofluorescence staining for polκ was performed on A375 cells treated with DMSO or 5 μM PLX4032 for 24 hours and then DMSO or 10 μM LMB for 24 hours (washout assay). Representative images shown in (E), and quantification of the percentage of cells with nuclear enrichment of polκ shown in (F). At least 100 cells were counted for each sample across 7 fields of view. All graphs are represented as mean ± S.E.M. Statistical analysis was performed using paired two-tailed t-tests (*$P < 0.05$, **$P < 0.01$, ***$P < 0.001$). All scale bars 10 μm.

2.3 Discussion

polκ belongs to a family of related Y family DNA polymerases which all function in TLS, a major DNA damage tolerance pathway (*159*, *333*). In normal physiology, these polymerases play an important role in bypassing stalled replication forks that are induced by DNA-damaging agents. Because they all lack proofreading domains, they have a propensity to introduce errors during replication, although depending on the specific lesion, they can also act in an error-free manner. For this reason, these Y family polymerases can be a double-edged sword since they enable cell survival by replicating past regions of damaged DNA but may do so at a cost of new mutations (*371*). Various *in vitro* studies have demonstrated that these polymerases can act with extraordinarily low fidelity, with error rates ranging from 10^{-1} to 10^{-4}, compared to 10^{-5} to 10^{-6} for the normal replicative polymerases polδ and polε (*5*, *6*, *339*, *372*). Therefore, it is important that cells regulate the expression and localization of these polymerases such that they only act when the cell is under genomic stress. Furthermore, several studies have now identified overexpression of polκ in human tumors such as lung cancer or glioma (*132*, *136*), and this has been associated with increased mutation rates as well as drug resistance (*137*, *334*). However, despite the potential importance of polκ in promoting tumor progression, little was previously known about the mechanisms by which it is regulated.

Although DNA damage is likely the major inducer of polκ, our data would suggest that mammalian cells harbor the capacity to influence the expression and localization of polκ under other forms of cell stress, namely loss of oncogenic signaling and/or nutrient starvation. This may be analogous to *E. coli*, whereby cells under starvation stress can upregulate DinB/pol IV (the bacterial ortholog of polκ) (*99*, *140*). However, whereas bacteria use a two-step system for SIM: the SOS response to regulate DinB expression (*139*, *147*) and then the RpoS response to regulate its access to DNA (*140*, *163*), our data would suggest that mammalian cells instead mainly regulate polκ via the nuclear import/export machinery. Activation of the DDR pathway (the human equivalent of the SOS response (*62*, *147*, *160*)) is not required for this regulation, but the mTOR pathway (the human equivalent of the RpoS response (*161–164*)) plays a key role in regulating the localization of polκ. The mPI3K-mTOR pathway and starvation more broadly are known to affect nuclear-cytoplasmic shuttling of multiple proteins (*319*, *323*, *324*, *327*, *329*, *330*, *332*, *373*), and one possible explanation for our observed results is that mTOR (or one of its downstream substrates) could directly phosphorylate polκ, and this phosphorylation could affect its localization as has been shown for other proteins that undergo nuclear-cytoplasmic shuttling (*297*, *298*, *374*, *375*). An important area for future exploration is understanding the ways in which mTOR may interact with the maintenance of genome stability.

Finally, an unexpected finding in our study was the observation that polκ can exist in a cytoplasmic form. Prior studies have shown that polκ is primarily a nuclear protein, but these relied upon overexpression of an eGFP-polκ fusion protein (*273*, *274*). In our hands, overexpression of polκ also strongly upregulated nuclear expression, which we

believe likely reflects saturation of the export machinery. This would be consistent with our data using leptomycin B, which suggested that one important mechanism of regulation for polκ is nuclear-cytoplasmic shuttling. A few other studies have also observed scant cytoplasmic polκ in HeLa cells, including data from the Human Protein Atlas (*356*), which used antibodies raised against peptide antigens. One important difference in our studies is that we used a monoclonal antibody raised against the full-length protein. Examination of polκ transcript variants in Ensembl (*376*) reveals that humans transcribe up to 5 protein-coding transcripts of polκ, such that antibodies raised against short peptides versus full-length protein may recognize different transcripts with different localizations. Interestingly, another Y family polymerase polη has also been reported to have nuclear localization when overexpressed as an eGFP fusion protein (*271*), yet data from the Human Protein Atlas (*356*) shows a predominantly cytoplasmic localization with nuclear enrichment in some cells, similar to what we see with polκ. The exact reasons for these discrepancies will await further studies of the polκ/polη structure with regards to post-translational modifications of nuclear localization/export signals or variations in transcript abundance in different cell types.

CHAPTER 3: FUNCTIONAL CONSEQUENCES OF HIGH LEVELS OF NUCLEAR POLK

3.1 Introduction

Chapter 2 detailed a mechanism by which polκ's expression and localization are regulated in response to cellular stresses. In unstressed cells, polκ is predominantly cytoplasmic, but it shifts into the nucleus in response to stressors like MAPK inhibition and glucose starvation. Furthermore, removal of the stress results in a rapid return of polκ back to the cytoplasm. This dynamic regulation of polκ's localization suggests that well-adapted cells actively sequester polκ in the cytoplasm, likely to keep it from accessing DNA. The reasons for this and the potential functional consequences of inappropriate access of DNA by polκ are explored in this chapter.

polκ plays a major role in TLS, where it replicates past bulky lesions, including minor-groove N_2-deoxyguanine adducts, benzo[a]pyrene adducts, and ICLs (*6*, *20*), and it has also been implicated in NER and HR (*34*, *82*). However, despite its role in multiple DNA damage repair/tolerance pathways, polκ has a much higher mutation rate than the replicative DNA polymerases polδ and polε, especially when replicating on undamaged DNA. This is due to lack of a proofreading domain and decreased nucleotide selectivity due to a larger active site (*6*, *20*). As a result, polκ can be a double-edged sword since it can allow for error-free TLS (which is necessary for cell survival) but may introduce new mutations (which can be detrimental to cell survival) (*371*). This means that both loss and overexpression of polκ can be mutagenic (*37*, *38*, *338*, *377*) albeit for different reasons: whereas knockout abrogates high fidelity TLS and DNA repair on damaged DNA,

overexpression is directly mutagenic to undamaged DNA. As would be expected with a higher mutation rate, overexpression of polκ has been identified in both lung cancer and glioma (*132*, *136*), and it has also been linked to increased resistance to temozolomide in glioblastoma (*137*).

We had previously demonstrated that overexpression of polκ subverts the normal dynamic regulation of its subcellular localization and results in increased nuclear levels of polκ (Figure 23, B and C), likely due to saturation of the nuclear export machinery. We thus decided to use a polκ overexpression construct in the A375 human melanoma cell line as well as a zebrafish model of melanoma to explore potential functional consequences of having high levels of nuclear polκ. This allowed us to mirror the nuclear shift of polκ observed in response to MAPK inhibition and glucose starvation but in a simpler system (ex: no cell cycle inhibition). We specifically focused on the functional consequences of mutagenesis, drug resistance, and tumorigenesis.

3.2 Results

3.2.1 polκ overexpression can lead to increased mutagenesis

We hypothesized that the major reason that cells actively sequester polκ in the cytoplasm is due to its potential mutagenic capabilities when replicating on undamaged DNA. This is because ectopic expression of polκ has been demonstrated to promote its nuclear localization, enable it to become part of the replication machinery in the absence of external stress, and generate new mutations (*273*). To test this in our A375 human melanoma cells, we generated a dox-inducible polκ overexpression construct. We transduced this construct into our cells and then isolated multiple single cell clones from

this population (Clone #1 and Clone #2) and expanded them for future use. As expected, these cells showed strong induction with increased nuclear localization of polκ after addition of dox compared to uninduced control cells (Figure 23, B and C).

The hypoxanthine phosphorybosyl transferase (HPRT) gene mutation assay is the gold standard for investigating mutagenesis in mammalian cells (*378–380*). HPRT is a transferase that normally catalyzes the conversion of guanine into guanine monophosphate as part of the nucleotide salvage pathway. 6-thioguanine (6-TG) is an analogue of guanine that can also be processed by HPRT into 6-thioguanosine monophosphate, which is toxic to cells. Therefore, in the presence of 6-TG, cells with functional HPRT will die while those with mutant HPRT will survive. As the *HPRT* gene is encoded on the X chromosome (meaning only one copy is expressed per cell), the HPRT gene mutation assay can be used to determine mutation rate in response to chemical treatments and genetic manipulations (*378*). We attempted to use this assay with our dox-inducible polκ overexpression cells to investigate the effects of polκ overexpression on the mutation rate; however, the results were inconclusive (data not shown).

Therefore, we developed a flow cytometry-based GFP mutagenesis assay as an alternative approach. The cDNA for green fluorescent protein (GFP) was originally isolated from the jellyfish *Aequorea victoria* and shown to be capable of being expressed in prokaryotic and eukaryotic cells in order to monitor gene expression and protein localization (*381*). When exposed to blue light, GFP emits green light, and modifications to the original GFP molecule have increased its stability and brightness, allowing its use in flow cytometry, immunofluorescence, and live-cell imaging (*381*, *382*). Previous work in bacteria, mammalian cell lines, and whole animals has demonstrated that GFP can be used

to measure cellular mutation rates. In those systems, mutant GFP (often containing a premature STOP codon) is expressed, and the mutation rate is determined using gain-of-function mutations that restore fluorescence (*383–387*). However, because only certain mutations will restore functionality, it is not a complete measurement.

We decided to use a similar concept but instead express a functional copy of GFP and then use loss-of-function mutations to compare mutation rates between cells overexpressing polκ and those expressing normal levels. To do so, we used our dox-inducible polκ overexpression A375 cell line and transduced in a SV40p-GFP construct, which allows for constitutive expression of GFP under the SV40 promoter. We could then treat our cells either with dox (to induce polκ) or without dox (acting as control cells) and use flow cytometry to determine the mean GFP intensity of each population (Figure 36A). Comparison of polκ-OE samples to the - CTRL sample for both clones revealed a small but significant decrease in the mean GFP intensity (Figure 36B). This confirms that in melanoma, as in other cell types (*37*), polκ overexpression can act to increase the mutation rate. Because the rate of mutagenesis we observed was modest, this data also suggested that other defects in DNA repair (i.e. MMR) would likely be required to achieve a higher mutation rate.

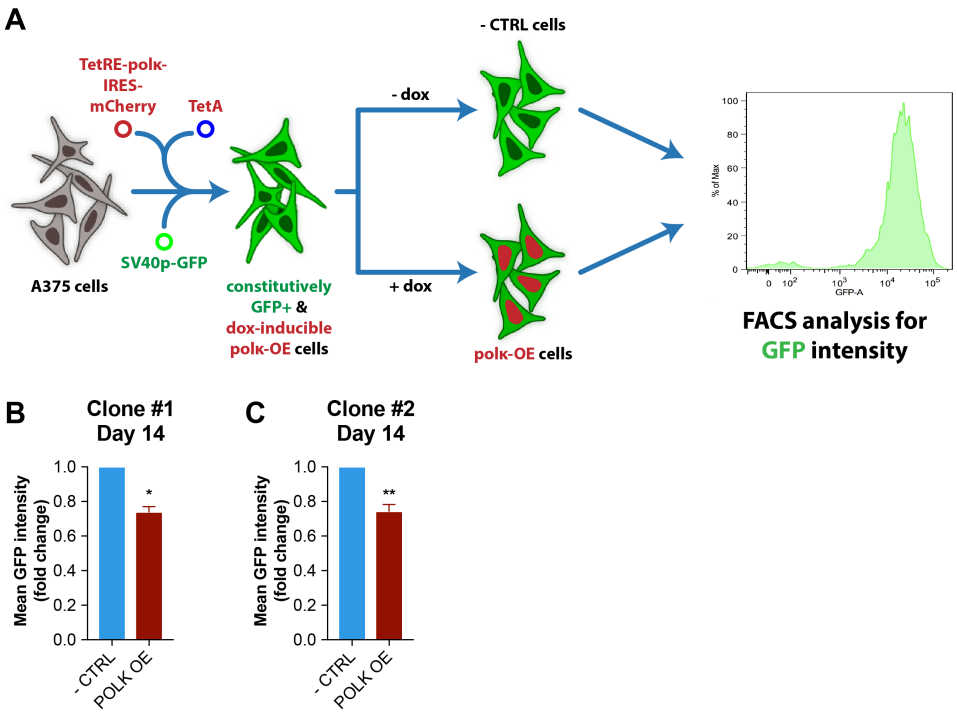

Figure 36. polκ overexpression is mutagenic in human melanoma cells.
(A) Schema detailing how single cell clones of A375 cells containing the SV40p-GFP and dox-inducible polκ overexpression constructs were created and how the dox- and dox+ populations were generated and then used to measure mean GFP intensity (as a proxy for mutagenesis). **(B)** Mean GFP intensity of dox- (- CTRL) and dox+ (polκ OE) populations of two different clones of dox-inducible polκ overexpression cells was determined via flow cytometry after 14 days of treatment, and then both samples were normalized to the dox- population (n=3-5 experiments). All graphs are represented as mean ± S.E.M. Statistical analysis was performed using paired two-tailed t-tests (*P < 0.05, **P < 0.01, ***P < 0.001).

3.2.2 polκ overexpression can lead to increased drug resistance

In bacteria, activation of the stress-induced DinB response leads to new mutations, and any individual harboring a beneficial mutation will then overtake the population. This has been shown to occur in response to starvation but also during the development of antibiotic resistance (*141*, *388*, *389*). Therefore, we hypothesized that subverting the normal shuttling of polκ and forcing it to remain nuclear could contribute to drug resistance due to its capacity for inducing new mutations. To test this, we used our dox-

inducible polκ overexpression A375 cells (without the GFP expression) and expanded them in culture in the presence or absence of dox for 3 months. We then tested both populations for sensitivity to the $BRAF^{V600E}$ inhibitor PLX4032 (Figure 37A). For both clones, the population that had experienced long-term polκ overexpression showed a modest increase in growth in PLX4032 across multiple different doses compared to its respective negative control cells (Figure 37B), consistent with increased resistance to the drug. This is consistent with the concept that prolonged nuclear expression of polκ is associated with resistance to certain clinically relevant cancer therapeutics, such as BRAF inhibitors.

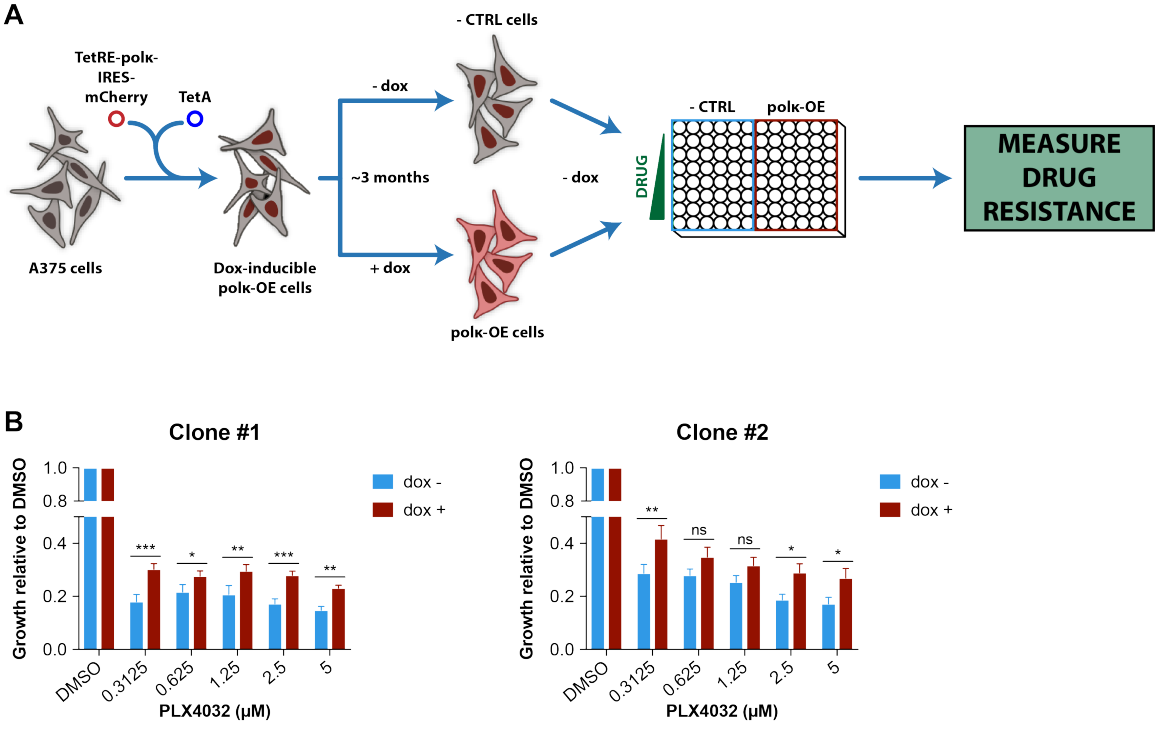

Figure 37. polκ overexpression can lead to increased drug resistance.
(A) Schema detailing how single cell clones of A375 cells containing the dox-inducible polκ overexpression construct were created and how the dox- and dox+ populations were generated and then used to measure drug resistance. **(B)** Drug resistance of the dox- and dox+ populations of two different clones of dox-inducible polκ overexpression cells to

PLX4032 was determined by the CyQuant Direct assay. For each population, the relative cell viability at each dose, compared with the 0 μM dose control (DMSO), was calculated for 4-5 experiments. All graphs are represented as mean ± S.E.M. Statistical analysis was performed using Fisher's Least Significant Difference test (*$P < 0.05$, **$P < 0.01$, ***$P < 0.001$). A comparison between the two populations in their response to PLX4032 by two-way ANOVA gave a p-value of 0.0130 for Clone #1 and of 0.0294 for Clone #2.

3.2.3 polκ overexpression can lead to increased tumorigenesis in zebrafish

Finally, we wished to determine if the mutagenic capabilities of polκ could accelerate tumor development *in vivo*. To test this, we used our previously developed zebrafish model of melanoma (*266*). In this model, expression of $BRAF^{V600E}$ is confined to melanocytes via the mitfa promoter. When crossed with p53-deficient zebrafish, 100% of the resultant animals develop highly stereotyped melanomas by 2 years. To test the effect of polκ in this model, we generated a new transgenic animal in which the ubiquitin promoter drives zebrafish polκ-2A-GFP, allowing us to directly compare tumor onset in mitfa-$BRAF^{V600E}$;$p53^{-/-}$;ubi-zpolκ-2A-GFP zebrafish versus mitfa-$BRAF^{V600E}$;$p53^{-/-}$ sibling controls (Figure 38A). One advantage of this system is that because polκ is driven ubiquitously, it allows us to see effects on both melanoma and other non-melanoma tumors generated by polκ. Kaplan-Meier analysis of melanoma burden showed a significant acceleration of tumor formation in the mitfa-$BRAF^{V600E}$;$p53^{-/-}$;ubi-zpolκ-2A-GFP animals when compared to the control fish (Figure 38B) without any differences in overall histology (Figure 38C).

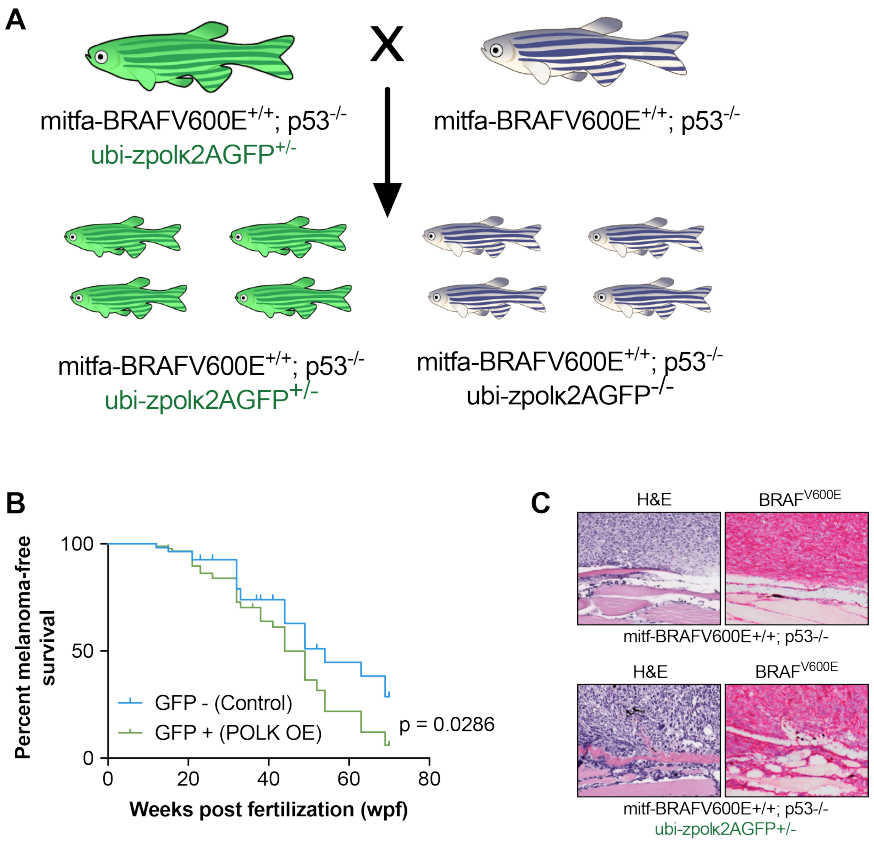

Figure 38. polκ overexpression augments tumorigenesis.
(A-B) Melanoma-free survival was measured in melanoma-prone zebrafish (mitfa-BRAF^{V600E};p53$^{-/-}$) overexpressing zebrafish polκ (ubi-zpolκ2AGFP) (n=89) and negative sibling controls (n=55). Diagram detailing the cross to produce each population (A) and Kaplan–Meier survival curve (B) showing melanoma-free survival of polκ-overexpressing (GFP-positive) zebrafish and sibling controls (GFP-negative), p = 0.0286, log-rank (Mantel-Cox) test. **(C)** H&E and BRAF^{V600E} staining in mitfa-BRAF^{V600E};p53$^{-/-}$ and mitfa-BRAF^{V600E};p53$^{-/-}$;ubi-zpolκ2AGFP melanomas.

Interestingly, some polκ-overexpressing animals developed atypical (i.e. non-melanoma) tumors that do not express BRAF^{V600E}, including a neuroblastoma (Figure 39). There were not enough atypical tumors to properly do statistics, and so we are unable to make any strong conclusions from this data. However, the lack of BRAF^{V600E} in these tumors does suggest that it is the combination of polκ and p53$^{-/-}$ that is responsible, and that the mutagenic capabilities of polκ are potentially capable of generating a new

oncogenic driver. Overall, in line with the *in vitro* effects, these data demonstrate that overexpression of polκ can accelerate tumor development *in vivo*.

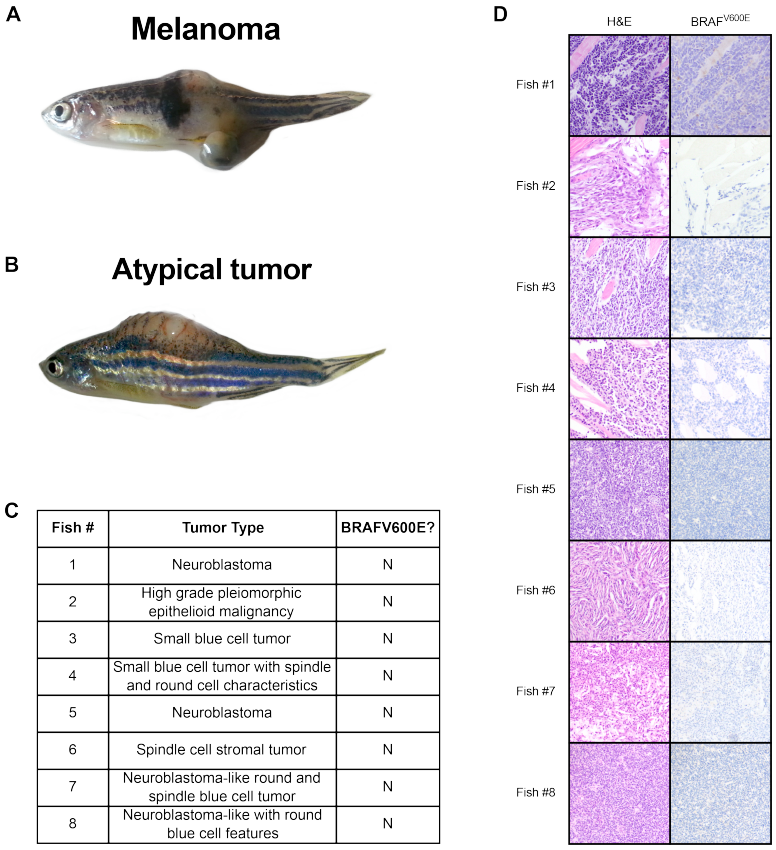

Fish #	Tumor Type	BRAFV600E?
1	Neuroblastoma	N
2	High grade pleiomorphic epithelioid malignancy	N
3	Small blue cell tumor	N
4	Small blue cell tumor with spindle and round cell characteristics	N
5	Neuroblastoma	N
6	Spindle cell stromal tumor	N
7	Neuroblastoma-like round and spindle blue cell tumor	N
8	Neuroblastoma-like with round blue cell features	N

Figure 39. Examples of atypical tumors found in polκ-overexpressing zebrafish. **(A-B)** Representative fish with melanoma (A) or an atypical tumor (B). **(C)** Table listing the fish with atypical tumors, their tumor type diagnosis, and $BRAF^{V600E}$ status. Fish #1 is shown as the representative fish in (B). **(D)** H&E and $BRAF^{V600E}$ staining in mitfa-$BRAF^{V600E}$;$p53^{-/-}$;ubi-zpolκ2AGFP atypical tumors.

3.3 Discussion

Our data suggest a mechanism by which mammalian cancer cells regulate the levels and localization of the error-prone DNA polymerase polκ, dysregulation of which can contribute to drug resistance and tumorigenesis. One implication of this is that polκ may play a role in resistance to targeted therapies. A previous study showed that polκ

could mediate resistance to the DNA-damaging agent temozolomide (*137*), but no studies have directly linked polκ to non-mutagenic therapies such as $BRAF^{V600E}$ inhibitors. Increased resistance to BRAF inhibitors is sometimes linked to the emergence of new clones with distinct mutational profiles (*212*, *222*, *223*, *227*, *229*, *390*, *391*). There has been much debate whether mutations causing drug resistance are pre-existing or acquired as they are often, although not always, found to be pre-existing upon deep sequencing (*392*). However, the two possibilities are not mutually exclusive. Here we have demonstrated a mechanism through which certain forms of cell stress could lead to prolonged overexpression of polκ, resulting in new mutations in the population (i.e. acquired resistance). Furthermore, we observed that stresses other than targeted inhibitors (ex: glucose starvation) resulted in a similar activation of polκ, suggesting stress-induced polκ activity could be responsible for the generation of pre-existing mutations as well. Given the fact that the resistance phenotype we saw from such overexpression was modest, it is highly likely that there would need to be other defects in DNA repair, such as MMR, for this to become a major mechanism of drug resistance. Nevertheless, it is important to note that we cannot exclude other, non-mutagenic functions of polκ that could account for the increased drug resistance, the elucidation of which will require future evaluation.

One interesting outcome of our study is the possibility that one could therapeutically target polκ, which has been proposed as a form of anti-evolution therapy. By decreasing the mutation rate, one could delay tumor progression and thus decrease the fitness of the tumor (*393*). However, because polκ is essential for physiologic DNA repair and TLS, complete inhibition or deletion of polκ can itself be mutagenic (*38*, *377*). Indeed,

mouse models and patient biopsies have shown that overexpression (*37*, *136*, *334*, *338*) as well as loss (*34*, *38*, *344*, *377*) of polκ are both tumor-inducing and mutagenic and can be associated with changes in sensitivity to chemotherapy (*137*). Whether there is a therapeutic window in which selective application of polκ inhibitors (*394*, *395*) could be advantageous is a major unanswered question in the field that awaits further study.

Alternatively, therapies could instead be created to exploit this increased mutation rate and push it over the edge, such that the cells start accumulating deleterious mutations (Figure 40) as is seen in patients with constitutive hypermutagenesis due a mutation in the proofreading domain of the replicative DNA polymerases polδ and polε (*3*, *126*, *127*).

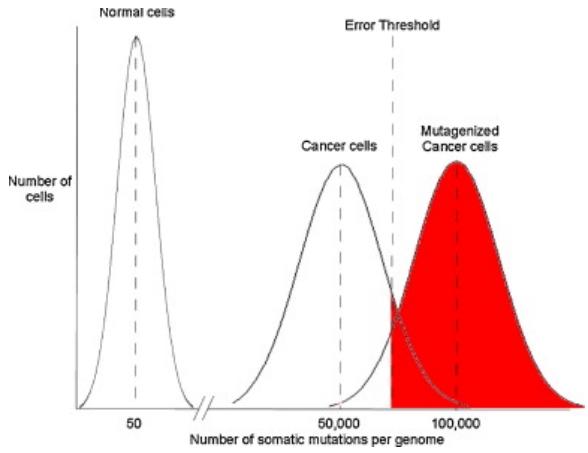

Figure 40. Lethal mutagenesis of cancer.
Normal cells maintain a low mutation rate due to high fidelity DNA replication and various DNA damage repair pathways. These pathways are often dysregulated in cancer, resulting in a mutator phenotype. While this increased mutation rate can promote tumor progression, a threshold exists above which viability greatly declines. Therapies that push cancer cells past that threshold could potentially be effective at treating cancer. Figure adapted from (*393*).

Support for this idea comes from the concept of lethal mutagenesis, which has been demonstrated in viruses (*396–399*) and theorized could be possible in bacteria (*400*,

401) and human cancer (*393*). Since the majority of mutations are neutral or deleterious in the absence of selective pressures (*402*, *403*), lethal mutagenesis operates on the principle that raising the mutation rate past a specific threshold will generate a load of deleterious mutations that results in population decline. In addition, because the detrimental consequences of lethal mutagenesis will not manifest for many generations, the mechanism of killing is uncoupled from drug exposure, which decreases the risk of resistance developing (*393*).

CHAPTER 4: CONCLUSION AND FUTURE DIRECTIONS

4.1 General conclusions and summary

In this study, we have investigated the effects of cellular stresses on the activity of the error-prone DNA polymerase polκ, the mechanism behind those effects, and the functional consequences of polκ overexpression on mutagenesis, drug resistance, and tumorigenesis. Based on all our data, we propose the following mechanism for the regulation of polκ localization under both normal and stressful conditions (Figure 41). Under normal conditions, mTOR signaling is high, and polκ is predominantly cytoplasmic. Some polκ is imported into the nucleus, but it is rapidly exported out by exportin-1. On the other hand, during stressful conditions, such as glucose starvation, MAPK inhibition, or ER stress, there is a decrease in mTOR signaling. Via a yet-to-be-determined mechanism, this reduction in mTOR signaling enables polκ to localize to the nucleus, and exportin-1 is unable to remove it. Removal of the stress reverses the effects on mTOR signaling and exportin-1, and polκ is rapidly returned to the cytoplasm. Further study is still required to determine the exact connection between mTOR and polκ, but it likely involves a post-translational modification and/or a polκ binding partner.

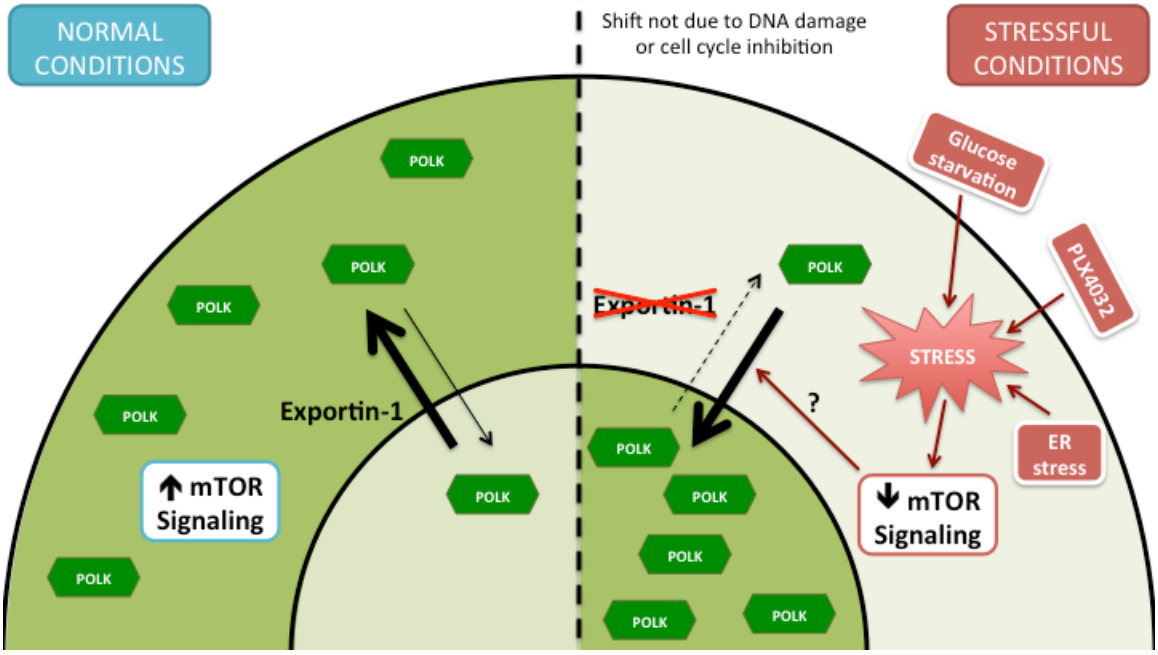

Figure 41. Mechanism by which cells regulate polκ's subcellular localization under normal and stressful conditions.
Summary of polκ regulation in well-adapted (left) and maladapted (right) cells. In this figure, green shading represents the predominant localization of polκ (cytoplasm or nucleus). The question mark represents the unknown connection between decreased mTOR signaling and nuclear import of polκ. See text for further details.

In addition to elucidating major parts of the mechanism through which polκ's subcellular localization is regulated, we also demonstrated that overexpression of polκ can have small but significant effects on mutagenesis, drug resistance, and tumorigenesis. The modest size of these effects is likely due to differences between cells shuttling polκ to the nucleus due to overexpression versus due to stress. The robust increase in mutation rate observed in bacteria in response to stress is due to increased activity of DinB and decreased effectiveness of the MMR (*99*, *155–157*). This higher mutation rate translates into increased fitness, such as increased resistance to antibiotics (*141*, *388*, *389*). Additional studies are necessary to demonstrate any synergy between increased nuclear

polκ and decreased MMR in human cancer. Moreover, it is likely other additional factors are regulated in response to stress that further enhance polκ's mutagenic capabilities.

4.2 Future directions

4.2.1 Further investigate the connection between mTOR signaling and polκ's subcellular localization

While we were able to elucidate many of the components required for the regulation of polκ in cells exposed to stress, many questions still remain. For example, the exact connection between mTOR signaling and polκ's localization remains elusive. Because mTOR and its downstream target S6K both act as kinases (*243*, *244*), and phosphorylation has been shown to be a factor in the subcellular localization of multiple proteins (*297*, *298*, *374*, *375*), we hypothesize that mTOR/S6K might have a similar effect on polκ such that phosphorylated polκ is predominantly cytoplasmic and unphosphorylated polκ predominantly nuclear. There are many possible mechanisms through which this can occur. For example, phosphorylation of polκ by mTOR/S6K could induce a conformation change that prevents recognition of its NLS and/or exposes its proposed NES. Alternatively, phosphorylation of polκ could generate a binding site for a cytoplasmic sequestration protein, such as 14-3-3. Additional possibilities exist, and much future work will be required to determine if a post-translation modification is involved, the responsible enzyme, and any necessary binding partners. The results of these studies will hopefully not only shed on a light on how mTOR signaling regulates the nuclear import/export of polκ but also on how mTOR regulates subcellular localization more generally. This is important as the nuclear-cytoplasmic shuttling of multiple proteins has

already been linked to starvation/the PI3K-mTOR pathway (*319*, *323*, *324*, *327*, *329*, *330*, *332*, *373*).

Another potential regulator of polκ's localization that needs exploring is HSP90. We previously performed a chemical screen that tested over 4000 compounds across 4 different chemical libraries for their ability to induce nuclear localization of polκ (Figure 42). This screen validated much of our previous work as many of the top hits belonged to the MAPK pathway, PI3K-mTOR pathway, or tyrosine kinase superfamily. Exportin-1 was also a hit. An unexpected hit was the chaperone HSP90: all 17 HSP90 inhibitors tested gave a score of 5 (i.e. 100% nuclear polκ).

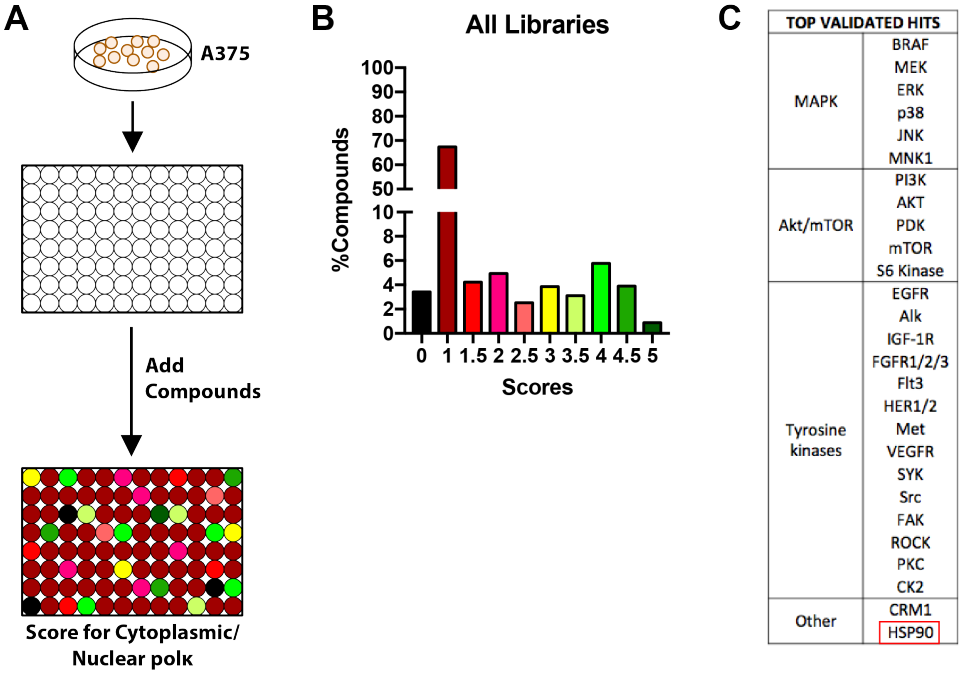

Figure 42. Chemical screen for regulators of polκ's localization.
(A) Over 4000 compounds from 4 different chemical libraries were tested for their ability to induce a nuclear shift after 24 hours. **(B)** Each compound was given a score between 1 and 5 (with 1 meaning 100% cytoplasmic and 5 meaning 100% nuclear). 0 was used to denote compounds that killed the cells. **(C)** A list of the top validated hits organized into pathways.

A literature search revealed connections of HSP90 to DNA polymerases, ER stress, and mTOR signaling. For example, a role has been identified for HSP90 in regulating polη-mediated TLS in human cells. HSP90 associates with both polη and Rev1 and then regulates their levels and localization in response to UV damage (*404*, *405*). Furthermore, the bacterial chaperone GroE regulates the levels of DinB, and *groE* mutant strains show reduced levels of SIM (*406*). These data suggest that HSP90 could function as a chaperone for polκ; however, the chemical screen demonstrated that loss of HSP90 increases polκ activity whereas loss of HSP90/GroE decreases polη/DinB activity, so a different mechanism of action would be required. HSP90 could instead function to sequester polκ in the cytoplasm of well-adapted cells as it has been shown to do for glucocorticoid receptor and AID (*407–410*). Similar to what we observed for polκ, treatment with HSP90 inhibitors increases nuclear localization of glucocorticoid receptor (*408*). Since HSP90 functions as a chaperone, induction of ER stress/the UPR could compromise interaction of HSP90 with some clients due to an increased load of unfolded/misfolded proteins (*411*, *412*). If HSP90 does sequester polκ, ER-stress mediated repression of the HSP90-polκ interaction could promote its release and subsequent nuclear localization. Furthermore, phosphorylation of polκ by mTOR/S6K could promote the interaction and/or hide polκ's NLS (*298*). Alternatively, a more direct interaction between HSP90 and mTOR signaling is possible. HSP90 interacts with the mTOR binding partner raptor, and this association promotes mTORC1 activity. Furthermore, HSP90 inhibitors have been shown to suppress the phosphorylation of S6K and 4E-BP1 by mTOR (*412*, *413*). A similar decrease in mTOR activity would be expected during ER stress-mediated repression of HSP90. Therefore, HSP90 could affect polκ's localization without acting as

a direct chaperone/cytoplasmic sequestration partner. These mechanisms are not mutually exclusive and require additional study to fully sort through.

4.2.2 Demonstrate synergy between polκ and MMR

Our flow cytometry-based GFP mutagenesis assay revealed a modest increase in mutagenesis upon overexpression of polκ, which likely did not reveal the true mutagenic capabilities of polκ due to compensation by the MMR machinery. In bacterial SIM, the upregulation/activation of DinB is accompanied by a decrease in the effectiveness of MMR. This saturation of the MMR machinery increases the number of mutations that are inherited, thereby increasing the effectiveness of SIM (*99*, *155–157*). Work in human cell lines supports this idea as suppression of MMR is required to decipher the true error rates of polε mutants that have lost their proofreading capabilities (*129*), and these two events co-occur in human cancer (*128*). Therefore, we propose that combining polκ overexpression with MMR loss will synergistically increase the mutation rate further.

To investigate this hypothesis, we decided to first investigate the effects of BRAF inhibition on expression of key MMR genes: MLH1, MSH2, MSH6, and PMS2. Loss of MMR proteins has been implicated in Lynch syndrome-associated colorectal and gynecologic cancers (*4*, *101*, *102*). The majority of mutations are seen in MLH1 and MSH2 (*103–105*), but mutations in MSH6 and PMS2 are also observed (*106*, *107*). This correlates with their importance in MMR. Analysis of RNAseq data generated using A375 cells treated with DMSO or PLX4032 for 48 hours (*414*) revealed a significant downregulation of three of the four genes assayed with only PMS2 showing no effect (Figure 43). Further work is ongoing to demonstrate a similar decrease in MMR protein

also occurs after BRAF inhibition. Overall, this demonstrates that our polκ overexpression system does not fully capitulate what happens in cells exposed to stress, and this could explain the modest effects of polκ overexpression alone.

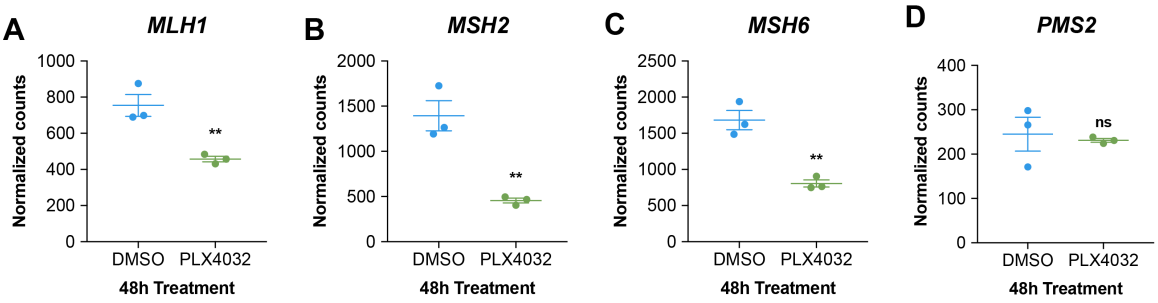

Figure 43. BRAF inhibition downregulates expression of MMR genes.
(A-D) RNAseq data was generated using A375 cells treated with DMSO or 0.1 μM PLX4032 for 48 hours (*414*), and normalized counts for MLH1 (A), MSH2 (B), MSH6 (C), and PMS2 (D) were determined for three different replicates. All graphs are represented as mean ± S.E.M. Statistical analysis was performed using unpaired two-tailed t-tests (ns = non-significant, *P < 0.05, **P < 0.01, ***P < 0.001).

In order to determine the effects of combining polκ overexpression with loss of MMR, we plan to use CRISPR/Cas9-mediated knockout of MMR genes (*415–418*). We have validated two different crRNAs against each gene using Western blot analysis (data not shown) and immunofluorescence (Figure 44). We plan to use these in our SV40p-GFP + dox-inducible polκ overexpression A375 cells and then compare the following four populations for each crRNA: 1) no MMR knockout – dox, 2) no MMR knockout + dox, 3) MMR knockout – dox, and 4) MMR knockout + dox. This will allow us to determine the effects of each event (polκ overexpression or MMR knockout) as well as the effect of combining them.

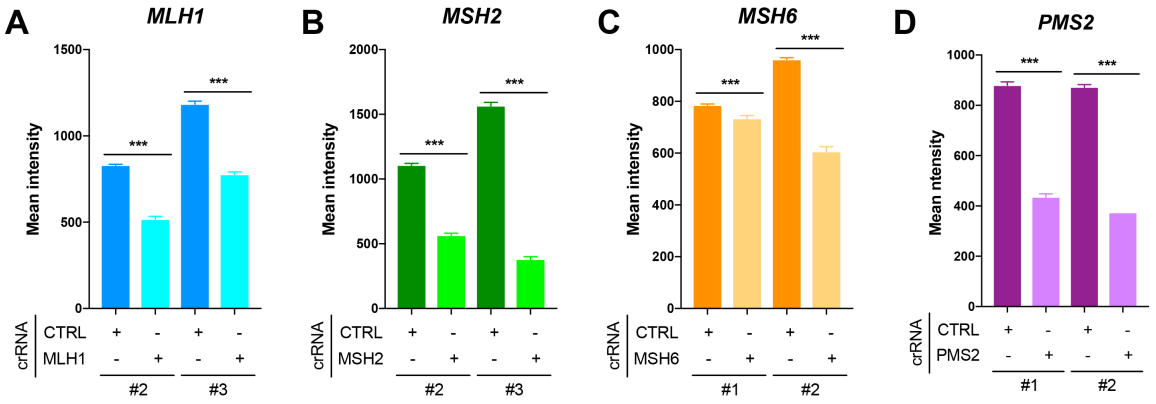

Figure 44. Validation of crRNAs against MMR genes.
(A-D) Immunofluorescence staining for MLH1 (A), MSH2 (B), MSH6, (C), or PMS2 (D) was performed on A375 cells nucleofected with a CTRL or gene-specific crRNA (2 per gene). The bar graphs show the mean intensity determined for at least 250 cells in each sample. All graphs are represented as mean ± S.E.M. Statistical analysis was performed using paired two-tailed t-tests (*P < 0.05, **P < 0.01, ***P < 0.001).

While we think it is highly likely that combining MMR downregulation with polκ overexpression is required to better recapitulate "stress-induced mutagenesis" in human cancer cells exposed to a BRAF inhibitor than polκ overexpression alone, we also know that there are likely other required changes that take place. In bacteria, RpoS functions to both increase expression of DinB and license it to replicate on undamaged DNA (*99*, *149*, *150*), so perhaps licensing factors are also required for the full activity of polκ in response to stress. The localization of polκ in response to DNA damage is dependent upon mono-ubiquitination of PCNA by RAD18 and also likely involves scaffolding by Rev1 (*67*, *70*). It is unknown if there is a similar requirement in cancer cells exposed to stress. Experiments by Bergoglio *et al* demonstrated that when expressed at high enough levels, polκ can become part of the replication machinery in the absence of DNA damage (*273*). Overexpression of polκ and exposure of cancer cells to certain stresses both cause a dramatic shift of polκ from the cytoplasm into the nucleus, resulting in a local increase of

polκ near DNA. This suggests it should be able to become part of the replication machinery in the absence of normal DNA damage signals, but this has not been fully explored.

4.2.3 What is the clinical significance of stress-induced polκ activity?

While polκ overexpression has been observed clinically in both lung cancer and glioma (*132*, *136*), it is much harder to demonstrate that transient induction of polκ occurs in patients treated with targeted therapies. Samples are typically collected before treatment begins and after resistance emerges but rarely if ever during the actual treatment, and this is what would be required to show that our observations in human cell culture also occur in human tumors. However, we could potentially detect polκ's induction indirectly using its mutational signature. Work by Michael Stratton has identified a number of different mutational signatures observed in human tumors, and only some of them have been linked to specific external (ex: UV) or internal (ex: APOBEC) causes (*419*). Therefore, if we could determine polκ's specific mutational signature, we could look for it in samples taken before treatment and after resistance emerges (specifically in patients who appear to acquire their resistance mutation). If stress-induced polκ is playing a role in drug resistance via increased mutagenesis, we would expect to see an enrichment of its signature in samples taken after resistance develops.

4.2.4 Determine the role of polκ/SIM in somatic mosaicism and normal development

One of the biggest questions arising from this work is why multicellular organisms like humans would retain a mechanism for SIM. SIM is very adaptive in unicellular

organisms like bacteria because beneficial mutations within a single cell will promote its continued survival, and these mutations along with the SIM phenotype will be passed onto its progeny. However, in multicellular organisms, an increased mutation rate would result in beneficial mutations in some cells and deleterious mutations in others, and unless the organism has mechanisms to eliminate cells with those deleterious mutations, they could be detrimental to the entire organism and potentially contribute to diseases, such as cancer.

One possibility is that multicellular organisms have maintained mechanisms for induced mutagenesis to allow for some degree of somatic mosaicism. Somatic mosaicism refers to the presence of two or more genetically distinct populations of cells within an individual and occurs due to post-zygotic mutations that are inherited by all subsequent cells in that lineage. These can include point mutations, small insertions/deletions, and large-scale chromosomal changes. Depending on when it occurs, it can affect varying fractions of the organism with the earlier the mutation, the greater the percentage of cells carrying it (Figure 45) (*420–424*). A physiological example of this is the generation of diversity via V(D)J recombination and somatic hypermutation as part of the development of a robust immune system (*425*). By re-wiring the input for SIM from cellular stress to developmental signals, multicellular organisms could retain a mechanism for SIM but mostly restrain its use to carefully regulated developmental processes, such as the creation of antibody diversity (*425*, *426*).

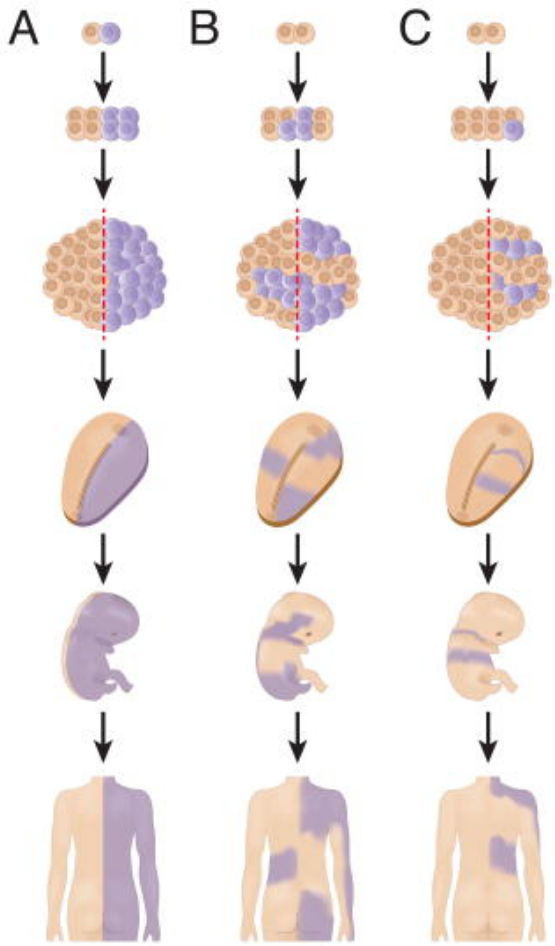

Figure 45. Somatic mosaicism.
(A-C) This figure demonstrates how when a post-zygotic mutation (indicated by a purple cell) arises influences the distribution of mutant cells in the organism. Mutations arising during the two-cell stage (A) will affect either the left or right half of the individual while mutations arising in later stages (B and C) will affect smaller percentages of cells but can be widely distributed throughout the body depending on cellular migration patterns. Figure adapted from (*421*).

The exact function of somatic mosaicism in development and all the responsible factors are still mostly unknown, but many examples of it exist in humans (*421*, *427–431*). This is particularly true in the human brain, where the resulting mutations/chromosomal alterations have even been proposed to play a role in normal brain function (*432–437*). This is particularly interesting because *in situ* hybridization using probes against polκ in

zebrafish embryos at 24 hours post fertilization (hpf) reveals that polκ expression is predominantly localized in the brain during early development (Figure 46). This suggests that induced expression of polκ could be a mechanism through which somatic mosaicism occurs, and that cancer cells could later co-opt the same pathway to increase their fitness in response to stress. While largely unexplored, this would be a useful area of investigation for future studies.

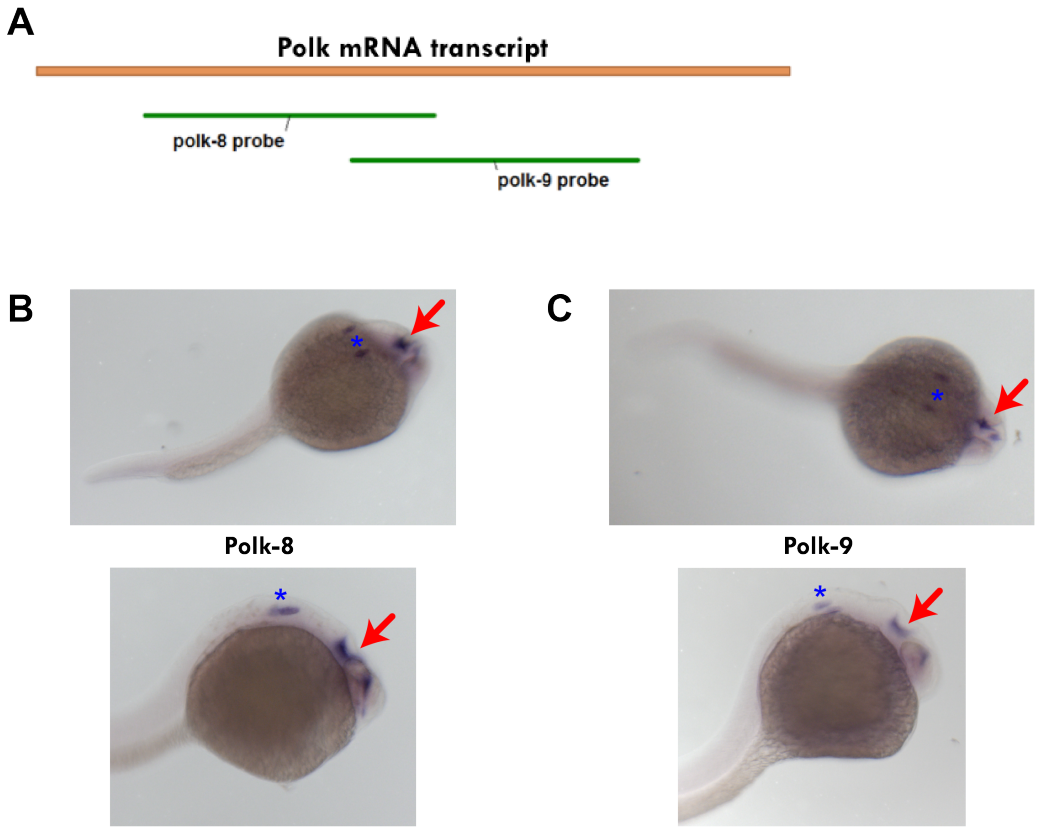

Figure 46. polκ is predominantly localized in the brain during development.
(A) Location of the *in situ* hybridization probes against polκ. **(B-C)** *in situ* hybridization was performed using the anti-sense probes polk-8 (B) and polk-9 (C) in wild-type embryos at 24 hpf. Dorsal (top) and side (bottom) views of the embryos were taken, and a representative embryo is shown for each probe. Red arrows indicate staining in the brain. Blue asterisks indicate non-specific staining.

CHAPTER 5: MATERIALS AND METHODS

5.1 Experimental models

5.1.1 Cell lines

Cell culture conditions

Cell culture was performed at 37°C in a humidified atmosphere containing 5% CO_2. A375 and SK-MEL28 cells were obtained from ATCC. PC-9 cells were a gift from C. Rudin (MSKCC, NYC, USA). SK-BR3 cells were a gift from S. Chandarlapaty (MSKCC, NYC, USA). Cells were cultured in DMEM (A375 and SK-MEL28), RPMI1640 (PC-9), or DMEM/F12 (SK-BR3) supplemented with 2 mM glutamine, 100 IU/ml penicillin, 100 μg/ml streptomycin, and 10% heat-inactivated fetal bovine serum (FBS). Cell lines were regularly tested and verified to be mycoplasma negative by the MycoAlert Mycoplasma Detection Kit (Lonza).

Transgenic lines

The following were generated using the A375 human melanoma cell line: 1) dox-inducible polκ overexpression cells, 2) constitutively GFP-positive + dox-inducible polκ overexpression cells, 3) dox-inducible polκ knockdown cells, and 4) dox-inducible p53 knockdown cells. Further details regarding the plasmids used, the transduction conditions, and selection of the cells are provided in Sections 5.2.2 (lines 1 and 2) and 5.2.3 (lines 3 and 4).

5.1.2 Zebrafish

Fish Husbandry

Zebrafish stocks were reared under standard conditions at 28.5°C under 14:10 light:dark cycles. Animals were fed a standard diet of brine shrimp followed by Zeigler pellets. Healthy, immune-competent male and female adults of the wild-type and mitfa-BRAF^{V600E};p53$^{-/-}$ background (*266*) were used for breeding and creation of transgenic fish. Embryos were collected from natural matings and incubated in E3 buffer (5 mM NaCl, 0.17 mM KCl, 0.33 mM $CaCl_2$, 0.33 mM $MgSO_4$) at 28.5°C before being put on system around 7 dpf.

Transgenic lines

One-cell-stage mitfa-BRAF^{V600E};p53$^{-/-}$ embryos were injected with the construct Tg(ubi-zpolκ-2A-GFP;cmlc2:eGFP) at 25 ng/µl with Tol2 mRNA at 20 ng/µl. Embryos were screened at 24 hpf for the presence of GFP in the heart as well as the rest of the body. GFP-positive embryos were grown to adulthood and outcrossed to identify founders that gave germline transmission of the transgene.

5.2 Methods

5.2.1 Drug treatments

Inhibitors were maintained until sample collection unless otherwise noted: PLX4032 (Selleck), CI-1040 (Selleck), U0126 (Sigma Aldrich), Ulixertinib (Selleck), SCH772984 (Selleck), forskolin (Thermo Fisher Scientific), bleomycin (Sigma Aldrich), brefeldin A (Sigma Aldrich), thapsigargin (Sigma Aldrich), tunicamycin (Sigma Aldrich),

rapamycin (Selleck), PP242 (Abcam), LY294002 (Sigma Aldrich), PF-4708671 (Selleck), erlotinib (Selleck), importazole (Sigma Aldrich), and leptomycin B (Sigma Aldrich). Lapatinib and PD0332991 were gifts from S. Chandarlapaty. Complete media consisted of DMEM (without glucose or glutamine) supplemented with 25 mM glucose, 6 mM glutamine, and 10% heat-inactivated FBS. Media – glucose consisted of DMEM (without glucose or glutamine) supplemented with 6 mM glutamine and 10% heat-inactivated FBS. Media – glutamine consisted of DMEM (without glucose or glutamine) supplemented with 25 mM glucose and 10% heat-inactivated FBS. Media + 1% serum consisted of DMEM (without glucose or glutamine) supplemented with 25 mM glucose, 6 mM glutamine, and 1% heat-inactivated FBS.

5.2.2 Generation of doxycycline-inducible polκ overexpression cells

For inducible overexpression of polκ, the human polκ open reading frame was amplified from a constitutive polκ overexpression plasmid that was a gift from J.S. Hoffmann (Toulouse, France) and cloned using the In-Fusion Cloning kit (Clontech) into the pSIN-TREtight-MCS-IRES-mCherry-PGK-Hygro vector, which has a doxycycline (dox)-inducible promoter and adds an IRES-mCherry to the C-terminus of polκ, to generate pTRE-hpolκ-IRES-mCherry. The pSIN-TREtight-MCS-IRES-mCherry-PGK-Hygro vector and its corresponding tet-activator (rtTA3) RIEP vector were gifts from S. Lowe (MSKCC, NYC, USA). Amplification of polκ was performed using the TRE-hpolκ F1 FW and TRE-hpolκ F1 RV primers (Table 6).

Table 6. Primers for cloning.

Construct	Primer name	Sequence (5′ → 3’)
pTRE-hpolκ-IRES-mCherry	TRE-hpolκ F1 FW	CGGTACCCGGGGATCCCACCATGGATAG CACAAAG
	TRE-hpolκ F1 RV	TTAGTCTTCGCGGCCGCTTACTTAAAAAA TATATCAAGGG
dox-inducible polκ shRNAs	miRE_XhoF	TACAATACTCGAGAAGGTATATTGCTGTT GACAGTGAGCG
	miRE_EcoRI	TTAGATGAATTCTAGCCCCTTGAAGTCCG AGGCAGTAGGCA
ubi-zpolκ-2A-GFP	zPOLK_FWD	ATGAGGCAGCAGTGCGAAAG
	zPOLK_REV	GACGTTCTGTCTGGTGTTTC
pCRII-TOPO + polk-8 ISH probe	POLK_F8	AAACCGATGGCAGTGGGATC
	POLK_R8	CGCCCATGAGTCTGAGTTTC
pCRII-TOPO + polk-9 ISH probe	POLK_F9	CATGAGCACTGAGAGGACGT
	POLK_R9	TGAAGTCATTGCCGTCATCG

Lentivirus was produced by transfection of HEK-293T cells with pTRE-hpolκ-IRES-mCherry and the packaging plasmid psiAmpho (which was a gift from R. Levine, MSKCC, NYC, USA) at a 1:1 ratio. Transfection was performed using Fugene (Promega) reagent. The viral supernatant was collected 48 and 72 hours following transfection, filtered through a 0.45 μm filter (Thermo Fisher Scientific), and added to A375 cells with 8 μg/ml polybrene (Thermo Fisher Scientific). Infected cells were selected by treatment with 1 mg/ml hygromycin (Thermo Fisher Scientific). Lentivirus for RIEP was produced the same way and then used to infect A375 cells already containing pTRE-hpolκ-IRES-mCherry. Doubly infected cells (pTRE-hpolκ-IRES-mCherry/RIEP) were selected by treatment with 10 μg/ml puromycin (Thermo Fisher Scientific) and 1 mg/ml hygromycin. Single cell clones were then isolated, and their induction efficiency was tested via flow cytometry for mCherry expression. Clones #1 and #2 showed the best induction after addition of 1 μg/ml dox (Sigma Aldrich) compared to uninduced controls, so they were selected for future experiments.

To add constitutive GFP expression to these cells, we used pBABE-GFP, which was a gift from William Hahn (Addgene plasmid #10668). pBABE-GFP expresses humanized *Renilla* GFP (hrGFP) under the SV40 promoter in the pBABE backbone. Lentivirus for pBABE-GFP was produced in HEK-293T cells using the same protocol detailed above and then used to infect A375 cells already containing pTRE-hpolκ-IRES-mCherry/RIEP (i.e. dox-inducible polκ overexpression cells). Infected cells were selected using flow cytometry for GFP-positive cells.

5.2.3 Inducible shRNA knockdown of polκ and p53

For inducible knockdown of polκ, two different shRNAs (*438*) targeting polκ were generated using PCR. The two polκ shRNAs (sh-polκ-1 and sh-polκ-2) were each cloned using restriction digestion and ligation into the LT3GEPIR vector (*354*), which allows dox-inducible expression of a shRNA and GFP. Amplification was performed using the miRE_XhoF and miRE_EcoRI primers (Table 6) and sh-polκ-1 or sh-polκ-2 oligo template (Table 7).

Table 7. Validated shRNA sequences for polκ knockdown.

shRNA	Sequence (5′ → 3’)
sh-polκ-1	TGCTGTTGACAGTGAGCGCAAGAAGAGTTTCTTTGATAAATAGTGAAGC CACAGATGTATTTATCAAAGAAACTCTTCTTATGCCTACTGCCTCGGA
sh-polκ-2	TGCTGTTGACAGTGAGCGCAAGGATTTATGTAGTTGAATATAGTGAAGC CACAGATGTATATTCAACTACATAAATCCTTATGCCTACTGCCTCGGA

Plasmids containing either a control hairpin (sh-Ctrl) or 2 different hairpins targeting p53 (sh-p53-1 and sh-p53-2) were gifts from S. Lowe. For all hairpins, lentivirus was produced by transfection of HEK-293T cells with each hairpin plasmid plus the

packaging plasmids psPAX2 and pMD2G at a 4:3:1 ratio. Transfection was performed using Lipofectamine 2000 (Life Technologies) reagent. The viral supernatant was collected at 48 and 72 hours following transfection and frozen at -80°C. Virus was later thawed and added to A375 cells, and infected cells were selected by treatment with 1 μg/ml puromycin. Induction after treatment with 1 μg/ml dox was verified using flow cytometry for GFP expression.

5.2.4 Total RNA extraction, cDNA isolation, and qRT-PCR analysis

Total RNA from treated cells was extracted using the Quick-RNA Mini-Prep kit (Zymo), and RNA concentration was determined using a Synergy H1 Hybrid Multi-Mode Microplate Reader (BioTek). Reverse transcription of total RNA was performed using SuperScript III First-Strand Synthesis SuperMix (Thermo Fisher Scientific) according to the manufacturer's guidelines. qRT-PCR reactions were detected on a CFX384 Touch machine (Bio-Rad) using iQ SYBR Green Supermix (Bio-Rad). RNA expression levels were calculated using the comparative C_t method ($2^{-\Delta\Delta CT}$) normalized to β-actin. The primer pairs used for each target are listed in Table 8.

Table 8. Primers for qRT-PCR.

Target	Forward primer sequence (5′ → 3')	Reverse primer sequence (5′ → 3')
POLH	GCTACTGGACAGGATCGAGTG	CACCACCCTTCCATGATTTGTA
POLI	CACTGGGTATCAATAGTGTGCG	GTATCACAGGGGAGTTATCCTCT
POLK	TGAGGGACAATCCAGAATTGAAG	CTGCACGAACACCAAATCTCC
REV1	ATGCTGCTATGCAGAAGGATG	CAGCGGAAGGATCTGTGTATC
B-ACTIN	CATGTACGTTGCTATCCAGGC	CTCCTTAATGTCACGCACGAT
ATF4 (*193*)	GTTCTCCAGCGACAAGGCTA	ATCCTGCTTGCTGTTGTTGG
CHOP (*193*)	AGAACCAGGAAACGGAAACAGA	TCTCCTTCATGCGCTGCTTT

5.2.5 Western blot analysis

For whole cell lysates, cells were washed 1x with phosphate buffered saline (PBS, Invitrogen) and then lysed in RIPA buffer (EMD Millipore) containing 1x HALT Combined Protease and Phosphatase Inhibitor Cocktail (Thermo Fisher Scientific) for 20 minutes at 4°C. Cell lysates were clarified by centrifugation at 10,000 RPM for 10 min at 4°C. For cytoplasmic or nuclear fractions, the Subcellular Protein Fractionation Kit for Cultured Cells (Thermo Fisher Scientific) was used according to the manufacturer's protocol. Protein concentration was measured with Bradford reagent (Sigma Aldrich), and samples were resolved by 4-15% or 12% SDS-PAGE gels (Bio-Rad) depending on the protein size. Proteins were transferred onto nitrocellulose membranes and subjected to standard immunoblotting. ECL Prime (Amersham) was used as the developing reagent.

Western blot antibodies: polκ (ab57070, Abcam, 1:10,000), p53 (sc-126, Santa Cruz Biotechnology, 1:10,000), mCherry (ab167453, Abcam, 1:1000), Lamin B1 (ab133741, Abcam, 1:10,000), β-Actin (A5441, Sigma Aldrich, 1:20,000), Akt (9272, Cell Signaling, 1:4000), p-Akt (4058, Cell Signaling, 1:1000), S6 (2317, Cell Signaling, 1:1000), p-S6 (2215, Cell Signaling, 1:1000), 4E-BP1 (9644, Cell Signaling, 1:4000), p-4EBP1 (2855, Cell Signaling, 1:1000), MLH1 (ab92312, Abcam, 1:20,000), MSH2 (ab227942, Abcam, 1:10,000), MSH6 (ab92471, Abcam, 1:10,000), PMS2 (ab110638, Abcam, 1:1000), anti-mouse (ab97046, Abcam, 1:10,000 – 1:30,000), anti-rabbit (ab97051, Abcam, 1:10,000 – 1:30,000)

5.2.6 Immunofluorescence

Cells were cultured on Millicell EZ SLIDE 4 or 8-well glass slides (EMD Millipore). Cells were fixed with 4% paraformaldehyde (Santa Cruz Biotechnology) at 37°C for 15 minutes, washed with PBS, and then blocked with 5% goat serum (Thermo Fisher Scientific) and 0.2% Triton X-100 (Thermo Fisher Scientific) in PBS for 1 h. The cells were incubated with primary antibody in antibody dilution buffer (PBS with 1% bovine serum albumin (Sigma Aldrich) and 0.2% Triton X-100) at 4°C overnight, then washed 3 times with PBS, and incubated with Alexa-conjugated secondary antibody for 2 h at RT. After washing 3 more times with PBS, cells were stained with 0.1 μg/ml DAPI (Thermo Fisher Scientific) and then mounted with Dako fluorescence mounting media (Agilent) and imaged on a Zeiss Axio Imager A2.

Immunofluorescence antibodies: polκ (ab57070, Abcam, 1:500), γH2AX (2577, Cell Signaling, 1:200), 53BP1 (ab175933, Abcam, 1:200), p-Chk1 (2348, Cell Signaling, 1:100), p-Chk2 (2661, Cell signaling, 1:500), p-S6 (5364, Cell Signaling, 1:1000), MLH1 (ab92312, Abcam, 1:1000), MSH2 (ab227942, Abcam, 1:250), MSH6 (ab92471, Abcam, 1:800), PMS2 (ab110638, Abcam, 1:250), anti-mouse Alexa-488 (4408, Cell signaling, 1:1000), anti-rabbit Alexa-488 (4412, Cell Signaling, 1:1000), anti-rabbit Alexa-594 (8889, Cell Signaling, 1:1000)

5.2.7 CREB ELISA

The CREB1 pS133 + CREB1 ELISA Kit (ab176659, Abcam) was used to determine the amount of phosphorylated and total CREB present in A375 cells treated

with DMSO, PLX4032, or forskolin. Control and sample lysates were prepared and analyzed according to the manufacturer's protocol.

5.2.8 Cell cycle analysis

Cells were treated with the indicated inhibitors for 24 hours and fixed in 70% ethanol (Thermo Fisher Scientific) at 4°C for at least 4 hours. Later, the cells were washed with PBS and stained with 20 μg of propidium iodide (Thermo Fisher Scientific), 200 μg of RNase A (Thermo Fisher Scientific), and 0.1% Triton X-100 in PBS for at least 30 minutes. The labeled cells were analyzed using a Fortessa flow cytometer, and the Dean-Jett Fox model in FlowJo was used to determine which cells were in G1, S, and G2/M.

5.2.9 Mutagenesis assay

Dox-inducible polκ overexpression A375 cells (Clone #1 and Clone #2) constitutively expressing GFP under the SV40 promoter were generated. We then divided each population equally and treated with or without 1 μg/ml dox to generate polκ-overexpressing cells and their corresponding negative control population. After 14 days of treatment, both populations were tryspinized, stained with 1 μg/ml DAPI, and analyzed using a Fortessa flow cytometer. FlowJo was used to determine the mean GFP intensity of each population.

5.2.10 Drug resistance assay

Two different clones of dox-inducible polκ overexpression cells (Clone #1 and Clone #2) were generated. We then divided each population equally and treated with or

without 1 μg/ml dox for ~3 months to generate polκ-overexpressing cells and their corresponding negative control population. All populations were then switched to media without dox, plated in 96 well plates, and exposed to various doses of PLX4032. After 4 days, cell number was determined using the CyQUANT Direct Cell Proliferation Assay kit (Thermo Fisher Scientific). The technical replicates for each dose were averaged and then normalized against the 0 μM dose condition to determine the growth relative to DMSO.

5.2.11 Chemical screen

We aimed to identify compounds that induced a nuclear enrichment of polκ by treating A375 cells in 96 well plates for 24 hours with 10 μM of over 4000 chemicals from four different libraries (the Sigma LOPAC 1280 Library, the Selleck Bioactive Compound Library, the NIH Clinical Collection, and the Roche Kinase Inhibitors Library). Chemicals were prepared from 10 mM stock and diluted to 10 μM using DMEM supplemented with 2 mM glutamine, 100 IU/ml penicillin, 100 μg/ml streptomycin, and 10% heat-inactivated FBS at 1% (v/v) DMSO. At least four DMSO-only negative control wells and four 5 μM PLX4032-only positive control wells were included per plate. After 24 hours of treatment, cells were fixed and stained for polκ immunofluorescence (see section 5.2.6). Each well was then screened by eye using a Zeiss Axio Observer microscope and scored from 1 to 5. 1 indicated 100% cytoplasmic polκ in 100% of cells while 5 indicated 100% nuclear polκ in 100% of cells. 0 was used to indicate wells with large amounts of cell death. Chemicals with scores ≥ 4 were subject to a second round of validation.

5.2.12 Analysis of MMR mRNA levels using RNAseq

RNAseq data from A375 cells treated with DMSO or 0.1 μM vemurafenib for 48 hours was generated by Obenauf *et al* (*414*). We obtained normalized counts from them for the MMR genes MLH1, MSH2, MSH6, and PMS2 for further analysis.

5.2.13 Knockout of MMR genes using the Alt-R CRISPR-Cas9 system

crRNAs for each MMR gene (Table 9) were designed using the CHOPCHOP online tool (*439*). Knockout was performed in A375 cells using the Alt-R CRISPR-Cas9 system (IDT), which utilizes crRNAs against the gene of interest and labeled tracrRNAs to guide Cas9 protein to a specific genomic location. Proper cutting by Cas9 was verified using the Surveyor Mutation Detection Kit (IDT) after amplification of the targeted area using the associated forward and reverse primers (Table 9).

Table 9. Validated crRNAs and associated primer sequences for MMR knockout.

Target	crRNA number	crRNA sequence (5′ → 3’)	Forward primer sequence (5′ → 3’)	Reverse primer sequence (5′ → 3’)
MLH1	#2	ATGAGGGTACGTAAACGCTG	AGAGACATCGGGAAGATTCTGA	ACTGCTTTCTCCATTTCCAAAA
	#3	AGCATGGCAAGGTCAAAGAG	ACCTGCCATTCTGATAGTGGAT	GTCACACCTCATCAATTTCCAA
MSH2	#2	CTAGGAGATGCACTTACCTG	GAGTCAGCAGAAGTGTCCATTG	TCCTTCTCACAGGACAGAGACA
	#3	AGAGGAACTTCTACCTACGA	AGGTCTGCAACCAAAGATTCAT	GTCTCTTCAGTGGTGAGTGCTG
MSH6	#1	TTTAAGCTCTAAGAAGGGGG	AGATGTTTTACTGTGCCTGGCT	TTTGGTCCAGTAACAAGCACAC
	#2	TTGTTGGCATCACTCAGCGC	GTAGATGCGGTGCTTTTAGGAG	CGTTGAGGTTCTTCGCCTT
PMS2	#1	GTGGAGAAGGACTCGGGGCA	AAAGAGTCGTCAGTTTTAGGCG	CCTCAGAAAGAGGCAGTGAGTT
	#2	CAAACCGTACTCTTCACACA	TGTAGTTCTCTTGCCAGCAATC	TTTTTGCGCTTGTAATGTCAAT

5.2.14 Generation of polκ-overexpressing zebrafish

Zebrafish polκ cDNA was amplified from a wild-type embryos cDNA library and cloned into a pENTR/D-TOPO vector with primers zPOLK_FWD and zPOLK_REV (Table 6). The final ubi-zpolκ2AGFP/395 backbone (cmlc2:eGFP) plasmid was constructed using the Gateway Tol2 kit.

5.2.15 Tumorigenesis assay

Transgenic zebrafish were generated via injection into melanoma-prone (mitfa-$BRAF^{V600E}$; $p53^{-/-}$) one-cell embryos, and stable lines were selected for using fluorescence. Melanoma-prone zebrafish with and without the ubi-zpolκ2AGFP construct were mated to generate polκ-overexpressing zebrafish (GFP-positive) and negative control siblings (GFP-negative). Fish were checked weekly for tumors from 5 weeks post fertilization (wpf) to 70 wpf. Fish with tumors were removed from the study. A Kaplan-Meier survival curve was generated using GraphPad Prism 7.

5.2.16 Histology

Zebrafish with tumors were euthanized, and the tumor was dissected, washed in PBS, and fixed overnight in 4% paraformaldehyde at 4°C. Samples were then transferred into 70% ethanol and submitted to HistoWiz. HistoWiz performed the sectioning and H&E staining. Additional unstained slides were stained with a $BRAF^{V600E}$ antibody (clone VE1, Spring Bio, 1:800, 30' ER2). The Bond Polymer Refine Detection kit (Leica Biosystems) was used to detect $BRAF^{V600E}$ protein expression.

5.2.17 *in situ* hybridization

in situ hybridization was performed as previously described (*440*). Embryos were fixed at 24 hpf, and probes were diluted to a working solution of 0.8 ng/µl. A staining time of 3.5 hours at room temperature was used. The zebrafish polκ probe DNA template was amplified from a WT adult cDNA library using the primers POLK_F8 and POLK_R8 (for polk-8) or POLK_F9 and POLK_R9 (for polk-9) (Table 6) and TOPO-TA cloned into the pCRII-TOPO vector. The anti-sense probe for each was digested with KpnI and then *in vitro* transcribed using T7 RNA polymerase. The sense probe (- control) for each was digested with EcoRV and then *in vitro* transcribed using Sp6 RNA polymerase.

5.3 Quantification and statistical analysis

The following statistical tests were used: paired 2-tailed t-test (all q-RT-PCR, Western blot analysis, immunofluorescence, ELISAs, and mutagenesis assay), unpaired 2-tailed t-test (RNAseq analysis), chi-square test (cell cycle analysis), Pearson correlation coefficient (comparison of rates of p-S6 loss vs. nuclear polκ enrichment), log-rank (Mantel-Cox) test (tumorigenesis assay), and two-way ANOVA and Fisher's least significant difference test (drug resistance assay). Statistical details, including sample size, can be found in the figure legends. In all graphs, ns indicates non-significant, * indicates $P < 0.05$, ** indicates $P < 0.01$, and *** indicates $P < 0.001$.

CHAPTER 6: BIBLIOGRAPHY

1. L. A. Loeb, K. R. Loeb, J. P. Anderson, Multiple mutations and cancer. *Proc. Natl. Acad. Sci. USA*. **100**, 776–781 (2003).
2. C. Masutani *et al.*, The XPV (xeroderma pigmentosum variant) gene encodes human DNA polymerase eta. *Nature*. **399**, 700–704 (1999).
3. C. Palles *et al.*, Germline mutations affecting the proofreading domains of POLE and POLD1 predispose to colorectal adenomas and carcinomas. *Nat. Genet.* **45**, 136–144 (2013).
4. M. S. Pino *et al.*, Deficient DNA mismatch repair is common in Lynch syndrome-associated colorectal adenomas. *J Mol Diagn*. **11**, 238–247 (2009).
5. J.-S. Hoffmann, C. Cazaux, Aberrant expression of alternative DNA polymerases: a source of mutator phenotype as well as replicative stress in cancer. *Semin. Cancer Biol.* **20**, 312–319 (2010).
6. S. D. McCulloch, T. A. Kunkel, The fidelity of DNA synthesis by eukaryotic replicative and translesion synthesis polymerases. *Cell Res.* **18**, 148–161 (2008).
7. M. Garcia-Diaz, K. Bebenek, Multiple functions of DNA polymerases. *CRC. Crit. Rev. Plant Sci.* **26**, 105–122 (2007).
8. J. H. Hoeijmakers, Genome maintenance mechanisms for preventing cancer. *Nature*. **411**, 366–374 (2001).
9. S. P. Jackson, J. Bartek, The DNA-damage response in human biology and disease. *Nature*. **461**, 1071–1078 (2009).
10. J. D. Watson, F. H. Crick, Molecular structure of nucleic acids; a structure for deoxyribose nucleic acid. *Nature*. **171**, 737–738 (1953).
11. I. R. Lehman, M. J. Bessman, E. S. Simms, A. Kornberg, Enzymatic synthesis of deoxyribonucleic acid. I. Preparation of substrates and partial purification of an enzyme from Escherichia coli. *J. Biol. Chem.* **233**, 163–170 (1958).
12. P. M. Burgers *et al.*, Eukaryotic DNA polymerases: proposal for a revised nomenclature. *J. Biol. Chem.* **276**, 43487–43490 (2001).
13. M. J. Longley, D. Nguyen, T. A. Kunkel, W. C. Copeland, The fidelity of human DNA polymerase gamma with and without exonucleolytic proofreading and the p55 accessory subunit. *J. Biol. Chem.* **276**, 38555–38562 (2001).
14. M. A. Graziewicz, M. J. Longley, W. C. Copeland, DNA polymerase gamma in mitochondrial DNA replication and repair. *Chem. Rev.* **106**, 383–405 (2006).

15. K. Takata, T. Shimizu, S. Iwai, R. D. Wood, Human DNA polymerase N (POLN) is a low fidelity enzyme capable of error-free bypass of 5S-thymine glycol. *J. Biol. Chem.* **281**, 23445–23455 (2006).

16. M. Seki *et al.*, High-efficiency bypass of DNA damage by human DNA polymerase Q. *EMBO J.* **23**, 4484–4494 (2004).

17. K. Masuda *et al.*, Absence of DNA polymerase theta results in decreased somatic hypermutation frequency and altered mutation patterns in Ig genes. *DNA Repair (Amst.)*. **5**, 1384–1391 (2006).

18. M. Yoshimura *et al.*, Vertebrate POLQ and POLbeta cooperate in base excision repair of oxidative DNA damage. *Mol. Cell*. **24**, 115–125 (2006).

19. P. A. Mateos-Gomez *et al.*, Mammalian polymerase θ promotes alternative NHEJ and suppresses recombination. *Nature*. **518**, 254–257 (2015).

20. J. L. Parsons, N. H. Nicolay, R. A. Sharma, Biological and therapeutic relevance of nonreplicative DNA polymerases to cancer. *Antioxid. Redox Signal.* **18**, 851–873 (2013).

21. Y. I. Pavlov *et al.*, Evidence that errors made by DNA polymerase alpha are corrected by DNA polymerase delta. *Curr. Biol.* **16**, 202–207 (2006).

22. R. E. Johnson, M. T. Washington, L. Haracska, S. Prakash, L. Prakash, Eukaryotic polymerases iota and zeta act sequentially to bypass DNA lesions. *Nature*. **406**, 1015–1019 (2000).

23. M. Diaz, C. Lawrence, An update on the role of translesion synthesis DNA polymerases in Ig hypermutation. *Trends Immunol.* **26**, 215–220 (2005).

24. A. F. Moon *et al.*, The X family portrait: structural insights into biological functions of X family polymerases. *DNA Repair (Amst.)*. **6**, 1709–1725 (2007).

25. M. García-Díaz, K. Bebenek, T. A. Kunkel, L. Blanco, Identification of an intrinsic 5'-deoxyribose-5-phosphate lyase activity in human DNA polymerase lambda: a possible role in base excision repair. *J. Biol. Chem.* **276**, 34659–34663 (2001).

26. A. J. Podlutsky, I. I. Dianova, S. H. Wilson, V. A. Bohr, G. L. Dianov, DNA Synthesis and dRPase Activities of Polymerase β Are Both Essential for Single-Nucleotide Patch Base Excision Repair in Mammalian Cell Extracts. *Biochemistry*. **40**, 809–813 (2001).

27. B. Bertocci, A. De Smet, J.-C. Weill, C.-A. Reynaud, Nonoverlapping functions of DNA polymerases mu, lambda, and terminal deoxynucleotidyltransferase during immunoglobulin V(D)J recombination in vivo. *Immunity*. **25**, 31–41 (2006).

28. F. Boudsocq *et al.*, Investigating the role of the little finger domain of Y-family DNA polymerases in low fidelity synthesis and translesion replication. *J. Biol. Chem.* **279**, 32932–32940 (2004).

29. S. D. McCulloch *et al.*, Preferential cis-syn thymine dimer bypass by DNA polymerase eta occurs with biased fidelity. *Nature*. **428**, 97–100 (2004).

30. M. J. McIlwraith *et al.*, Human DNA polymerase eta promotes DNA synthesis from strand invasion intermediates of homologous recombination. *Mol. Cell*. **20**, 783–792 (2005).

31. A. Tissier *et al.*, Misinsertion and bypass of thymine-thymine dimers by human DNA polymerase iota. *EMBO J.* **19**, 5259–5266 (2000).

32. M. Wang *et al.*, Pol iota is a candidate for the mouse pulmonary adenoma resistance 2 locus, a major modifier of chemically induced lung neoplasia. *Cancer Res.* **64**, 1924–1931 (2004).

33. K. Bebenek *et al.*, 5'-Deoxyribose phosphate lyase activity of human DNA polymerase iota in vitro. *Science*. **291**, 2156–2159 (2001).

34. T. Ogi, A. R. Lehmann, The Y-family DNA polymerase kappa (pol kappa) functions in mammalian nucleotide-excision repair. *Nat. Cell Biol.* **8**, 640–642 (2006).

35. S. Lone *et al.*, Human DNA polymerase kappa encircles DNA: implications for mismatch extension and lesion bypass. *Mol. Cell*. **25**, 601–614 (2007).

36. N. M. King *et al.*, Overproduction of DNA polymerase eta does not raise the spontaneous mutation rate in diploid human fibroblasts. *DNA Repair (Amst.)*. **4**, 714–724 (2005).

37. T. Ogi, T. Kato, T. Kato, H. Ohmori, Mutation enhancement by DINB1, a mammalian homologue of the Escherichia coli mutagenesis protein dinB. *Genes Cells*. **4**, 607–618 (1999).

38. J. N. K. Stancel *et al.*, Polk mutant mice have a spontaneous mutator phenotype. *DNA Repair (Amst.)*. **8**, 1355–1362 (2009).

39. J. R. Nelson, C. W. Lawrence, D. C. Hinkle, Deoxycytidyl transferase activity of yeast REV1 protein. *Nature*. **382**, 729–731 (1996).

40. G. X. Reyes, T. T. Schmidt, R. D. Kolodner, H. Hombauer, New insights into the mechanism of DNA mismatch repair. *Chromosoma*. **124**, 443–462 (2015).

41. J. Jiricny, The multifaceted mismatch-repair system. *Nat. Rev. Mol. Cell Biol.* **7**, 335–346 (2006).

42. P. Ross-Macdonald, G. S. Roeder, Mutation of a meiosis-specific MutS homolog decreases crossing over but not mismatch correction. *Cell*. **79**, 1069–1080 (1994).

43. N. M. Hollingsworth, L. Ponte, C. Halsey, MSH5, a novel MutS homolog, facilitates meiotic reciprocal recombination between homologs in Saccharomyces cerevisiae but not mismatch repair. *Genes Dev.* **9**, 1728–1739 (1995).

44. Y. Habraken, P. Sung, L. Prakash, S. Prakash, Enhancement of MSH2-MSH3-mediated mismatch recognition by the yeast MLH1-PMS1 complex. *Curr. Biol.* **7**, 790–793 (1997).

45. F. A. Kadyrov, L. Dzantiev, N. Constantin, P. Modrich, Endonucleolytic function of MutLalpha in human mismatch repair. *Cell*. **126**, 297–308 (2006).

46. A. Pluciennik *et al.*, PCNA function in the activation and strand direction of MutLα endonuclease in mismatch repair. *Proc. Natl. Acad. Sci. USA*. **107**, 16066–16071 (2010).

47. T. A. Kunkel, D. A. Erie, Eukaryotic mismatch repair in relation to DNA replication. *Annu. Rev. Genet.* **49**, 291–313 (2015).

48. K. M. Welsh, A. L. Lu, S. Clark, P. Modrich, Isolation and characterization of the Escherichia coli mutH gene product. *J. Biol. Chem.* **262**, 15624–15629 (1987).

49. H. Hombauer, A. Srivatsan, C. D. Putnam, R. D. Kolodner, Mismatch repair, but not heteroduplex rejection, is temporally coupled to DNA replication. *Science*. **334**, 1713–1716 (2011).

50. L. D. Langston, M. O'Donnell, DNA replication: keep moving and don't mind the gap. *Mol. Cell*. **23**, 155–160 (2006).

51. Y. I. Pavlov, I. M. Mian, T. A. Kunkel, Evidence for preferential mismatch repair of lagging strand DNA replication errors in yeast. *Curr. Biol.* **13**, 744–748 (2003).

52. M. M. Ghodgaonkar *et al.*, Ribonucleotides misincorporated into DNA act as strand-discrimination signals in eukaryotic mismatch repair. *Mol. Cell*. **50**, 323–332 (2013).

53. S. Chakarov, R. Petkova, G. Russev, N. Zhelev, DNA damage and mutation. Types of DNA damage. *Biodiscovery*, 1 (2014).

54. B. B. Zhou, S. J. Elledge, The DNA damage response: putting checkpoints in perspective. *Nature*. **408**, 433–439 (2000).

55. M. A. Troester *et al.*, Cell-type-specific responses to chemotherapeutics in breast cancer. *Cancer Res.* **64**, 4218–4226 (2004).

56. H. Stevens, A. B. Williams, W. M. Michael, Cell-Type Specific Responses to DNA Replication Stress in Early C. elegans Embryos. *PLoS One*. **11**, e0164601 (2016).

57. M. Patil, N. Pabla, Z. Dong, Checkpoint kinase 1 in DNA damage response and cell cycle regulation. *Cell Mol. Life Sci.* **70**, 4009–4021 (2013).

58. X. Huang, Z. Darzynkiewicz, Cytometric assessment of histone H2AX phosphorylation: a reporter of DNA damage. *Methods Mol. Biol.* **314**, 73–80 (2006).

59. A. Kinner, W. Wu, C. Staudt, G. Iliakis, Gamma-H2AX in recognition and signaling of DNA double-strand breaks in the context of chromatin. *Nucleic Acids Res.* **36**, 5678–5694 (2008).

60. R. Scully, A. Xie, Double strand break repair functions of histone H2AX. *Mutat. Res.* **750**, 5–14 (2013).

61. S. J. Elledge, The DNA Damage Response, (available at http://elledgelab.med.harvard.edu/?page_id=264).

62. C. J. Bakkenist, M. B. Kastan, DNA damage activates ATM through intermolecular autophosphorylation and dimer dissociation. *Nature*. **421**, 499–506 (2003).

63. T. Iyama, D. M. Wilson, DNA repair mechanisms in dividing and non-dividing cells. *DNA Repair (Amst.)*. **12**, 620–636 (2013).

64. A. A. Goodarzi, P. A. Jeggo, The repair and signaling responses to DNA double-strand breaks. *Adv Genet*. **82**, 1–45 (2013).

65. N. D. Lakin, S. P. Jackson, Regulation of p53 in response to DNA damage. *Oncogene*. **18**, 7644–7655 (1999).

66. L. S. Waters *et al.*, Eukaryotic translesion polymerases and their roles and regulation in DNA damage tolerance. *Microbiol. Mol. Biol. Rev.* **73**, 134–154 (2009).

67. P. A. Knobel, T. M. Marti, Translesion DNA synthesis in the context of cancer research. *Cancer Cell Int.* **11**, 39 (2011).

68. J. K. Hicks, The Cellular Roles of the Translesion Polymerases Eta, REV1 and Zeta in Bypass and Repair of DNA Damage Induced by Anti-Cancer Agents. (2010).

69. K. Watanabe *et al.*, Rad18 guides poleta to replication stalling sites through physical interaction and PCNA monoubiquitination. *EMBO J.* **23**, 3886–3896 (2004).

70. X. Bi *et al.*, Rad18 regulates DNA polymerase kappa and is required for recovery from S-phase checkpoint-mediated arrest. *Mol. Cell. Biol.* **26**, 3527–3540 (2006).

71. M. Bienko *et al.*, Ubiquitin-binding domains in Y-family polymerases regulate translesion synthesis. *Science*. **310**, 1821–1824 (2005).

72. A. Ahmad, S. L. Nay, T. R. O'Connor, in *Advances in DNA repair*, C. C. Chen, Ed. (InTech, 2015).

73. J. C. Fromme, G. L. Verdine, Base excision repair. *Adv. Protein Chem.* **69**, 1–41 (2004).

74. S. S. Wallace, Base excision repair: a critical player in many games. *DNA Repair (Amst.)*. **19**, 14–26 (2014).

75. J. T. Reardon, A. Sancar, Nucleotide excision repair. *Prog Nucleic Acid Res Mol Biol*. **79**, 183–235 (2005).

76. J. A. Marteijn, H. Lans, W. Vermeulen, J. H. J. Hoeijmakers, Understanding nucleotide excision repair and its roles in cancer and ageing. *Nat. Rev. Mol. Cell Biol.* **15**, 465–481 (2014).

77. K. W. Caldecott, Single-strand break repair and genetic disease. *Nat. Rev. Genet.* **9**, 619–631 (2008).

78. R. Ceccaldi, B. Rondinelli, A. D. D'Andrea, Repair Pathway Choices and Consequences at the Double-Strand Break. *Trends Cell Biol.* **26**, 52–64 (2016).

79. T. H. Stracker, J. H. J. Petrini, The MRE11 complex: starting from the ends. *Nat. Rev. Mol. Cell Biol.* **12**, 90–103 (2011).

80. R. Anand, L. Ranjha, E. Cannavo, P. Cejka, Phosphorylated CtIP Functions as a Co-factor of the MRE11-RAD50-NBS1 Endonuclease in DNA End Resection. *Mol. Cell*. **64**, 940–950 (2016).

81. L. R. Myler *et al.*, Single-Molecule Imaging Reveals How Mre11-Rad50-Nbs1 Initiates DNA Break Repair. *Mol. Cell*. **67**, 891–898.e4 (2017).

82. M. Sebesta, L. Krejci, in *DNA replication, recombination, and repair*, F. Hanaoka, K. Sugasawa, Eds. (Springer Japan, Tokyo, 2016), pp. 73–109.

83. M. Jasin, R. Rothstein, Repair of strand breaks by homologous recombination. *Cold Spring Harb. Perspect. Biol.* **5**, a012740 (2013).

84. D. C. van Gent, H. IJspeert, M. van der Burg, in *DNA replication, recombination, and repair*, F. Hanaoka, K. Sugasawa, Eds. (Springer Japan, Tokyo, 2016), pp. 341–362.

85. H. H. Y. Chang, N. R. Pannunzio, N. Adachi, M. R. Lieber, Non-homologous DNA end joining and alternative pathways to double-strand break repair. *Nat. Rev. Mol. Cell Biol.* **18**, 495–506 (2017).

86. J.-H. Seol, E. Y. Shim, S. E. Lee, Microhomology-mediated end joining: Good, bad and ugly. *Mutat. Res.* **809**, 81–87 (2018).

87. S. Hashimoto, H. Anai, K. Hanada, Mechanisms of interstrand DNA crosslink repair and human disorders. *Genes Environ.* **38**, 9 (2016).

88. M. Räschle *et al.*, Mechanism of replication-coupled DNA interstrand crosslink repair. *Cell*. **134**, 969–980 (2008).

89. P. D. Sniegowski, P. J. Gerrish, R. E. Lenski, Evolution of high mutation rates in experimental populations of E. coli. *Nature*. **387**, 703–705 (1997).

90. J. E. LeClerc, B. Li, W. L. Payne, T. A. Cebula, High mutation frequencies among Escherichia coli and Salmonella pathogens. *Science*. **274**, 1208–1211 (1996).

91. I. Matic *et al.*, Highly variable mutation rates in commensal and pathogenic Escherichia coli. *Science*. **277**, 1833–1834 (1997).

92. T. C. Gibson, M. L. Scheppe, E. C. Cox, Fitness of an Escherichia coli mutator gene. *Science*. **169**, 686–688 (1970).

93. W. Tröbner, R. Piechocki, Competition between isogenic mutS and mut+ populations of Escherichia coli K12 in continuously growing cultures. *Molecular and General Genetics MGG*. **198**, 175–176 (1984).

94. C. F. Gentile, S.-C. Yu, S. A. Serrano, P. J. Gerrish, P. D. Sniegowski, Competition between high- and higher-mutating strains of Escherichia coli. *Biol. Lett.* **7**, 422–424 (2011).

95. E. F. Mao, L. Lane, J. Lee, J. H. Miller, Proliferation of mutators in A cell population. *J. Bacteriol.* **179**, 417–422 (1997).

96. A. Giraud *et al.*, Costs and benefits of high mutation rates: adaptive evolution of bacteria in the mouse gut. *Science*. **291**, 2606–2608 (2001).

97. O. Tenaillon, B. Toupance, H. Le Nagard, F. Taddei, B. Godelle, Mutators, population size, adaptive landscape and the adaptation of asexual populations of bacteria. *Genetics*. **152**, 485–493 (1999).

98. J. M. Smith, J. Haigh, The hitch-hiking effect of a favourable gene. *Genet Res*. **23**, 23–35 (1974).

99. R. S. Galhardo, P. J. Hastings, S. M. Rosenberg, Mutation as a stress response and the regulation of evolvability. *Crit Rev Biochem Mol Biol*. **42**, 399–435 (2007).

100. I. Bjedov *et al.*, Stress-induced mutagenesis in bacteria. *Science*. **300**, 1404–1409 (2003).

101. H. T. Lynch, A. de la Chapelle, Genetic susceptibility to non-polyposis colorectal cancer. *J. Med. Genet.* **36**, 801–818 (1999).

102. J. P. Mecklin, H. J. Järvinen, Tumor spectrum in cancer family syndrome (hereditary nonpolyposis colorectal cancer). *Cancer*. **68**, 1109–1112 (1991).

103. C. E. Bronner *et al.*, Mutation in the DNA mismatch repair gene homologue hMLH1 is associated with hereditary non-polyposis colon cancer. *Nature*. **368**, 258–261 (1994).

104. N. Papadopoulos *et al.*, Mutation of a mutL homolog in hereditary colon cancer. *Science*. **263**, 1625–1629 (1994).

105. R. Fishel *et al.*, The human mutator gene homolog MSH2 and its association with hereditary nonpolyposis colon cancer. *Cell*. **75**, 1027–1038 (1993).

106. M. Miyaki *et al.*, Germline mutation of MSH6 as the cause of hereditary nonpolyposis colorectal cancer. *Nat. Genet.* **17**, 271–272 (1997).

107. N. C. Nicolaides *et al.*, Mutations of two PMS homologues in hereditary nonpolyposis colon cancer. *Nature*. **371**, 75–80 (1994).

108. F. Duraturo *et al.*, Association of low-risk MSH3 and MSH2 variant alleles with Lynch syndrome: probability of synergistic effects. *Int. J. Cancer*. **129**, 1643–1650 (2011).

109. F. Duraturo, R. Liccardo, P. Izzo, Coexistence of MLH3 germline variants in colon cancer patients belonging to families with Lynch syndrome-associated brain tumors. *J. Neurooncol.* (2016), doi:10.1007/s11060-016-2203-0.

110. C. R. Boland, A. Goel, Microsatellite instability in colorectal cancer. *Gastroenterology*. **138**, 2073–2087.e3 (2010).

111. M. F. Kane *et al.*, Methylation of the hMLH1 promoter correlates with lack of expression of hMLH1 in sporadic colon tumors and mismatch repair-defective human tumor cell lines. *Cancer Res.* **57**, 808–811 (1997).

112. J. E. Cleaver, Defective repair replication of DNA in xeroderma pigmentosum. *Nature*. **218**, 652–656 (1968).

113. J. H. Epstein, K. Fukuyama, W. B. Reed, W. L. Epstein, Defect in DNA synthesis in skin of patients with xeroderma pigmentosum demonstrated in vivo. *Science*. **168**, 1477–1478 (1970).

114. K. H. Kraemer, M. M. Lee, J. Scotto, Xeroderma Pigmentosum: Cutaneous, Ocular, and Neurologic Abnormalities in 830 Published Cases. *Arch. Dermatol.* (1987).

115. K. H. Kraemer, M.-M. Lee, A. D. Andrews, W. C. Lambert, The Role of Sunlight and DNA Repair in Melanoma and Nonmelanoma Skin Cancer: The Xeroderma Pigmentosum Paradigm. *Arch. Dermatol.* (1994).

116. K. H. Kraemer, M. M. Lee, J. Scotto, DNA repair protects against cutaneous and internal neoplasia: evidence from xeroderma pigmentosum. *Carcinogenesis*. **5**, 511–514 (1984).

117. K. H. Kraemer *et al.*, Genetic heterogeneity in xeroderma pigmentosum: complementation groups and their relationship to DNA repair rates. *Proc. Natl. Acad. Sci. USA*. **72**, 59–63 (1975).

118. K. H. Kraemer *et al.*, Five complementation groups in xeroderma pigmentosum. *Mutat. Res.* **33**, 327–340 (1975).

119. S. Arase, T. Kozuka, K. Tanaka, M. Ikenaga, H. Takebe, A sixth complementation group in xeroderma pigmentosum. *Mutat. Res.* **59**, 143–146 (1979).

120. W. Keijzer *et al.*, A seventh complementation group in excision-deficient xeroderma pigmentosum. *Mutat. Res.* **62**, 183–190 (1979).

121. A. R. Lehmann *et al.*, Xeroderma pigmentosum cells with normal levels of excision repair have a defect in DNA synthesis after UV-irradiation. *Proc. Natl. Acad. Sci. USA*. **72**, 219–223 (1975).

122. K. H. Kraemer, Sunlight and skin cancer: another link revealed. *Proc. Natl. Acad. Sci. USA*. **94**, 11–14 (1997).

123. S. Briggs, I. Tomlinson, Germline and somatic polymerase ε and δ mutations define a new class of hypermutated colorectal and endometrial cancers. *J. Pathol.* **230**, 148–153 (2013).

124. T. M. Albertson *et al.*, DNA polymerase epsilon and delta proofreading suppress discrete mutator and cancer phenotypes in mice. *Proc. Natl. Acad. Sci. USA*. **106**, 17101–17104 (2009).

125. D. N. Church *et al.*, DNA polymerase ε and δ exonuclease domain mutations in endometrial cancer. *Hum. Mol. Genet.* **22**, 2820–2828 (2013).

126. B. Meng *et al.*, POLE exonuclease domain mutation predicts long progression-free survival in grade 3 endometrioid carcinoma of the endometrium. *Gynecol. Oncol.* **134**, 15–19 (2014).

127. E. Z. Erson-Omay *et al.*, Somatic POLE mutations cause an ultramutated giant cell high-grade glioma subtype with better prognosis. *Neuro. Oncol.* **17**, 1356–1364 (2015).

128. R. Yoshida *et al.*, Concurrent genetic alterations in DNA polymerase proofreading and mismatch repair in human colorectal cancer. *Eur. J. Hum. Genet.* **19**, 320–325 (2011).

129. K. P. Hodel *et al.*, Explosive mutation accumulation triggered by heterozygous human Pol ε proofreading-deficiency is driven by suppression of mismatch repair. *Elife*. **7** (2018), doi:10.7554/eLife.32692.

130. A. Paul, S. Paul, The breast cancer susceptibility genes (BRCA) in breast and ovarian cancers. *Front. Biosci. (Landmark Ed)*. **19**, 605–618 (2014).

131. F. Yuan *et al.*, Overexpressed DNA polymerase iota regulated by JNK/c-Jun contributes to hypermutagenesis in bladder cancer. *PLoS One*. **8**, e69317 (2013).

132. H. Wang *et al.*, Analysis of specialized DNA polymerases expression in human gliomas: association with prognostic significance. *Neuro. Oncol.* **12**, 679–686 (2010).

133. J. Yang, Z. Chen, Y. Liu, R. J. Hickey, L. H. Malkas, Altered DNA polymerase iota expression in breast cancer cells leads to a reduction in DNA replication fidelity and a higher rate of mutagenesis. *Cancer Res.* **64**, 5597–5607 (2004).

134. H. Sun *et al.*, Elevated DNA polymerase iota (Poli) is involved in the acquisition of aggressive phenotypes of human esophageal squamous cell cancer. *Int J Clin Exp Pathol*. **8**, 3591–3601 (2015).

135. S. Zou *et al.*, DNA polymerase iota (Pol ι) promotes invasion and metastasis of esophageal squamous cell carcinoma. *Oncotarget*. **7**, 32274–32285 (2016).

136. J. O-Wang *et al.*, DNA polymerase kappa, implicated in spontaneous and DNA damage-induced mutagenesis, is overexpressed in lung cancer. *Cancer Res.* **61**, 5366–5369 (2001).

137. C. Peng *et al.*, The Error-Prone DNA Polymerase κ Promotes Temozolomide Resistance in Glioblastoma through Rad17-Dependent Activation of ATR-Chk1 Signaling. *Cancer Res.* **76**, 2340–2353 (2016).

138. W. A. Rosche, P. L. Foster, The role of transient hypermutators in adaptive mutation in Escherichia coli. *Proc. Natl. Acad. Sci. USA*. **96**, 6862–6867 (1999).

139. G. J. McKenzie, R. S. Harris, P. L. Lee, S. M. Rosenberg, The SOS response regulates adaptive mutation. *Proc. Natl. Acad. Sci. USA*. **97**, 6646–6651 (2000).

140. R. G. Ponder, N. C. Fonville, S. M. Rosenberg, A switch from high-fidelity to error-prone DNA double-strand break repair underlies stress-induced mutation. *Mol. Cell*. **19**, 791–804 (2005).

141. D. M. Fitzgerald, P. J. Hastings, S. M. Rosenberg, Stress-Induced Mutagenesis: Implications in Cancer and Drug Resistance. *Annu. Rev. Cancer Biol.* **1**, 119–140 (2017).

142. C. Shee *et al.*, Engineered proteins detect spontaneous DNA breakage in human and bacterial cells. *Elife*. **2**, e01222 (2013).

143. R. S. Harris, S. Longerich, S. M. Rosenberg, Recombination in adaptive mutation. *Science*. **264**, 258–260 (1994).

144. J. Cairns, P. L. Foster, Adaptive reversion of a frameshift mutation in Escherichia coli. *Genetics*. **128**, 695–701 (1991).

145. P. L. Foster, J. M. Trimarchi, R. A. Maurer, Two enzymes, both of which process recombination intermediates, have opposite effects on adaptive mutation in Escherichia coli. *Genetics*. **142**, 25–37 (1996).

146. R. S. Harris, K. J. Ross, S. M. Rosenberg, Opposing roles of the holliday junction processing systems of Escherichia coli in recombination-dependent adaptive mutation. *Genetics*. **142**, 681–691 (1996).

147. R. S. Galhardo *et al.*, DinB upregulation is the sole role of the SOS response in stress-induced mutagenesis in Escherichia coli. *Genetics*. **182**, 55–68 (2009).

148. H. Weber, T. Polen, J. Heuveling, V. F. Wendisch, R. Hengge, Genome-wide analysis of the general stress response network in Escherichia coli: sigmaS-dependent genes, promoters, and sigma factor selectivity. *J. Bacteriol.* **187**, 1591–1603 (2005).

149. M.-J. Lombardo, I. Aponyi, S. M. Rosenberg, General stress response regulator RpoS in adaptive mutation and amplification in Escherichia coli. *Genetics*. **166**, 669–680 (2004).

150. J. C. Layton, P. L. Foster, Error-prone DNA polymerase IV is controlled by the stress-response sigma factor, RpoS, in Escherichia coli. *Mol. Microbiol.* **50**, 549–561 (2003).

151. P. J. Hastings *et al.*, Competition of Escherichia coli DNA polymerases I, II and III with DNA Pol IV in stressed cells. *PLoS One*. **5**, e10862 (2010).

152. R. L. Frisch *et al.*, Separate DNA Pol II- and Pol IV-dependent pathways of stress-induced mutation during double-strand-break repair in Escherichia coli are controlled by RpoS. *J. Bacteriol.* **192**, 4694–4700 (2010).

153. G. J. McKenzie, P. L. Lee, M. J. Lombardo, P. J. Hastings, S. M. Rosenberg, SOS mutator DNA polymerase IV functions in adaptive mutation and not adaptive amplification. *Mol. Cell*. **7**, 571–579 (2001).

154. P. L. Foster, G. Gudmundsson, J. M. Trimarchi, H. Cai, M. F. Goodman, Proofreading-defective DNA polymerase II increases adaptive mutation in Escherichia coli. *Proc. Natl. Acad. Sci. USA*. **92**, 7951–7955 (1995).

155. H. C. Tsui, G. Feng, M. E. Winkler, Negative regulation of mutS and mutH repair gene expression by the Hfq and RpoS global regulators of Escherichia coli K-12. *J. Bacteriol.* **179**, 7476–7487 (1997).

156. R. S. Harris *et al.*, Mismatch repair protein MutL becomes limiting during stationary-phase mutation. *Genes Dev.* **11**, 2426–2437 (1997).

157. G. Feng, H. C. Tsui, M. E. Winkler, Depletion of the cellular amounts of the MutS and MutH methyl-directed mismatch repair proteins in stationary-phase Escherichia coli K-12 cells. *J. Bacteriol.* **178**, 2388–2396 (1996).

158. N. S. Persky, S. T. Lovett, Mechanisms of recombination: lessons from E. coli. *Crit Rev Biochem Mol Biol*. **43**, 347–370 (2008).

159. H. Ohmori *et al.*, The Y-family of DNA polymerases. *Mol. Cell*. **8**, 7–8 (2001).

160. C. Janion, Inducible SOS response system of DNA repair and mutagenesis in Escherichia coli. *Int. J. Biol. Sci.* **4**, 338–344 (2008).

161. A. Battesti, N. Majdalani, S. Gottesman, The RpoS-mediated general stress response in Escherichia coli. *Annu. Rev. Microbiol.* **65**, 189–213 (2011).

162. A. M. Heberle *et al.*, Molecular mechanisms of mTOR regulation by stress. *Molecular & Cellular Oncology*. **2**, e970489 (2015).

163. K. A. M. Storvik, P. L. Foster, RpoS, the stress response sigma factor, plays a dual role in the regulation of Escherichia coli's error-prone DNA polymerase IV. *J. Bacteriol.* **192**, 3639–3644 (2010).

164. J. Aramburu, M. C. Ortells, S. Tejedor, M. Buxadé, C. López-Rodríguez, Transcriptional regulation of the stress response by mTOR. *Sci. Signal.* **7**, re2 (2014).

165. K. Fukui, DNA mismatch repair in eukaryotes and bacteria. *J. Nucleic Acids*. **2010** (2010), doi:10.4061/2010/260512.

166. R. L. Mort, I. J. Jackson, E. E. Patton, The melanocyte lineage in development and disease. *Development*. **142**, 620–632 (2015).

167. B. Shannan, M. Perego, R. Somasundaram, M. Herlyn, Heterogeneity in Melanoma. *Cancer Treat. Res.* **167**, 1–15 (2016).

168. W. H. Clark *et al.*, A study of tumor progression: the precursor lesions of superficial spreading and nodular melanoma. *Hum. Pathol.* **15**, 1147–1165 (1984).

169. J. D. Wolchok *et al.*, Overall Survival with Combined Nivolumab and Ipilimumab in Advanced Melanoma. *N. Engl. J. Med.* **377**, 1345–1356 (2017).

170. J. Longstreth, Cutaneous malignant melanoma and ultraviolet radiation: A review. *Cancer Metast. Rev.* **7**, 321–333 (1988).

171. B. C. Bastian, The molecular pathology of melanoma: an integrated taxonomy of melanocytic neoplasia. *Annu. Rev. Pathol.* **9**, 239–271 (2014).

172. C. Cohen *et al.*, Mitogen-actived protein kinase activation is an early event in melanoma progression. *Clin. Cancer Res.* **8**, 3728–3733 (2002).

173. B. Govindarajan *et al.*, Malignant transformation of melanocytes to melanoma by constitutive activation of mitogen-activated protein kinase kinase (MAPKK) signaling. *J. Biol. Chem.* **278**, 9790–9795 (2003).

174. A. L. Pritchard, N. K. Hayward, Molecular pathways: mitogen-activated protein kinase pathway mutations and drug resistance. *Clin. Cancer Res.* **19**, 2301–2309 (2013).

175. M. Cargnello, P. P. Roux, Activation and function of the MAPKs and their substrates, the MAPK-activated protein kinases. *Microbiol. Mol. Biol. Rev.* **75**, 50–83 (2011).

176. A. Gorden *et al.*, Analysis of BRAF and N-RAS mutations in metastatic melanoma tissues. *Cancer Res.* **63**, 3955–3957 (2003).

177. Cancer Genome Atlas Network, Genomic classification of cutaneous melanoma. *Cell*. **161**, 1681–1696 (2015).

178. H. Davies *et al.*, Mutations of the BRAF gene in human cancer. *Nature*. **417**, 949–954 (2002).

179. P. A. Ascierto *et al.*, The role of BRAF V600 mutation in melanoma. *J. Transl. Med.* **10**, 85 (2012).

180. E. Hodis *et al.*, A landscape of driver mutations in melanoma. *Cell*. **150**, 251–263 (2012).

181. D. B. Solit *et al.*, BRAF mutation predicts sensitivity to MEK inhibition. *Nature*. **439**, 358–362 (2006).

182. A.-X. Wang, X.-Y. Qi, Targeting RAS/RAF/MEK/ERK signaling in metastatic melanoma. *IUBMB Life*. **65**, 748–758 (2013).

183. K. T. Flaherty *et al.*, Improved survival with MEK inhibition in BRAF-mutated melanoma. *N. Engl. J. Med.* **367**, 107–114 (2012).

184. J. Tsai *et al.*, Discovery of a selective inhibitor of oncogenic B-Raf kinase with potent antimelanoma activity. *Proc. Natl. Acad. Sci. USA*. **105**, 3041–3046 (2008).

185. E. W. Joseph *et al.*, The RAF inhibitor PLX4032 inhibits ERK signaling and tumor cell proliferation in a V600E BRAF-selective manner. *Proc. Natl. Acad. Sci. USA*. **107**, 14903–14908 (2010).

186. K. T. Flaherty *et al.*, Inhibition of mutated, activated BRAF in metastatic melanoma. *N. Engl. J. Med.* **363**, 809–819 (2010).

187. J. A. Sosman *et al.*, Survival in BRAF V600-mutant advanced melanoma treated with vemurafenib. *N. Engl. J. Med.* **366**, 707–714 (2012).

188. P. B. Chapman *et al.*, Improved survival with vemurafenib in melanoma with BRAF V600E mutation. *N. Engl. J. Med.* **364**, 2507–2516 (2011).

189. G. V. Long *et al.*, Combined BRAF and MEK inhibition versus BRAF inhibition alone in melanoma. *N. Engl. J. Med.* **371**, 1877–1888 (2014).

190. F. S. Hodi *et al.*, Improved survival with ipilimumab in patients with metastatic melanoma. *N. Engl. J. Med.* **363**, 711–723 (2010).

191. D. Beck *et al.*, Vemurafenib potently induces endoplasmic reticulum stress-mediated apoptosis in BRAFV600E melanoma cells. *Sci. Signal.* **6**, ra7 (2013).

192. S. Haferkamp *et al.*, Vemurafenib induces senescence features in melanoma cells. *J. Invest. Dermatol.* **133**, 1601–1609 (2013).

193. C. M. Oslowski, F. Urano, Measuring ER stress and the unfolded protein response using mammalian tissue culture system. *Meth. Enzymol.* **490**, 71–92 (2011).

194. C. Appenzeller-Herzog, M. N. Hall, Bidirectional crosstalk between endoplasmic reticulum stress and mTOR signaling. *Trends Cell Biol.* **22**, 274–282 (2012).

195. L. Qin, Z. Wang, L. Tao, Y. Wang, ER stress negatively regulates AKT/TSC/mTOR pathway to enhance autophagy. *Autophagy*. **6**, 239–247 (2010).

196. K. Eigner *et al.*, The unfolded protein response impacts melanoma progression by enhancing FGF expression and can be antagonized by a chemical chaperone. *Sci. Rep.* **7**, 17498 (2017).

197. C. Holohan, S. Van Schaeybroeck, D. B. Longley, P. G. Johnston, Cancer drug resistance: an evolving paradigm. *Nat. Rev. Cancer*. **13**, 714–726 (2013).

198. W. Chen, H. Yuan, Z. Wang, in *Myeloid Leukemia - Basic Mechanisms of Leukemogenesis*, S. Koschmieder, Ed. (InTech, 2011).

199. K. Kochanowski, L. Morinishi, S. J. Altschuler, L. F. Wu, Drug persistence – From antibiotics to cancer therapies. *Current Opinion in Systems Biology*. **10**, 1–8 (2018).

200. S. V. Sharma *et al.*, A chromatin-mediated reversible drug-tolerant state in cancer cell subpopulations. *Cell*. **141**, 69–80 (2010).

201. S. Pearl Mizrahi, O. Gefen, I. Simon, N. Q. Balaban, Persistence to anti-cancer treatments in the stationary to proliferating transition. *Cell Cycle*. **15**, 3442–3453 (2016).

202. N. R. Cohen, M. A. Lobritz, J. J. Collins, Microbial persistence and the road to drug resistance. *Cell Host Microbe*. **13**, 632–642 (2013).

203. M. Ramirez *et al.*, Diverse drug-resistance mechanisms can emerge from drug-tolerant cancer persister cells. *Nat. Commun.* **7**, 10690 (2016).

204. A. N. Hata *et al.*, Tumor cells can follow distinct evolutionary paths to become resistant to epidermal growth factor receptor inhibition. *Nat. Med.* **22**, 262–269 (2016).

205. F. Michor *et al.*, Dynamics of chronic myeloid leukaemia. *Nature*. **435**, 1267–1270 (2005).

206. A. Azvolinsky, How Cancers Evolve Drug Resistance. *The Scientist* (2017), (available at https://www.the-scientist.com/features/how-cancers-evolve-drug-resistance-31742).

207. N. P. Shah *et al.*, Multiple BCR-ABL kinase domain mutations confer polyclonal resistance to the tyrosine kinase inhibitor imatinib (STI571) in chronic phase and blast crisis chronic myeloid leukemia. *Cancer Cell*. **2**, 117–125 (2002).

208. C. Kim *et al.*, Chemoresistance Evolution in Triple-Negative Breast Cancer Delineated by Single-Cell Sequencing. *Cell*. **173**, 879–893.e13 (2018).

209. H. Kim *et al.*, Whole-genome and multisector exome sequencing of primary and post-treatment glioblastoma reveals patterns of tumor evolution. *Genome Res.* **25**, 316–327 (2015).

210. K.-Y. Su *et al.*, Pretreatment epidermal growth factor receptor (EGFR) T790M mutation predicts shorter EGFR tyrosine kinase inhibitor response duration in patients with non-small-cell lung cancer. *J. Clin. Oncol.* **30**, 433–440 (2012).

211. L. A. Diaz *et al.*, The molecular evolution of acquired resistance to targeted EGFR blockade in colorectal cancers. *Nature*. **486**, 537–540 (2012).

212. E. M. Van Allen *et al.*, The genetic landscape of clinical resistance to RAF inhibition in metastatic melanoma. *Cancer Discov.* **4**, 94–109 (2014).

213. C. Roche-Lestienne *et al.*, Several types of mutations of the Abl gene can be found in chronic myeloid leukemia patients resistant to STI571, and they can pre-exist to the onset of treatment. *Blood*. **100**, 1014–1018 (2002).

214. T. Ernst *et al.*, Dynamics of BCR-ABL mutated clones prior to hematologic or cytogenetic resistance to imatinib. *Haematologica*. **93**, 186–192 (2008).

215. L. Ding *et al.*, Clonal evolution in relapsed acute myeloid leukaemia revealed by whole-genome sequencing. *Nature*. **481**, 506–510 (2012).

216. A.-M. Patch *et al.*, Whole-genome characterization of chemoresistant ovarian cancer. *Nature*. **521**, 489–494 (2015).

217. M. Inukai *et al.*, Presence of epidermal growth factor receptor gene T790M mutation as a minor clone in non-small cell lung cancer. *Cancer Res.* **66**, 7854–7858 (2006).

218. C. Bettegowda *et al.*, *Sci. Transl. Med.*, in press, doi:10.1126/scitranslmed.3007094.

219. N. Wagle *et al.*, Dissecting therapeutic resistance to RAF inhibition in melanoma by tumor genomic profiling. *J. Clin. Oncol.* **29**, 3085–3096 (2011).

220. H. Yuan *et al.*, BCR-ABL gene expression is required for its mutations in a novel KCL-22 cell culture model for acquired resistance of chronic myelogenous leukemia. *J. Biol. Chem.* **285**, 5085–5096 (2010).

221. S. Misale *et al.*, Emergence of KRAS mutations and acquired resistance to anti-EGFR therapy in colorectal cancer. *Nature*. **486**, 532–536 (2012).

222. R. Nazarian *et al.*, Melanomas acquire resistance to B-RAF(V600E) inhibition by RTK or N-RAS upregulation. *Nature*. **468**, 973–977 (2010).

223. H. Shi *et al.*, Acquired resistance and clonal evolution in melanoma during BRAF inhibitor therapy. *Cancer Discov.* **4**, 80–93 (2014).

224. P. I. Poulikakos *et al.*, RAF inhibitor resistance is mediated by dimerization of aberrantly spliced BRAF(V600E). *Nature*. **480**, 387–390 (2011).

225. S. R. Whittaker *et al.*, A genome-scale RNA interference screen implicates NF1 loss in resistance to RAF inhibition. *Cancer Discov.* **3**, 350–362 (2013).

226. C. M. Johannessen *et al.*, COT drives resistance to RAF inhibition through MAP kinase pathway reactivation. *Nature*. **468**, 968–972 (2010).

227. C. M. Emery *et al.*, MEK1 mutations confer resistance to MEK and B-RAF inhibition. *Proc. Natl. Acad. Sci. USA*. **106**, 20411–20416 (2009).

228. J. Villanueva *et al.*, Concurrent MEK2 mutation and BRAF amplification confer resistance to BRAF and MEK inhibitors in melanoma. *Cell Rep.* **4**, 1090–1099 (2013).

229. D. B. Johnson *et al.*, Acquired BRAF inhibitor resistance: A multicenter meta-analysis of the spectrum and frequencies, clinical behaviour, and phenotypic associations of resistance mechanisms. *Eur. J. Cancer*. **51**, 2792–2799 (2015).

230. K. H. T. Paraiso *et al.*, PTEN loss confers BRAF inhibitor resistance to melanoma cells through the suppression of BIM expression. *Cancer Res.* **71**, 2750–2760 (2011).

231. R. Straussman *et al.*, Tumour micro-environment elicits innate resistance to RAF inhibitors through HGF secretion. *Nature*. **487**, 500–504 (2012).

232. E. Hirata *et al.*, Intravital imaging reveals how BRAF inhibition generates drug-tolerant microenvironments with high integrin β1/FAK signaling. *Cancer Cell*. **27**, 574–588 (2015).

233. J. Kunz *et al.*, Target of rapamycin in yeast, TOR2, is an essential phosphatidylinositol kinase homolog required for G1 progression. *Cell*. **73**, 585–596 (1993).

234. D. M. Sabatini, H. Erdjument-Bromage, M. Lui, P. Tempst, S. H. Snyder, RAFT1: a mammalian protein that binds to FKBP12 in a rapamycin-dependent fashion and is homologous to yeast TORs. *Cell*. **78**, 35–43 (1994).

235. M. Laplante, D. M. Sabatini, mTOR signaling in growth control and disease. *Cell*. **149**, 274–293 (2012).

236. A. R. Tee, B. D. Manning, P. P. Roux, L. C. Cantley, J. Blenis, Tuberous sclerosis complex gene products, Tuberin and Hamartin, control mTOR signaling by acting as a GTPase-activating protein complex toward Rheb. *Curr. Biol.* **13**, 1259–1268 (2003).

237. K. Inoki, Y. Li, T. Xu, K.-L. Guan, Rheb GTPase is a direct target of TSC2 GAP activity and regulates mTOR signaling. *Genes Dev.* **17**, 1829–1834 (2003).

238. G. Song, G. Ouyang, S. Bao, The activation of Akt/PKB signaling pathway and cell survival. *J. Cell Mol. Med.* (2005).

239. C. J. Potter, L. G. Pedraza, T. Xu, Akt regulates growth by directly phosphorylating Tsc2. *Nat. Cell Biol.* **4**, 658–665 (2002).

240. K. Inoki, Y. Li, T. Zhu, J. Wu, K.-L. Guan, TSC2 is phosphorylated and inhibited by Akt and suppresses mTOR signalling. *Nat. Cell Biol.* **4**, 648–657 (2002).

241. E. Vander Haar, S.-I. Lee, S. Bandhakavi, T. J. Griffin, D.-H. Kim, Insulin signalling to mTOR mediated by the Akt/PKB substrate PRAS40. *Nat. Cell Biol.* **9**, 316–323 (2007).

242. Y. Sancak *et al.*, PRAS40 is an insulin-regulated inhibitor of the mTORC1 protein kinase. *Mol. Cell*. **25**, 903–915 (2007).

243. P. E. Burnett, R. K. Barrow, N. A. Cohen, S. H. Snyder, D. M. Sabatini, RAFT1 phosphorylation of the translational regulators p70 S6 kinase and 4E-BP1. *Proc. Natl. Acad. Sci. USA*. **95**, 1432–1437 (1998).

244. B. Magnuson, B. Ekim, D. C. Fingar, Regulation and function of ribosomal protein S6 kinase (S6K) within mTOR signalling networks. *Biochem. J.* **441**, 1–21 (2012).

245. D. C. Fingar, S. Salama, C. Tsou, E. Harlow, J. Blenis, Mammalian cell size is controlled by mTOR and its downstream targets S6K1 and 4EBP1/eIF4E. *Genes Dev.* **16**, 1472–1487 (2002).

246. R. J. O. Dowling *et al.*, mTORC1-mediated cell proliferation, but not cell growth, controlled by the 4E-BPs. *Science*. **328**, 1172–1176 (2010).

247. K. K. Park, K. Liu, Y. Hu, J. L. Kanter, Z. He, PTEN/mTOR and axon regeneration. *Exp. Neurol.* **223**, 45–50 (2010).

248. D. D. Sarbassov *et al.*, Rictor, a novel binding partner of mTOR, defines a rapamycin-insensitive and raptor-independent pathway that regulates the cytoskeleton. *Curr. Biol.* **14**, 1296–1302 (2004).

249. E. Jacinto *et al.*, Mammalian TOR complex 2 controls the actin cytoskeleton and is rapamycin insensitive. *Nat. Cell Biol.* **6**, 1122–1128 (2004).

250. D. D. Sarbassov, D. A. Guertin, S. M. Ali, D. M. Sabatini, Phosphorylation and regulation of Akt/PKB by the rictor-mTOR complex. *Science*. **307**, 1098–1101 (2005).

251. D. A. Guertin *et al.*, Ablation in mice of the mTORC components raptor, rictor, or mLST8 reveals that mTORC2 is required for signaling to Akt-FOXO and PKCalpha, but not S6K1. *Dev. Cell*. **11**, 859–871 (2006).

252. M. C. Mendoza, E. E. Er, J. Blenis, The Ras-ERK and PI3K-mTOR pathways: cross-talk and compensation. *Trends Biochem. Sci.* **36**, 320–328 (2011).

253. S. Lehr *et al.*, Identification of major ERK-related phosphorylation sites in Gab1. *Biochemistry*. **43**, 12133–12140 (2004).

254. S. Zimmermann, K. Moelling, Phosphorylation and regulation of Raf by Akt (protein kinase B). *Science*. **286**, 1741–1744 (1999).

255. N. Dumaz, R. Marais, Protein kinase A blocks Raf-1 activity by stimulating 14-3-3 binding and blocking Raf-1 interaction with Ras. *J. Biol. Chem.* **278**, 29819–29823 (2003).

256. P. P. Roux, B. A. Ballif, R. Anjum, S. P. Gygi, J. Blenis, Tumor-promoting phorbol esters and activated Ras inactivate the tuberous sclerosis tumor suppressor complex via p90 ribosomal S6 kinase. *Proc. Natl. Acad. Sci. USA*. **101**, 13489–13494 (2004).

257. A. Carriere *et al.*, ERK1/2 phosphorylate Raptor to promote Ras-dependent activation of mTOR complex 1 (mTORC1). *J. Biol. Chem.* **286**, 567–577 (2011).

258. T. Kodaki *et al.*, The activation of phosphatidylinositol 3-kinase by Ras. *Curr. Biol.* **4**, 798–806 (1994).

259. P. Rodriguez-Viciana *et al.*, Phosphatidylinositol-3-OH kinase as a direct target of Ras. *Nature*. **370**, 527–532 (1994).

260. J.-Y. Yang *et al.*, ERK promotes tumorigenesis by inhibiting FOXO3a via MDM2-mediated degradation. *Nat. Cell Biol.* **10**, 138–148 (2008).

261. W. H. Biggs, J. Meisenhelder, T. Hunter, W. K. Cavenee, K. C. Arden, Protein kinase B/Akt-mediated phosphorylation promotes nuclear exclusion of the winged

helix transcription factor FKHR1. *Proc. Natl. Acad. Sci. USA*. **96**, 7421–7426 (1999).

262. J. Zhu, J. Blenis, J. Yuan, Activation of PI3K/Akt and MAPK pathways regulates Myc-mediated transcription by phosphorylating and promoting the degradation of Mad1. *Proc. Natl. Acad. Sci. USA*. **105**, 6584–6589 (2008).

263. D. J. Giard *et al.*, In vitro cultivation of human tumors: establishment of cell lines derived from a series of solid tumors2. *JNCI: Journal of the National Cancer Institute*. **51**, 1417–1423 (1973).

264. T. E. Carey, T. Takahashi, L. A. Resnick, H. F. Oettgen, L. J. Old, Cell surface antigens of human malignant melanoma: mixed hemadsorption assays for humoral immunity to cultured autologous melanoma cells. *Proc. Natl. Acad. Sci. USA*. **73**, 3278–3282 (1976).

265. J. Fogh, J. M. Fogh, T. Orfeo, One Hundred and Twenty-Seven Cultured Human Tumor Cell Lines Producing Tumors in Nude Mice23. *JNCI: Journal of the National Cancer Institute*. **59**, 221–226 (1977).

266. E. E. Patton *et al.*, BRAF mutations are sufficient to promote nevi formation and cooperate with p53 in the genesis of melanoma. *Curr. Biol.* **15**, 249–254 (2005).

267. J. Yen *et al.*, The genetic heterogeneity and mutational burden of engineered melanomas in zebrafish models. *Genome Biol.* **14**, R113 (2013).

268. R. M. White *et al.*, DHODH modulates transcriptional elongation in the neural crest and melanoma. *Nature*. **471**, 518–522 (2011).

269. P. M. Pollock *et al.*, High frequency of BRAF mutations in nevi. *Nat. Genet.* **33**, 19–20 (2003).

270. N. Panté, M. Kann, Nuclear pore complex is able to transport macromolecules with diameters of about 39 nm. *Mol. Biol. Cell*. **13**, 425–434 (2002).

271. P. Kannouche *et al.*, Domain structure, localization, and function of DNA polymerase eta, defective in xeroderma pigmentosum variant cells. *Genes Dev.* **15**, 158–172 (2001).

272. P. Kannouche *et al.*, Localization of DNA polymerases eta and iota to the replication machinery is tightly co-ordinated in human cells. *EMBO J.* **22**, 1223–1233 (2003).

273. V. Bergoglio, C. Bavoux, V. Verbiest, J.-S. Hoffmann, C. Cazaux, Localisation of human DNA polymerase kappa to replication foci. *J. Cell Sci.* **115**, 4413–4418 (2002).

274. T. Ogi, P. Kannouche, A. R. Lehmann, Localisation of human Y-family DNA polymerase kappa: relationship to PCNA foci. *J. Cell Sci.* **118**, 129–136 (2005).

275. C. Guo *et al.*, REV1 protein interacts with PCNA: significance of the REV1 BRCT domain in vitro and in vivo. *Mol. Cell*. **23**, 265–271 (2006).

276. F. J. Bollum, V. R. Potter, Incorporation of thymidine into deoxyribonucleic acid by enzymes from rat tissues. *J. Biol. Chem.* **233**, 478–482 (1958).

277. D. M. Prescott, F. J. Bollum, B. C. Kluss, Is DNA polymerase a cytoplasmic enzyme? *J. Cell Biol.* **13**, 172–174 (1962).

278. J. W. Littlefield, A. P. McGOVERN, K. B. Margeson, Changes in the distribution of polymerase activity during DNA synthesis in mouse fibroblasts. *Proc. Natl. Acad. Sci. USA*. **49**, 102–107 (1963).

279. M. Beck, E. Hurt, The nuclear pore complex: understanding its function through structural insight. *Nat. Rev. Mol. Cell Biol.* **18**, 73–89 (2017).

280. C. Strambio-De-Castillia, M. Niepel, M. P. Rout, The nuclear pore complex: bridging nuclear transport and gene regulation. *Nat. Rev. Mol. Cell Biol.* **11**, 490–501 (2010).

281. I. G. Macara, Transport into and out of the Nucleus. *Microbiol. Mol. Biol. Rev.* **65**, 570–594 (2001).

282. M. S. Moore, G. Blobel, The GTP-binding protein Ran/TC4 is required for protein import into the nucleus. *Nature*. **365**, 661–663 (1993).

283. S. A. Adam, L. Gerace, Cytosolic proteins that specifically bind nuclear location signals are receptors for nuclear import. *Cell*. **66**, 837–847 (1991).

284. B. Cautain, R. Hill, N. de Pedro, W. Link, Components and regulation of nuclear transport processes. *FEBS J.* **282**, 445–462 (2015).

285. J. F. Soderholm *et al.*, Importazole, a small molecule inhibitor of the transport receptor importin-β. *ACS Chem. Biol.* **6**, 700–708 (2011).

286. C. Dingwall, S. V. Sharnick, R. A. Laskey, A polypeptide domain that specifies migration of nucleoplasmin into the nucleus. *Cell*. **30**, 449–458 (1982).

287. D. Kalderon, B. L. Roberts, W. D. Richardson, A. E. Smith, A short amino acid sequence able to specify nuclear location. *Cell*. **39**, 499–509 (1984).

288. C. V. Dang, W. M. Lee, Identification of the human c-myc protein nuclear translocation signal. *Mol. Cell. Biol.* **8**, 4048–4054 (1988).

289. C. Dingwall, J. Robbins, S. M. Dilworth, B. Roberts, W. D. Richardson, The nucleoplasmin nuclear location sequence is larger and more complex than that of SV-40 large T antigen. *J. Cell Biol.* **107**, 841–849 (1988).

290. A. Lange, L. M. McLane, R. E. Mills, S. E. Devine, A. H. Corbett, Expanding the definition of the classical bipartite nuclear localization signal. *Traffic*. **11**, 311–323 (2010).

291. M.-H. Chen *et al.*, Phospholipid scramblase 1 contains a nonclassical nuclear localization signal with unique binding site in importin alpha. *J. Biol. Chem.* **280**, 10599–10606 (2005).

292. P. Wang, P. Palese, R. E. O'Neill, The NPI-1/NPI-3 (karyopherin alpha) binding site on the influenza a virus nucleoprotein NP is a nonconventional nuclear localization signal. *J. Virol.* **71**, 1850–1856 (1997).

293. M. Stewart, Molecular mechanism of the nuclear protein import cycle. *Nat. Rev. Mol. Cell Biol.* **8**, 195–208 (2007).

294. M. Fukuda *et al.*, CRM1 is responsible for intracellular transport mediated by the nuclear export signal. *Nature*. **390**, 308–311 (1997).

295. K. Nishi *et al.*, Leptomycin B targets a regulatory cascade of crm1, a fission yeast nuclear protein, involved in control of higher order chromosome structure and gene expression. *J. Biol. Chem.* **269**, 6320–6324 (1994).

296. H. P. Bogerd, R. A. Fridell, R. E. Benson, J. Hua, B. R. Cullen, Protein sequence requirements for function of the human T-cell leukemia virus type 1 Rex nuclear export signal delineated by a novel in vivo randomization-selection assay. *Mol. Cell. Biol.* **16**, 4207–4214 (1996).

297. C. R. Beals, N. A. Clipstone, S. N. Ho, G. R. Crabtree, Nuclear localization of NF-ATc by a calcineurin-dependent, cyclosporin-sensitive intramolecular interaction. *Genes Dev.* **11**, 824–834 (1997).

298. J. D. Nardozzi, K. Lott, G. Cingolani, Phosphorylation meets nuclear import: a review. *Cell Commun. Signal.* **8**, 32 (2010).

299. A. Kaffman, E. K. O'Shea, Regulation of nuclear localization: a key to a door. *Annu. Rev. Cell Dev. Biol.* **15**, 291–339 (1999).

300. A. Kaffman, N. M. Rank, E. K. O'Shea, Phosphorylation regulates association of the transcription factor Pho4 with its import receptor Pse1/Kap121. *Genes Dev.* **12**, 2673–2683 (1998).

301. A. Kaffman, N. M. Rank, E. M. O'Neill, L. S. Huang, E. K. O'Shea, The receptor Msn5 exports the phosphorylated transcription factor Pho4 out of the nucleus. *Nature*. **396**, 482–486 (1998).

302. A. Komeili, E. K. O'Shea, Roles of phosphorylation sites in regulating activity of the transcription factor Pho4. *Science*. **284**, 977–980 (1999).

303. A. Kumagai, W. G. Dunphy, Binding of 14-3-3 proteins and nuclear export control the intracellular localization of the mitotic inducer Cdc25. *Genes Dev.* **13**, 1067–1072 (1999).

304. N. Davezac *et al.*, Regulation of CDC25B phosphatases subcellular localization. *Oncogene*. **19**, 2179–2185 (2000).

305. H. Seimiya *et al.*, Involvement of 14-3-3 proteins in nuclear localization of telomerase. *EMBO J.* **19**, 2652–2661 (2000).

306. K. Fineberg *et al.*, Inhibition of nuclear import mediated by the Rev-arginine rich motif by RNA molecules. *Biochemistry*. **42**, 2625–2633 (2003).

307. C. W. Chow, R. J. Davis, Integration of calcium and cyclic AMP signaling pathways by 14-3-3. *Mol. Cell. Biol.* **20**, 702–712 (2000).

308. J. Zhu, F. McKeon, NF-AT activation requires suppression of Crm1-dependent export by calcineurin. *Nature*. **398**, 256–260 (1999).

309. F. Shibasaki, E. R. Price, D. Milan, F. McKeon, Role of kinases and the phosphatase calcineurin in the nuclear shuttling of transcription factor NF-AT4. *Nature*. **382**, 370–373 (1996).

310. K. Kondoh, K. Terasawa, H. Morimoto, E. Nishida, Regulation of nuclear translocation of extracellular signal-regulated kinase 5 by active nuclear import and export mechanisms. *Mol. Cell. Biol.* **26**, 1679–1690 (2006).

311. S. Malek, Y. Chen, T. Huxford, G. Ghosh, IkappaBbeta, but not IkappaBalpha, functions as a classical cytoplasmic inhibitor of NF-kappaB dimers by masking both NF-kappaB nuclear localization sequences in resting cells. *J. Biol. Chem.* **276**, 45225–45235 (2001).

312. C. Yan, L. H. Lee, L. I. Davis, Crm1p mediates regulated nuclear export of a yeast AP-1-like transcription factor. *EMBO J.* **17**, 7416–7429 (1998).

313. W. A. Smith, B. T. Schurter, F. Wong-Staal, M. David, Arginine methylation of RNA helicase a determines its subcellular localization. *J. Biol. Chem.* **279**, 22795–22798 (2004).

314. L. C. Trotman *et al.*, Ubiquitination regulates PTEN nuclear import and tumor suppression. *Cell*. **128**, 141–156 (2007).

315. T. Meyer, A. Begitt, I. Lödige, M. van Rossum, U. Vinkemeier, Constitutive and IFN-gamma-induced nuclear import of STAT1 proceed through independent pathways. *EMBO J.* **21**, 344–354 (2002).

316. W. F. Tam, L. H. Lee, L. Davis, R. Sen, Cytoplasmic sequestration of rel proteins by IkappaBalpha requires CRM1-dependent nuclear export. *Mol. Cell. Biol.* **20**, 2269–2284 (2000).

317. E. W. Harhaj, S. C. Sun, Regulation of RelA subcellular localization by a putative nuclear export signal and p50. *Mol. Cell. Biol.* **19**, 7088–7095 (1999).

318. J. M. Stommel *et al.*, A leucine-rich nuclear export signal in the p53 tetramerization domain: regulation of subcellular localization and p53 activity by NES masking. *EMBO J.* **18**, 1660–1672 (1999).

319. J. A. Martina, Y. Chen, M. Gucek, R. Puertollano, MTORC1 functions as a transcriptional regulator of autophagy by preventing nuclear transport of TFEB. *Autophagy*. **8**, 903–914 (2012).

320. H. Takaishi *et al.*, Regulation of nuclear translocation of forkhead transcription factor AFX by protein kinase B. *Proc. Natl. Acad. Sci. USA*. **96**, 11836–11841 (1999).

321. A. Brunet *et al.*, Akt promotes cell survival by phosphorylating and inhibiting a Forkhead transcription factor. *Cell*. **96**, 857–868 (1999).

322. A. M. Brownawell, G. J. Kops, I. G. Macara, B. M. Burgering, Inhibition of nuclear import by protein kinase B (Akt) regulates the subcellular distribution and activity of the forkhead transcription factor AFX. *Mol. Cell. Biol.* **21**, 3534–3546 (2001).

323. M. Bechard, S. Dalton, Subcellular localization of glycogen synthase kinase 3beta controls embryonic stem cell self-renewal. *Mol. Cell. Biol.* **29**, 2092–2104 (2009).

324. S. J. Bautista *et al.*, mTORC1 controls glycogen synthase kinase 3β nuclear localization and function. *BioRxiv* (2018), doi:10.1101/277657.

325. F. Guo *et al.*, mTOR regulates DNA damage response through NF-κB-mediated FANCD2 pathway in hematopoietic cells. *Leukemia*. **27**, 2040–2046 (2013).

326. J. A. Fielhaber *et al.*, Inactivation of mammalian target of rapamycin increases STAT1 nuclear content and transcriptional activity in alpha4- and protein phosphatase 2A-dependent fashion. *J. Biol. Chem.* **284**, 24341–24353 (2009).

327. W. Görner *et al.*, Acute glucose starvation activates the nuclear localization signal of a stress-specific yeast transcription factor. *EMBO J.* **21**, 135–144 (2002).

328. K. Düvel, A. Santhanam, S. Garrett, L. Schneper, J. R. Broach, Multiple roles of Tap42 in mediating rapamycin-induced transcriptional changes in yeast. *Mol. Cell*. **11**, 1467–1478 (2003).

329. T. Beck, M. N. Hall, The TOR signalling pathway controls nuclear localization of nutrient-regulated transcription factors. *Nature*. **402**, 689–692 (1999).

330. Z. S. Chughtai, R. Rassadi, N. Matusiewicz, U. Stochaj, Starvation promotes nuclear accumulation of the hsp70 Ssa4p in yeast cells. *J. Biol. Chem.* **276**, 20261–20266 (2001).

331. S.-O. Yoon *et al.*, Ran-binding protein 3 phosphorylation links the Ras and PI3-kinase pathways to nucleocytoplasmic transport. *Mol. Cell*. **29**, 362–375 (2008).

332. D. Kazyken *et al.*, The nuclear import of ribosomal proteins is regulated by mTOR. *Oncotarget*. **5**, 9577–9593 (2014).

333. J. E. Sale, A. R. Lehmann, R. Woodgate, Y-family DNA polymerases and their role in tolerance of cellular DNA damage. *Nat. Rev. Mol. Cell Biol.* **13**, 141–152 (2012).

334. C. Bavoux *et al.*, Up-regulation of the error-prone DNA polymerase {kappa} promotes pleiotropic genetic alterations and tumorigenesis. *Cancer Res.* **65**, 325–330 (2005).

335. Y. Zhang *et al.*, Error-free and error-prone lesion bypass by human DNA polymerase kappa in vitro. *Nucleic Acids Res.* **28**, 4138–4146 (2000).

336. P. L. Fischhaber *et al.*, Human DNA polymerase kappa bypasses and extends beyond thymine glycols during translesion synthesis in vitro, preferentially incorporating correct nucleotides. *J. Biol. Chem.* **277**, 37604–37611 (2002).

337. E. Ohashi *et al.*, Error-prone bypass of certain DNA lesions by the human DNA polymerase kappa. *Genes Dev.* **14**, 1589–1594 (2000).

338. E. Ohashi *et al.*, Fidelity and processivity of DNA synthesis by DNA polymerase kappa, the product of the human DINB1 gene. *J. Biol. Chem.* **275**, 39678–39684 (2000).

339. Y. Zhang *et al.*, Human DNA polymerase kappa synthesizes DNA with extraordinarily low fidelity. *Nucleic Acids Res.* **28**, 4147–4156 (2000).

340. A. Quinet *et al.*, Gap-filling and bypass at the replication fork are both active mechanisms for tolerance of low-dose ultraviolet-induced DNA damage in the human genome. *DNA Repair (Amst.)*. **14**, 27–38 (2014).

341. J. M. Pennington, S. M. Rosenberg, Spontaneous DNA breakage in single living Escherichia coli cells. *Nat. Genet.* **39**, 797–802 (2007).

342. V. L. Gerlach *et al.*, Human and mouse homologs of Escherichia coli DinB (DNA polymerase IV), members of the UmuC/DinB superfamily. *Proc. Natl. Acad. Sci. USA*. **96**, 11922–11927 (1999).

343. S. Velasco-Miguel *et al.*, Constitutive and regulated expression of the mouse Dinb (Polkappa) gene encoding DNA polymerase kappa. *DNA Repair (Amst.)*. **2**, 91–106 (2003).

344. F. Lemée *et al.*, Characterization of promoter regulatory elements involved in downexpression of the DNA polymerase kappa in colorectal cancer. *Oncogene*. **26**, 3387–3394 (2007).

345. H. Zhu, Y. Fan, J. Shen, H. Qi, J. Shao, Characterization of human DNA polymerase κ promoter in response to benzo[a]pyrene diol epoxide. *Environ Toxicol Pharmacol*. **33**, 205–211 (2012).

346. U. A. Germann *et al.*, Targeting the MAPK Signaling Pathway in Cancer: Promising Preclinical Activity with the Novel Selective ERK1/2 Inhibitor BVD-523 (ulixertinib). *Mol. Cancer Ther.* (2017), doi:10.1158/1535-7163.MCT-17-0456.

347. E. Atlas, M. Stramwasser, C. R. Mueller, A CREB site in the BRCA1 proximal promoter acts as a constitutive transcriptional element. *Oncogene*. **20**, 7110–7114 (2001).

348. G. Wang, Y. Yu, X. Chen, H. Xie, Low concentration N-methyl-N′-nitro-N-nitrosoguanidine activates DNA polymerase-β expression via cyclic-AMP-protein kinase A-cAMP response element binding protein pathway. *Mutation Research/Fundamental and Molecular Mechanisms of Mutagenesis*. **478**, 177–184 (2001).

349. M. Johannessen, M. P. Delghandi, U. Moens, What turns CREB on? *Cell Signal.* **16**, 1211–1227 (2004).

350. B. Mayr, M. Montminy, Transcriptional regulation by the phosphorylation-dependent factor CREB. *Nat. Rev. Mol. Cell Biol.* **2**, 599–609 (2001).

351. R. R. Braeuer, M. Zigler, G. J. Villares, A. S. Dobroff, M. Bar-Eli, Transcriptional control of melanoma metastasis: the importance of the tumor microenvironment. *Semin. Cancer Biol.* **21**, 83–88 (2011).

352. M. P. Delghandi, M. Johannessen, U. Moens, The cAMP signalling pathway activates CREB through PKA, p38 and MSK1 in NIH 3T3 cells. *Cell Signal.* **17**, 1343–1351 (2005).

353. H. Potu *et al.*, Usp5 links suppression of p53 and FAS levels in melanoma to the BRAF pathway. *Oncotarget*. **5**, 5559–5569 (2014).

354. C. Fellmann *et al.*, An optimized microRNA backbone for effective single-copy RNAi. *Cell Rep.* **5**, 1704–1713 (2013).

355. Y. Wang *et al.*, Elevated expression of DNA polymerase kappa in human lung cancer is associated with p53 inactivation: Negative regulation of POLK promoter activity by p53. *Int. J. Oncol.* **25**, 161–165 (2004).

356. M. Uhlén *et al.*, A human protein atlas for normal and cancer tissues based on antibody proteomics. *Mol. Cell Proteomics*. **4**, 1920–1932 (2005).

357. R. S. Finn *et al.*, PD 0332991, a selective cyclin D kinase 4/6 inhibitor, preferentially inhibits proliferation of luminal estrogen receptor-positive human breast cancer cell lines in vitro. *Breast Cancer Res.* **11**, R77 (2009).

358. J. W. Harper, S. J. Elledge, The DNA damage response: ten years after. *Mol. Cell*. **28**, 739–745 (2007).

359. Y. Kozutsumi, M. Segal, K. Normington, M. J. Gething, J. Sambrook, The presence of malfolded proteins in the endoplasmic reticulum signals the induction of glucose-regulated proteins. *Nature*. **332**, 462–464 (1988).

360. B. Ding *et al.*, Sestrin2 is induced by glucose starvation via the unfolded protein response and protects cells from non-canonical necroptotic cell death. *Sci. Rep.* **6**, 22538 (2016).

361. M. N. Lee *et al.*, Glycolytic flux signals to mTOR through glyceraldehyde-3-phosphate dehydrogenase-mediated regulation of Rheb. *Mol. Cell. Biol.* **29**, 3991–4001 (2009).

362. G. Xu *et al.*, Insulin mediates glucose-stimulated phosphorylation of PHAS-I by pancreatic beta cells. An insulin-receptor mechanism for autoregulation of protein synthesis by translation. *J. Biol. Chem.* **273**, 4485–4491 (1998).

363. L. M. Dickson *et al.*, Differential activation of protein kinase B and p70(S6)K by glucose and insulin-like growth factor 1 in pancreatic beta-cells (INS-1). *J. Biol. Chem.* **276**, 21110–21120 (2001).

364. K. Inoki, T. Zhu, K.-L. Guan, TSC2 mediates cellular energy response to control cell growth and survival. *Cell*. **115**, 577–590 (2003).

365. D.-H. Kim *et al.*, mTOR interacts with raptor to form a nutrient-sensitive complex that signals to the cell growth machinery. *Cell*. **110**, 163–175 (2002).

366. N. Ohoka, S. Yoshii, T. Hattori, K. Onozaki, H. Hayashi, TRB3, a novel ER stress-inducible gene, is induced via ATF4-CHOP pathway and is involved in cell death. *EMBO J.* **24**, 1243–1255 (2005).

367. K. Du, S. Herzig, R. N. Kulkarni, M. Montminy, TRB3: a tribbles homolog that inhibits Akt/PKB activation by insulin in liver. *Science*. **300**, 1574–1577 (2003).

368. F. A. Shepherd *et al.*, Erlotinib in previously treated non-small-cell lung cancer. *N. Engl. J. Med.* **353**, 123–132 (2005).

369. B. Kaufman *et al.*, Lapatinib monotherapy in patients with HER2-overexpressing relapsed or refractory inflammatory breast cancer: final results and survival of the

expanded HER2+ cohort in EGF103009, a phase II study. *Lancet Oncol.* **10**, 581–588 (2009).

370. NES Finder 0.2, (available at http://research.nki.nl/fornerodlab/NES-Finder.htm).

371. C. Bavoux, J. S. Hoffmann, C. Cazaux, Adaptation to DNA damage and stimulation of genetic instability: the double-edged sword mammalian DNA polymerase kappa. *Biochimie*. **87**, 637–646 (2005).

372. T. A. Kunkel, DNA replication fidelity. *J. Biol. Chem.* **279**, 16895–16898 (2004).

373. B. van der Vaart *et al.*, TORC1 signaling exerts spatial control over microtubule dynamics by promoting nuclear export of Stu2. *J. Cell Biol.* **216**, 3471–3484 (2017).

374. T. Tagawa, T. Kuroki, P. K. Vogt, K. Chida, The cell cycle-dependent nuclear import of v-Jun is regulated by phosphorylation of a serine adjacent to the nuclear localization signal. *J. Cell Biol.* **130**, 255–263 (1995).

375. M. H. Lam *et al.*, Phosphorylation at the cyclin-dependent kinases site (Thr85) of parathyroid hormone-related protein negatively regulates its nuclear localization. *J. Biol. Chem.* **274**, 18559–18566 (1999).

376. D. R. Zerbino *et al.*, Ensembl 2018. *Nucleic Acids Res.* **46**, D754–D761 (2018).

377. T. Ogi, Y. Shinkai, K. Tanaka, H. Ohmori, Polkappa protects mammalian cells against the lethal and mutagenic effects of benzo[a]pyrene. *Proc. Natl. Acad. Sci. USA*. **99**, 15548–15553 (2002).

378. G. E. Johnson, Mammalian cell HPRT gene mutation assay: test methods. *Methods Mol. Biol.* **817**, 55–67 (2012).

379. E. E. Furth, W. G. Thilly, B. W. Penman, H. L. Liber, W. M. Rand, Quantitative assay for mutation in diploid human lymphoblasts using microtiter plates. *Anal. Biochem.* **110**, 1–8 (1981).

380. W. E. Glaab *et al.*, Resistance to 6-thioguanine in mismatch repair-deficient human cancer cell lines correlates with an increase in induced mutations at the HPRT locus. *Carcinogenesis*. **19**, 1931–1937 (1998).

381. M. Chalfie, Y. Tu, G. Euskirchen, W. W. Ward, D. C. Prasher, Green fluorescent protein as a marker for gene expression. *Science*. **263**, 802–805 (1994).

382. J. D. Ropp *et al.*, Aequorea green fluorescent protein analysis by flow cytometry. *Cytometry*. **21**, 309–317 (1995).

383. N. F. Cariello, S. Narayanan, P. Kwanyuen, H. Muth, W. M. Casey, A novel bacterial reversion and forward mutation assay based on green fluorescent protein. *Mutation Research/Genetic Toxicology and Environmental Mutagenesis*. **414**, 95–105 (1998).

384. M. Standley, J. Allen, L. Cervantes, J. Lilly, M. Camps, Fluorescence-Based Reporters for Detection of Mutagenesis in E. coli. *Meth. Enzymol.* **591**, 159–186 (2017).

385. J. Bachl, M. Dessing, C. Olsson, R. C. von Borstel, C. Steinberg, An experimental solution for the Luria-Delbrück fluctuation problem in measuring hypermutation rates. *Proc. Natl. Acad. Sci. USA*. **96**, 6847–6849 (1999).

386. J. Bachl, C. Olsson, Hypermutation targets a green fluorescent protein-encoding transgene in the presence of immunoglobulin enhancers. *Eur. J. Immunol.* (1999).

387. S. Ro, B. Rannala, A stop-EGFP transgenic mouse to detect clonal cell lineages generated by mutation. *EMBO Rep.* **5**, 914–920 (2004).

388. J. F. Petrosino, R. S. Galhardo, L. D. Morales, S. M. Rosenberg, Stress-induced beta-lactam antibiotic resistance mutation and sequences of stationary-phase mutations in the Escherichia coli chromosome. *J. Bacteriol.* **191**, 5881–5889 (2009).

389. A. Gutierrez *et al.*, β-Lactam antibiotics promote bacterial mutagenesis via an RpoS-mediated reduction in replication fidelity. *Nat. Commun.* **4**, 1610 (2013).

390. R. S. Lo, H. Shi, Detecting mechanisms of acquired BRAF inhibitor resistance in melanoma. *Methods Mol. Biol.* **1102**, 163–174 (2014).

391. E. M. Goetz, M. Ghandi, D. J. Treacy, N. Wagle, L. A. Garraway, ERK mutations confer resistance to mitogen-activated protein kinase pathway inhibitors. *Cancer Res.* **74**, 7079–7089 (2014).

392. N. Wagle *et al.*, MAP kinase pathway alterations in BRAF-mutant melanoma patients with acquired resistance to combined RAF/MEK inhibition. *Cancer Discov.* **4**, 61–68 (2014).

393. E. J. Fox, L. A. Loeb, Lethal mutagenesis: targeting the mutator phenotype in cancer. *Semin. Cancer Biol.* **20**, 353–359 (2010).

394. Y. Mizushina *et al.*, 3-O-methylfunicone, a selective inhibitor of mammalian Y-family DNA polymerases from an Australian sea salt fungal strain. *Mar Drugs*. **7**, 624–639 (2009).

395. K. Yamanaka *et al.*, A comprehensive strategy to discover inhibitors of the translesion synthesis DNA polymerase κ. *PLoS One*. **7**, e45032 (2012).

396. L. A. Loeb *et al.*, Lethal mutagenesis of HIV with mutagenic nucleoside analogs. *Proc. Natl. Acad. Sci. USA*. **96**, 1492–1497 (1999).

397. N. Pariente, S. Sierra, P. R. Lowenstein, E. Domingo, Efficient virus extinction by combinations of a mutagen and antiviral inhibitors. *J. Virol.* **75**, 9723–9730 (2001).

398. S. Sierra, M. Dávila, P. R. Lowenstein, E. Domingo, Response of foot-and-mouth disease virus to increased mutagenesis: influence of viral load and fitness in loss of infectivity. *J. Virol.* **74**, 8316–8323 (2000).

399. J. D. Graci *et al.*, Lethal mutagenesis of poliovirus mediated by a mutagenic pyrimidine analogue. *J. Virol.* **81**, 11256–11266 (2007).

400. J. J. Bull, C. O. Wilke, Lethal mutagenesis of bacteria. *Genetics*. **180**, 1061–1070 (2008).

401. P. J. Gerrish, A. Colato, A. S. Perelson, P. D. Sniegowski, Complete genetic linkage can subvert natural selection. *Proc. Natl. Acad. Sci. USA*. **104**, 6266–6271 (2007).

402. J. C. Fay, G. J. Wyckoff, C. I. Wu, Positive and negative selection on the human genome. *Genetics*. **158**, 1227–1234 (2001).

403. F. Gao *et al.*, Unselected mutations in the human immunodeficiency virus type 1 genome are mostly nonsynonymous and often deleterious. *J. Virol.* **78**, 2426–2433 (2004).

404. T. Sekimoto *et al.*, The molecular chaperone Hsp90 regulates accumulation of DNA polymerase eta at replication stalling sites in UV-irradiated cells. *Mol. Cell*. **37**, 79–89 (2010).

405. F. M. Pozo *et al.*, Molecular chaperone Hsp90 regulates REV1-mediated mutagenesis. *Mol. Cell. Biol.* **31**, 3396–3409 (2011).

406. J. C. Layton, P. L. Foster, Error-prone DNA polymerase IV is regulated by the heat shock chaperone GroE in Escherichia coli. *J. Bacteriol.* **187**, 449–457 (2005).

407. K. Tago, F. Tsukahara, M. Naruse, T. Yoshioka, K. Takano, Regulation of nuclear retention of glucocorticoid receptor by nuclear Hsp90. *Mol. Cell. Endocrinol.* **213**, 131–138 (2004).

408. M. Kakar, C. Kanwal, J. R. Davis, H. Li, C. S. Lim, Geldanamycin, an inhibitor of Hsp90, blocks cytoplasmic retention of progesterone receptors and glucocorticoid receptors via their respective ligand binding domains. *AAPS J.* **8**, E718-28 (2006).

409. S. P. Methot *et al.*, Consecutive interactions with HSP90 and eEF1A underlie a functional maturation and storage pathway of AID in the cytoplasm. *J. Exp. Med.* **212**, 581–596 (2015).

410. A. Orthwein *et al.*, Regulation of activation-induced deaminase stability and antibody gene diversification by Hsp90. *J. Exp. Med.* **207**, 2751–2765 (2010).

411. K. B. Kaplan, R. Li, A prescription for 'stress'--the role of Hsp90 in genome stability and cellular adaptation. *Trends Cell Biol.* **22**, 576–583 (2012).

412. S.-B. Qian *et al.*, mTORC1 links protein quality and quantity control by sensing chaperone availability. *J. Biol. Chem.* **285**, 27385–27395 (2010).

413. G. Ohji *et al.*, Suppression of the mTOR-raptor signaling pathway by the inhibitor of heat shock protein 90 geldanamycin. *J. Biochem.* **139**, 129–135 (2006).

414. A. C. Obenauf *et al.*, Therapy-induced tumour secretomes promote resistance and tumour progression. *Nature*. **520**, 368–372 (2015).

415. M. Jinek *et al.*, A programmable dual-RNA-guided DNA endonuclease in adaptive bacterial immunity. *Science*. **337**, 816–821 (2012).

416. L. Cong *et al.*, Multiplex genome engineering using CRISPR/Cas systems. *Science*. **339**, 819–823 (2013).

417. M. Jinek *et al.*, RNA-programmed genome editing in human cells. *Elife*. **2**, e00471 (2013).

418. P. Mali *et al.*, RNA-guided human genome engineering via Cas9. *Science*. **339**, 823–826 (2013).

419. L. B. Alexandrov *et al.*, Signatures of mutational processes in human cancer. *Nature*. **500**, 415–421 (2013).

420. D. Freed, E. L. Stevens, J. Pevsner, Somatic mosaicism in the human genome. *Genes (Basel)*. **5**, 1064–1094 (2014).

421. I. M. Campbell, C. A. Shaw, P. Stankiewicz, J. R. Lupski, Somatic mosaicism: implications for disease and transmission genetics. *Trends Genet.* **31**, 382–392 (2015).

422. S. De, Somatic mosaicism in healthy human tissues. *Trends Genet.* **27**, 217–223 (2011).

423. A. C. M. Paquola, J. A. Erwin, F. H. Gage, Insights into the role of somatic mosaicism in the brain. *Current Opinion in Systems Biology*. **1**, 90–94 (2017).

424. J. C. Alcántara-Montiel *et al.*, Somatic mosaicism in B cells of a patient with autosomal dominant hyper IgE syndrome. *Eur. J. Immunol.* **46**, 2438–2443 (2016).

425. Z. Li, C. J. Woo, M. D. Iglesias-Ussel, D. Ronai, M. D. Scharff, The generation of antibody diversity through somatic hypermutation and class switch recombination. *Genes Dev.* **18**, 1–11 (2004).

426. L. Cisneros *et al.*, Ancient genes establish stress-induced mutation as a hallmark of cancer. *PLoS One*. **12**, e0176258 (2017).

427. A. Y. Huang *et al.*, Postzygotic single-nucleotide mosaicisms in whole-genome sequences of clinically unremarkable individuals. *Cell Res.* **24**, 1311–1327 (2014).

428. A. Goriely *et al.*, Germline and somatic mosaicism for FGFR2 mutation in the mother of a child with Crouzon syndrome: Implications for genetic testing in "paternal age-effect" syndromes. *Am. J. Med. Genet. A*. **152A**, 2067–2073 (2010).

429. M. J. McConnell *et al.*, Intersection of diverse neuronal genomes and neuropsychiatric disease: The Brain Somatic Mosaicism Network. *Science*. **356** (2017), doi:10.1126/science.aal1641.

430. M. O'Huallachain, K. J. Karczewski, S. M. Weissman, A. E. Urban, M. P. Snyder, Extensive genetic variation in somatic human tissues. *Proc. Natl. Acad. Sci. USA*. **109**, 18018–18023 (2012).

431. L. A. Forsberg *et al.*, Age-related somatic structural changes in the nuclear genome of human blood cells. *Am. J. Hum. Genet.* **90**, 217–228 (2012).

432. J. R. Lupski, Genetics. Genome mosaicism--one human, multiple genomes. *Science*. **341**, 358–359 (2013).

433. S. K. Rehen *et al.*, Constitutional aneuploidy in the normal human brain. *J. Neurosci.* **25**, 2176–2180 (2005).

434. A. R. Muotri, F. H. Gage, Generation of neuronal variability and complexity. *Nature*. **441**, 1087–1093 (2006).

435. J. K. Baillie *et al.*, Somatic retrotransposition alters the genetic landscape of the human brain. *Nature*. **479**, 534–537 (2011).

436. Y. B. Yurov *et al.*, The variation of aneuploidy frequency in the developing and adult human brain revealed by an interphase FISH study. *J. Histochem. Cytochem.* **53**, 385–390 (2005).

437. Y. B. Yurov *et al.*, Aneuploidy and confined chromosomal mosaicism in the developing human brain. *PLoS One*. **2**, e558 (2007).

438. R. Pelossof *et al.*, Prediction of potent shRNAs with a sequential classification algorithm. *Nat. Biotechnol.* **35**, 350–353 (2017).

439. T. G. Montague, J. M. Cruz, J. A. Gagnon, G. M. Church, E. Valen, CHOPCHOP: a CRISPR/Cas9 and TALEN web tool for genome editing. *Nucleic Acids Res.* **42**, W401-7 (2014).

440. C. Thisse, B. Thisse, High-resolution in situ hybridization to whole-mount zebrafish embryos. *Nat. Protoc.* **3**, 59–69 (2008).